IDENTIFICATION AND CHARACTERIZATION OF A MAJOR PROSTAGLANDIN GLYCEROL ESTER HYDROLASE IN HUMAN CANCER CELLS

By

Joseph Dominick Manna

Dissertation

Submitted to the Faculty of the

Graduate School of Vanderbilt University

in partial fulfillment of the requirements

for the degree of

DOCTOR OF PHILOSOPHY

In

Chemical and Physical Biology

August, 2014

Nashville, Tennessee

Approved:

H. Alex Brown. Ph.D

Lawrence J. Marnett Ph.D

Alan R. Brash Ph.D.

Richard M. Caprioli Ph.D.

Ned A. Porter Ph.D.

DEDICATION

In loving memory of my grandmother, Filomena D'Orazio, who never gave up and taught us all to do the same. She will always be an important part of me.

To my family for supporting me in my life journey in science

To my beloved fiancé, Febie, endlessly supportive and my personal cheerleader

ACKNOWLEDGEMENTS

My time here at Vanderbilt was a long and difficult road full of many failures and successes. Getting through the ups and downs would not have been so easy if it wasn't for the support and guidance of fellow researchers and friends. First, I have to thank my advisor, Professor Larry Marnett, for providing the guidance, encouragement, and willingness to provide me with all the resources I needed in my research and in my professional development. His support has allowed me to become a more productive, enthusiastic, and independent scientist and I know my future is going to be full of fruitful adventures in research and life thanks to him.

My scientific experience would not have been so successful if it wasn't for the help and guidance of a terrific committee. I am particularly appreciative of Richard Caprioli for providing me with the training and resources to develop all the MALDI-MS techniques used throughout this work. I am also appreciative of the guidance from my other committee members, Alex Brown, Alan Brash and Ned Porter. I was fortunate to have the opportunity to work with an remarkably knowledgeable and fun committee.

I am thankful to numerous lab mates for their support and guidance. Thanks to Chris Aluise , Jim Galligan and Will Beavers for providing a listening ear and helping me through many of the ups and downs of my research. Thank you to Shu Xu for helping in the beginning of my purification struggles. Phil Kingsley answered countless questions and providing training regarding many LC-MS problems. James Wepy, who helped in the beginning of kinetic characterization and who will continue this work once I leave. Carol Rouzer has been a careful editor of much of my writing, and I have appreciated her advice throughout graduate school. Finally, a special thanks to Brenda Crews for running

a tight but always fun and enjoyable ship, and all of my lab mates for their positive attitudes and willingness to share knowledge.

Thanks to Celeste Riley, Anne Lara, Mary Veazey and Stephen Doster who have provided valuable administrative support. They made everything easy; from getting time with Larry, scheduling rooms for practice talks or meetings, and helping with all my travel needs for courses and conferences. They made everything easy so I didn't have to worry and could focus on research.

Much the success would not have been possible if it was not for the willingness to share information, data, and resources of the Cravatt Lab at Scripps. Thanks particularly to Professor Ben Cravatt for openly sharing all the ABPP data they have generated, for providing inhibitors for our biochemical research, and for a knowledgeable resource in everything related to serine hydrolases.

Working and training at Vanderbilt has allowed me to take advantage of numerous core resources to further my research and I am thankful for that. The HTS Core provided me with the training, guidance, and instruments to develop our COX-2 HTS screen. The VAPR Core, particularly Erin Gribben, for all their help in protein expression in *E.coli* and for never getting aggravated whenever I came into their lab to ask for a new purification tag on my protein.

My friends and family have made my time in Nashville some of the best years of my life. The times with friends out of the lab made the worst days in lab that much easier. I am thankful to my friends in Massachusetts and Nashville, for their support during graduate school, even though many now refuse to call me doctor now that it’s over.
I am forever grateful for my parents who always supported me throughout my entire life

and taught me never to give up no matter how difficult something may seem. I have no doubt that these lessons gave me the drive and determination I needed to succeed in graduate school. Finally I am eternally grateful to my fiancé, Febie. She has been with me throughout every step of this process. She has gotten me through the lows, when I felt nothing would work, and celebrated with me through the highs. She made this entire process easier and I have our entire life to thank her for that.

TABLE OF CONTENTS

Page

LIST OF TABLES

LIST OF FIGURES

LIST OF ABBREVIATIONS

2-AG	2-arachidonoylglycerol
AA	arachidonic acid
ABHD	α/β-hydrolase domain
ABPP	activity based protein profiling
ACN	acetonitrile
AEA	*N*-arachidonoyl ethanolamide
cAMP	cyclic AMP
CB	cannabinoid receptor
cDNA	circular deoxyribonucleic acid
CES1	carboxylesterase 1
CHCA	cyano-4-hydroxy-cinnamic acid
CID	collision-induced dissociation
COX	cyclooxygenases
DDAH2	dimethylarginine dimethylaminohydrolase 2
DAG	diacylglycerol
DAGL	diacylglycerol lipase
DMSO	dimethyl sulfoxide
DTT	dithiothreitol
-EA	ethanolamine
EDTA	Ethylenediaminetetraacetic acid
FAAH	fatty acid amide hydrolase
FBS	fetal bovine serum

FP	fluorophosphonate
-G	glycerol
GPCR	G-protein coupled receptor
IC50	inhibitory concentration 50%
IP3	inositol 1,4,5-triphosphate
LC	liquid chromatography
LOX	lipoxygenase
LPS	lipopolysaccharide LPS
LYPLA1	lysophopholipase A1
LYPLA2	lysophopholipase A2
LysoPL	lysophospholipids
LysoPC	lysophosphatidylcholine
LysoPE	lysophosphatidylethanolamine
MAGL	monoacylglycerol lipase
MALDI	Matrix Assisted Laser Desorption Ionization
mRNA	micro ribonucleic acid
MS	mass spectrometry
MS/MS	tandem mass spectrometry
MudPIT	multidimensional protein identification technology
NAPE	N-arachidonoylphosphatidylethanolamine
NSAID	non-steroidal anti-inflammatory drugs
NAT	N-acyltranferase (NAT)
PAFAH1β3	platelet activating factor acetylhydrolase 1β3 subunit

PAGE	polyacrylamide gel electrophoresis
PE	phosphatidylethanolamine
PG	prostaglandin
PGHS	prostaglandin H_2 synthases
PGLS	6-phosphoglucolactonase
PLA	phospholipase A
PLC	phospholipase C
PLD	phospholipase D
POX	peroxidase
PPT1	palmitoyl protein thioesterase 1
-SA	serinol amide
SDS	sodium dodecyl sulfate
siRNA	small interfering ribonucleic acid
SRM	selected reaction monitoring
TAMRA	tetramethylrhodamine
THC	Δ^9-tetrahydrocannabinol
TXA2	thromboxane A2
WT	wild-type

Chapter I

INTRODUCTION

The Endocannabinoid System

Overview

The endocannabinoid system is a lipid signaling system that derives its name from the *Cannabis sativa* plant, more commonly known as marijuana. *Cannabis sativa* has been cultivated by humans for thousands of years and was predominantly used for fabric and binding. Scientists and physicians became interested in *Cannabis sativa* when Napoleon's troops returning from Egypt described the plants psychotropic effects (1). Medically, *Cannabis sativa* extracts began to be used for their analgesic and antispasmodic effects (2). Due to the psychotropic and analgesic effects of *Cannabis sativa,* modern applications have grown and include both medicinal and recreational uses.

The physiological and psychotropic effects of *Cannabis sativa* are predominantly caused by the plant's active component, the terpenoid derivative Δ^9-tetrahydrocannabinol (THC). Though the active agent was identified in the 1960s, it was not until the 1990s that the receptor activated by THC was identified in mammalian brain (3). Soon after this cannabinoid receptor, named CB1, was identified, another receptor (CB2) was cloned through sequence homology (4). Both receptors are expressed throughout the body with each being concentrated in specific locations. CB1 is expressed throughout the central nervous system, with highest expression in the basal ganglia, hippocampus, and

cerebellum, whereas CB2 is predominately expressed in the immune system. Receptor signaling plays a role in numerous biological processes including pain, motor function, cognition, food intake, body temperature, and inflammation. Following identification of the cannabinoid receptors, endogenously produced ligands were discovered. These compounds, which are arachidonic acid derivatives, were termed endocannabindoids and included *N*-arachidonoyl ethanolamide (AEA), more commonly known as anandamide (5), and 2-arachidonoyl glycerol (2-AG) (Figure 1) (6).

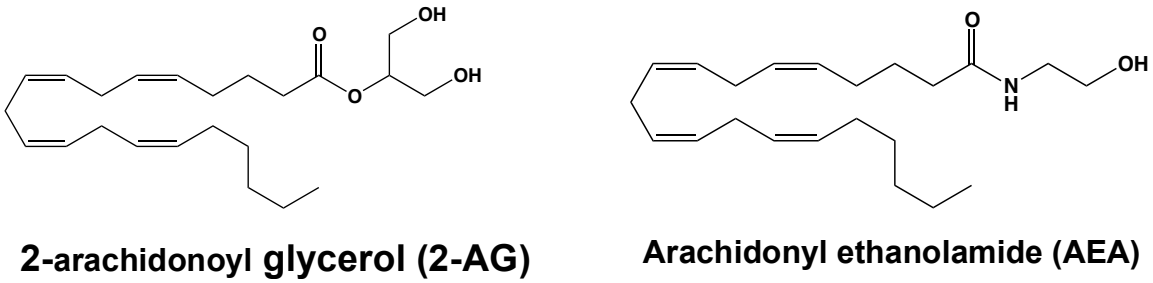

2-arachidonoyl glycerol (2-AG) **Arachidonyl ethanolamide (AEA)**

Figure 1: Structures of the endocannabinoids

AEA was the first endocannabinoid identified in 1992 by a screen for endogenous ligand for the cannabinoid receptors. Three years later, 2-AG was discovered and isolated from mammalian intestinal tissue.

Cannabinoid Receptors

As mentioned above, there are two major G-protein coupled receptors for endocannabinoids, the CB1 and CB2 receptors. The first receptor identified was named the CB1 receptor and is mainly present in nerve cells (central and peripheral neurons and glial cells) and reproductive system (7-10). The CB2 receptor was initially found in the

immune system, with highest expression in B lymphocytes, moderate expression in monocytes and neutrophils, and lowest expression in T lymphocytes and microglial cells (1, 4, 11). Interestingly, CB receptors play an important role during development of the brain, where they control differentiation (12). In adult brains, cannabinoid receptors (predominantly CB1) are the most abundant G-protein coupled receptors, with levels 10-50 fold higher than other receptors, such as dopamine or opioid receptors (8, 9).

Both CB receptors are coupled to similar transduction networks, including GPCR coupled pathways, ion channel regulation and protein kinase pathways. CB receptor GPCR pathway activation leads to either inhibition of cAMP through coupling to Gi proteins, resulting in decreased protein kinase A phosphorylation (7, 9), or stimulation of cAMP formation through coupling to the Gs proteins (13). Additionally, cannabinoid receptors can couple to ion channels and result in the inhibition of Ca^{2+} influx through interaction with multiple calcium channel types (N, P/Q, and L types, (14-16). This is related to endocannabinoid involvement in neurotransmitter release and synaptic plasticity (17, 18). Furthermore, cannabinoid receptors couple to a multitude of protein kinase cascades, including mitogen-activate protein kinase, phosphatidylinositol 3-kinase, and focal adhesion kinase (19-21).

Endocannabinoids differ in how they bind the cannabinoid receptors. AEA acts as a partial agonist at both receptors but has a higher affinity for the CB1 receptor, with activity at CB1 4-30 fold higher then at CB2 (21, 22). In contrast, 2-AG is a complete agonist of both cannabinoid receptors though it exhibits lower affinity then AEA for either receptor (21, 23).

Biosynthesis and Metabolism of Endocannabinoids

N-Arachidonoyl ethanolamine: AEA is primarily synthesized from membrane phospholipids through a two-step process. Initially, increased Ca^{2+} stimulates the N-acylation of phosphatidylethanolamine (PE), where an acyl group is specifically transferred from the sn-1 position of a glycerophospholipids to the amine of PE, to form N-arachidonoylphosphatidylethanolamine (NAPE) (24-26). The enzyme responsible for this transfer is N-acyltranferase (NAT) (24-26). The next step involves the hydrolysis of NAPE by a NAPE-phospholipase D (PLD) to produce AEA and phosphatidic acid (Figure 2) (24-26). NAT is inactive in the absence of Ca^{2+}, and increasing the concentrations of Ca^{2+} during synaptic transmission activates NAT (27).

Alternative pathways for the production of AEA exist in cellular systems. Phospholipases (PLA_1/A_2) catalyze the hydrolysis of *N*APEs to *N*-acyl-lysoPEs (Lyso-NAPEs) (28, 29), which are further cleaved at the phosphodiester bond by a lysophospholipase D to generate AEA (Figure 2). However, NAPE-PLD has low hydrolytic activity for lyso-NAPE, implying the role of another lysophospholipase (30). The serine hydrolase α/β-hydrolase domain 4 (ABHD4) has shown to accept a wide array of lyso-NAPEs, including ones containing arachidonoylethanolamine (31). Another alternative pathway for AEA biosynthesis was identified in macrophages, and involved the hydrolysis of NAPE to phosphoanandamide by phospholipase C, followed by dephosphorylation through a phosphatase to generate AEA. This pathway may account for findings showing anandamide tissue levels are unchanged in NAPE-PLD knockout mice (32).

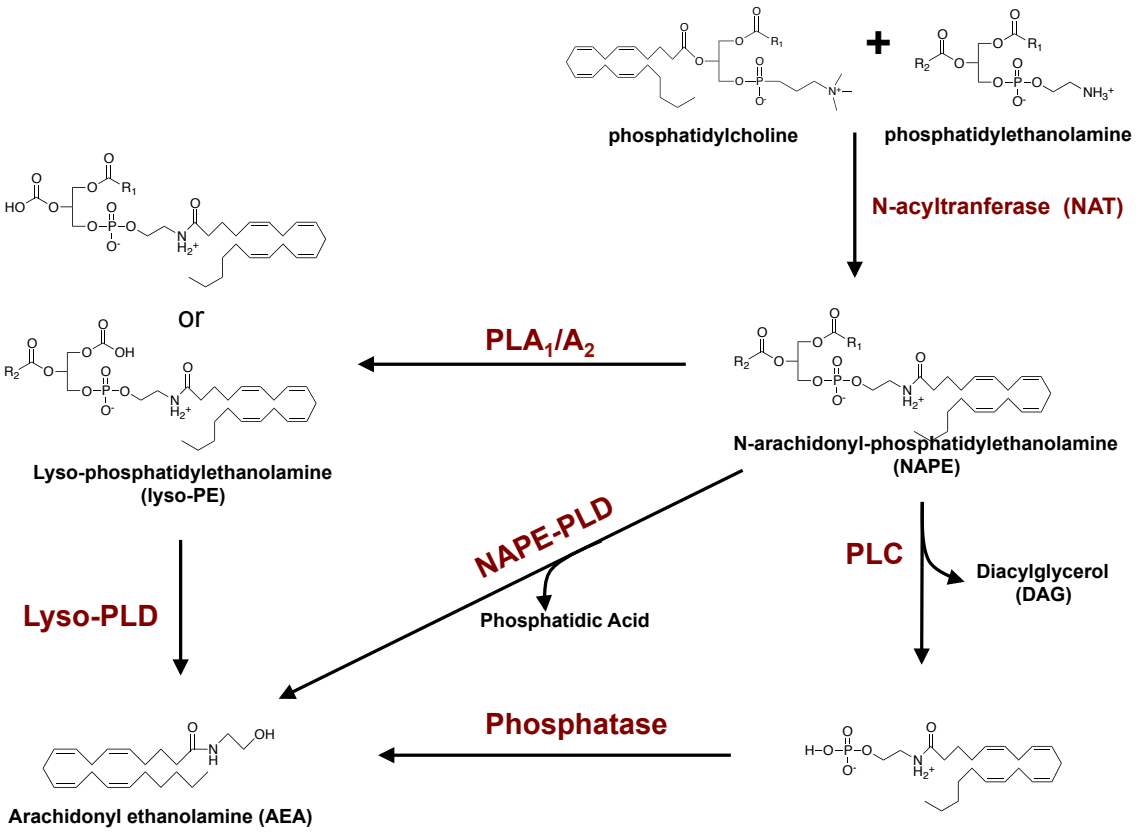

Figure 2: Biosynthesis pathway of AEA

Once AEA is synthesized in neurons, it passively diffuses through the postsynaptic membrane into the intracellular space where it can engage the cannabinoid receptors as well as catabolic enzymes (33). Additionally, AEA is trafficked by specific transporters, which are modulated by levels of intracellular AEA (34). Once in the cell, AEA is subject to hydrolysis, to form free arachidonic acid and ethanolamine. The major enzyme responsible for this hydrolysis was identified as the serine hydrolase fatty acid amide hydrolase (FAAH) (35-38). FAAH is an inter-cellular membrane-bound protein that hydrolyzes a wide array of ethanolamine containing lipids, including oleoylethanolamide (39) and palmitoylethanolamine (40, 41). Furthermore, AEA is subject to oxidative metabolic pathways; including lipoxygenases (LOXs), cyclooxygenases (COX-2) and cytochrome P450s (42). AEA oxidation by COX-2 results in the formation of ethanolamides of the prostaglandins, termed prostamides, which will be described in further detail below.

2-Arachidonoyl glycerol: Similar to AEA, the major pathways for the biosynthesis of 2-arachidonoyl glycerol (2-AG) begins in the lipid bilayer. Biochemical studies have indicated multiple pathways for the generation of 2-AG. Primarily, arachidonic acid containing inositol phospholipids are sequentially hydrolyzed by the serine hydrolases, phospholipase C (PLC) and diacylglycerol lipase (DAGL) (6, 43, 44). In response to extracellular stimulation, increases in cellular calcium trigger PLCs to catalyze the hydrolysis of phosphatidylinositol-4-5-bisphosphate (Figure 3) to produce two well-studied second messenger molecules, inositol 1,4,5-triphosphate (IP3) and diacylglycerol (DAG) (44-46). Next, DAGL hydrolyzes DAG at the sn-1 position to produce 2-AG,

which is released from cells to stimulate the CB receptors. Alternatively, 2-AG can be produced by the action of phospholipase A_1 (PLA_1) and lysophosphotidylinositol specific phospholipase C (lysoPLC). PLA_1 acting on inositol containing phospholipids generates the inositol-containing lysophospholipid (Figure 3) (6, 47, 48). From here, a lysoPLC generates 2-AG by cleavage of the phosphoinositol containing head group. Many of these biosynthetic pathways differ depending on stimulation conditions, e.g. calcium stimulation, receptor activation.

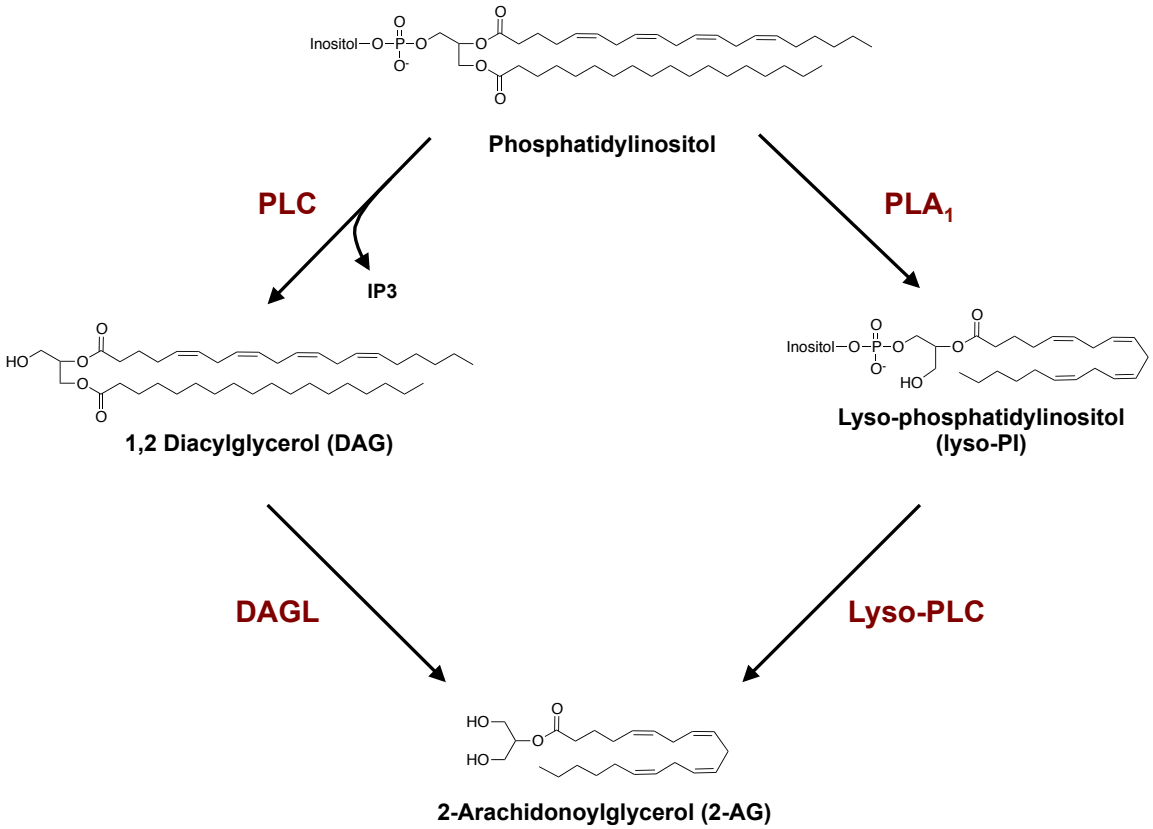

Figure 3: Biosynthesis pathway of 2-arachidonoyl glycerol

Similar to AEA, 2-AG signaling is terminated by enzymatic hydrolysis, generating arachidonic acid and glycerol (49). Due to the structural similarities between AEA and 2-AG, it was hypothesized that FAAH also hydrolyzes 2-AG (50). Though FAAH is capable of hydrolyzing 2-AG, it was determined that the major enzyme responsible for 2-AG metabolism is monoacylglycerol lipase (MAGL) (51). MAGL is abundantly expressed in the nervous system and localizes on neurons that express CB1 receptors (52, 53). Though MAGL accounts for ~85% of the degradation of 2-AG, the remaining 15% of 2-AG metabolism is attributed to two serine hydrolases, α/β hydrolase (ABHD) domain proteins, ABHD6 and ABHD12. 2-AG is also subject to oxidative metabolism by many of the same enzymes that oxygenate both arachidonic acid (AA) and AEA. The remainder of this work will focus on COX-2 oxidation products of the endocannabinoids.

Cyclooxygenase

Historical Overview

The history of cyclooxygenases is a long and fruitful one. It begins in ancient times where people unknowingly manipulated the enzyme for the treatment of pain and inflammation. The first examples of pain relief are mentioned in the Ebers papyrus which dates to 1500 BC where it is recommended to use myrtle leaves to relieve pain (54-56). Hippocrates followed in 400 BC with his recommendations for the consumption of bark from the willow tree to alleviate fever and pain (54-56). In 1763, Edward Stone used willow bark to treat fevers in 50 of his patients, and was one of the first to scientifically publish the results (54, 57). It wasn't until 1838 that Raffaelle Piria was

able to isolate and identify the active component of the willow bark as salicylic acid (Figure 4). Twenty years later, Hammond Kolbe was the first to synthesize salicylic acid which eventually led to industrial scale up and production of the compound (56, 57).

Though salicylic acid was a useful treatment for fever and pain, it had some undesirable qualities, including a bitter taste and irritability to both the mouth and stomach (55-57). These undesirable qualities led Felix Hoffman in 1897 to synthesize an acetylated version of salicylic acid, mainly to help his father tolerate the drug better. The new compound, named aspirin (Figure 4), caused less dyspepsia than salicylic acid (55-57). Detailed pharmacological and toxicological tests confirmed the actions of aspirin as an excellent analgesic and antipyretic (56-58). It would take another 70 years to identify prostaglandin H_2 synthases (PGHS), also known as cyclooxygenases (COX), as the targets for these newly developed non-steroidal anti-inflammatory drugs (NSAIDs) (56, 57, 59).

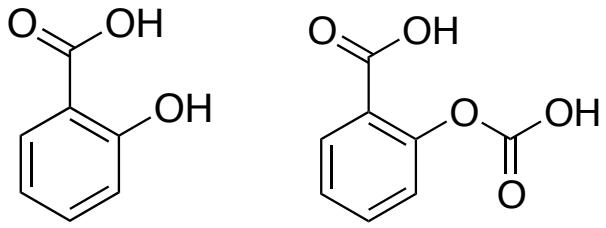

Salicylic Acid Aspirin

Figure 4: Structure of Salicylic Acid and Aspirin

With the mass production, commercialization and administration of aspirin as a drug, scientists began to study what effect this compound was having in the body. It was first shown in 1971 by Sir John Vane that aspirin, and other newly developed NSAIDs,

inhibited the synthesis of prostaglandins in guinea pig lungs (59). He concluded that the effects of NSAIDs were due to decreased production of prostaglandins by inhibition of COX. Smith and Willis's findings on the effect of aspirin on platelet behavior was published jointly with Vane's (60). They showed that platelets isolated from patients treated with aspirin were not able to aggregate, and produced lower levels of prostaglandins as compared to controls (58, 60). The effects of NSAIDs as a whole were due to inhibition of prostaglandin formation by COX, causing positive effects such as anti-inflammatory, analgesic and anti-pyretic responses; but also many of the side effects, including damage to stomach mucosa and the gastrointestinal system and kidney toxicity (58).

Cyclooxygenase Biochemistry

Cyclooxygenases (COXs) are membrane bound homodimeric proteins comprised of 70 kDa monomers. Each monomer of the protein contains both a cyclooxygenase active site and a peroxidase active site, and requires heme to catalyze its reactions (61-64). Structurally, COXs are homodimer proteins composed of tightly associated monomers with each protein consisting of three distinct regions; an epidermal growth factor domain near the dimer interface, a membrane binding domain which binds monotopically to the lipid bilayer, predominantly at the endoplasmic reticulum, and the catalytic domain, which possesses both a cyclooxygenase (COX) and a peroxidase (POX) functionality (Figure 5) (61-64). Monomers of COX differ in terms of activity, with maximal COX activity occurring when one molecule of heme is bound per dimer of protein (65). These leads to a protein that has one catalytically active subunit and one

non-catalytically active subunit that acts as an allosteric modulator of the catalytic subunit. Additionally, some NSAIDs, such as indomethacin, are able to inhibit COX at a stoichiometric ratio of one NSAID for each dimer (66). Multiple studies utilizing various fatty acids and COX inhibitors have shown that COX is a structural homodimer but a functional heterodimers during catalysis and inhibition (67-70).

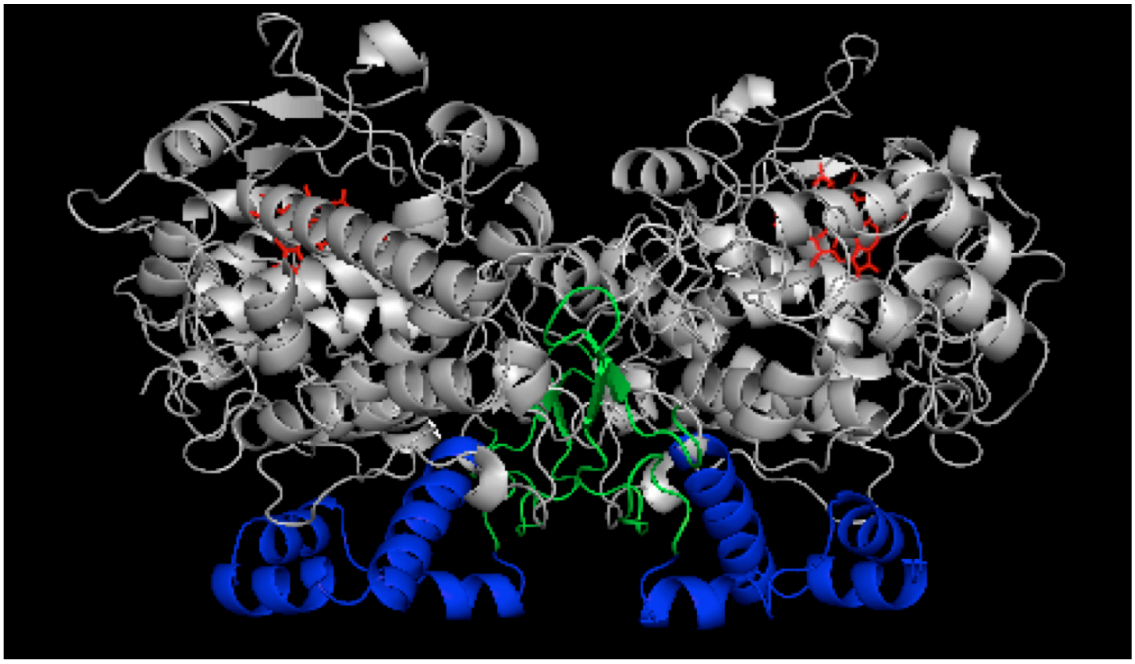

Figure 5: Structure of COX-2: Homodimer with the membrane-binding domain is in blue, EGF-like domain is in green and the catalytic domain in grey. The heme is shown (red) bound in the POX active site (PDB ID: 3PGH)

Cyclooxygenase Catalytic Mechanism

Cyclooxygenases are bi-functional enzymes that perform consecutive reactions in two active sites, the COX and POX active sites (61, 62, 64, 71). The *bis*-dioxygenation of arachidonic acid (AA) takes place in the L-shaped cavity of the COX active site, resulting in the production of prostaglandin G_2 (PGG_2). PGG_2 diffuses from the COX active site and is reduced in the POX active site to form PGH_2. Once produced, PGH_2 is further processed by various synthases to form a wide array of prostaglandins and thromboxanes (Figure 6) (61, 62, 64, 71).

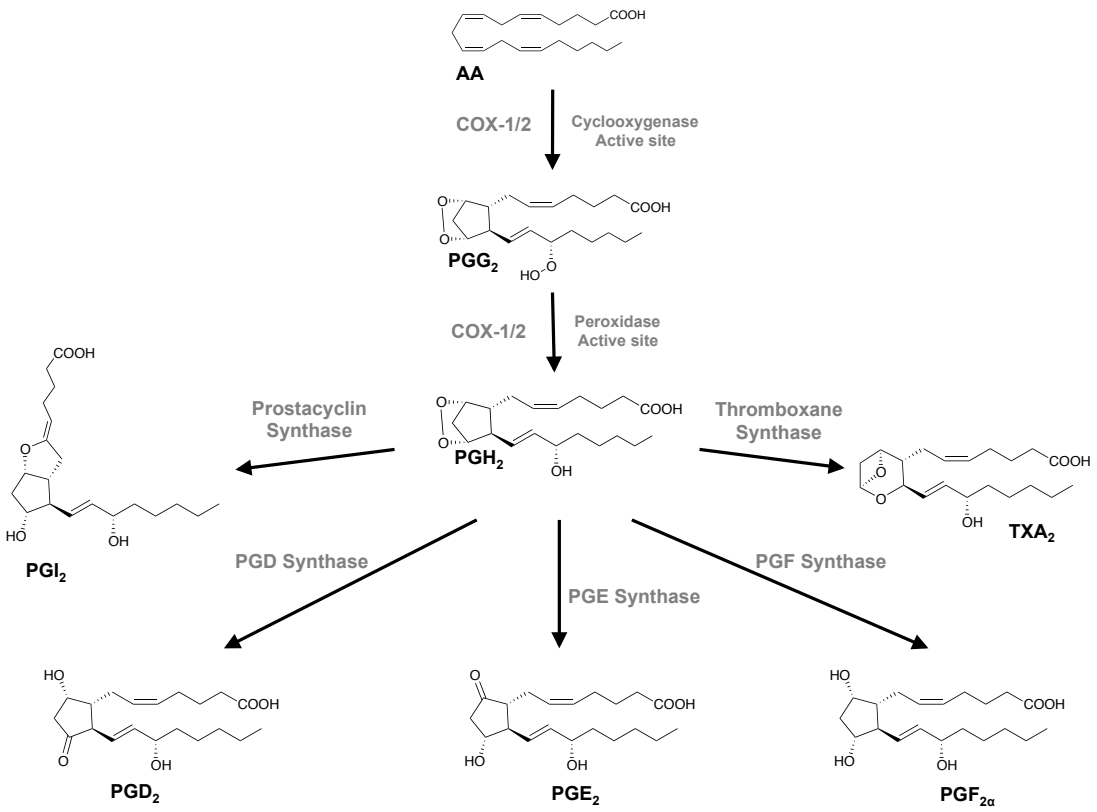

Figure 6: Products of Arachidonic Acid Oxidation by Cyclooxygenase

Importantly, initiation of the COX reaction is dependent upon a two-electron oxidation of the heme present in the POX active site. The need for heme oxidation in the cyclooxygenase enzyme is best described by the branched-chain mechanism (Figure 7), where the POX active site can function independently of the COX active site. Conversely, COX activity requires a two-electron oxidation of the POX active site protoporphyrin heme [(PPIX)Fe^{3+}] in combination with a two-electron reduction of a hydroperoxide substrate, to form a ferryloxo protoporphyrin radical cation ((PPIX□)$^{+}Fe^{4+}O$). It is this protoporphyrin radical that initiates the COX active site by

radical abstraction of the hydrogen from Tyr-385 in the COX active site, leading to formation of a tyrosyl radical and initiation of the cyclooxygenase reaction (62, 64).

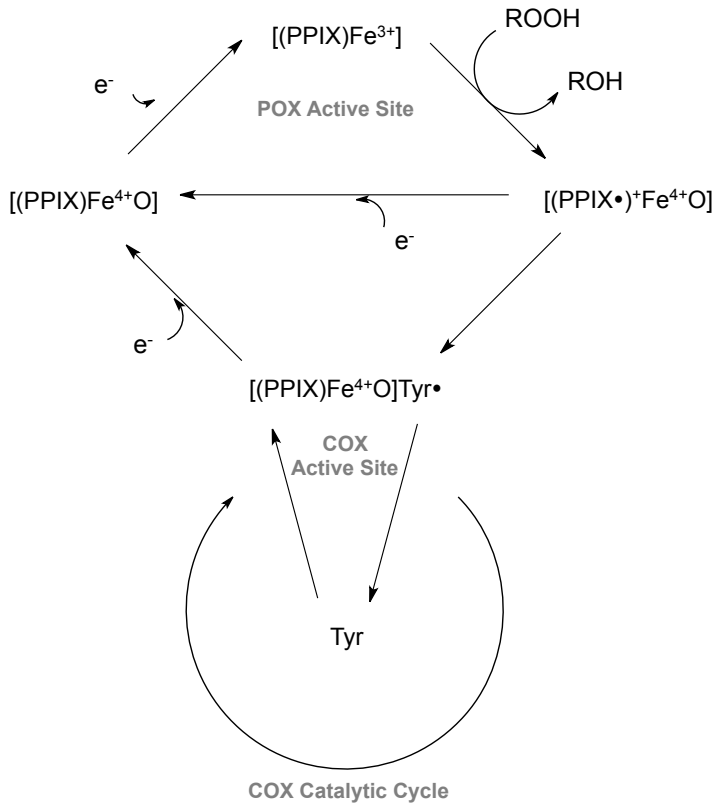

Figure 7: Branched Chain Mechanism of COX (62).

Once activated, the COX enzyme activity is initiated with the introduction of AA into the correct catalytic orientation in the COX active site (71). This involves the placement of the carboxylic acid group of AA near Arg-120 and Tyr-355 at the opening of the binding pocket. This orients the fatty acid chain of AA in the hydrophobic groove of COX, which orients carbon-13 below the catalytic Tyr-385 radical (Figure 8). This catalytic Tyr-385 radical can abstract the 13-*proS*-hydrogen of AA forming a carbon-centered radical. Formation of this radical leads to a series of radical rearrangements along the

AA backbone, allowing the addition of two molecules of oxygen and formation of the 15-hydroperoxyl radical of PGG_2, with is reduced by Tyr-385 regenerating the radical Tyr-385. PGG_2 migrates to the POX active site to be reduced to PGH_2 (61, 62, 64, 71).

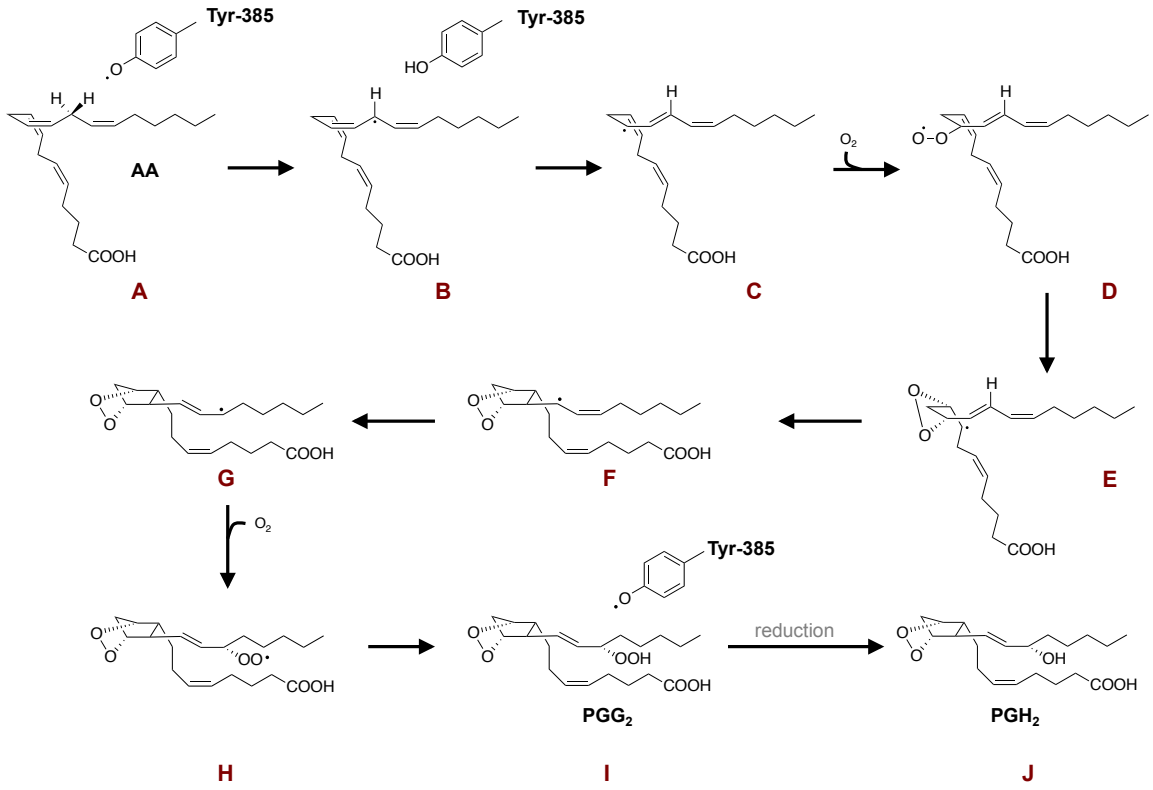

Figure 8: Mechanism of Cyclooxygenase Catalysis. Substrate binding in the COX active site results in radical abstraction of the 13-*proS*-hydrogen of AA (A). (B) The resulting oxygen radical shifts to the 11 position (C) which is then subject to addition of molecular oxygen (D). Following addition of oxygen, the endoperoxide is formed between carbons 9 and 11 (E) followed by the formation of a single carbon-carbon bond between carbons 8 and 12 (F). From here the radical shifts from carbon 13 to carbon 15 (G), which is subject to another addition of molecular oxygen to form the peroxyl radical (H). This radical is reduced by Tyr-385 to form PGG_2 (I) and regeneration of the radical Tyr-385. PGG_2 migrates to the POX active site to be reduced to PGH_2 (J)

Cyclooxygenase 1 versus Cyclooxygenase 2

Though Vane described the cyclooxygenase enzymes as the target for aspirin; the discovery of two COX isoforms wasn't made until 1990 (72). The two enzymes (named COX-1 and COX-2) share 60% sequence identity and metabolize AA at the same rate (63). COX-1, the first isoform discovered, is a constitutively expressed protein that is thought to maintain the homeostatic levels of prostaglandins throughout the body (73). COX-2 is the inducible form of the enzyme and its expression is triggered by multiple stimuli; including inflammatory cytokines, growth factors, and tumor promoters (73). The inducible nature of COX-2 has led many to believe the enzyme is responsible for prostaglandin formation during pathological states, including inflammation and tumorigenesis (73, 74).

In addition to expression differences, both enzymes have differential binding for a wide array of substrates. COX-1 is more selective in which substrates it utilizes and requires a free carboxyl group in fatty acid substrates in order to perform catalysis. COX-2 has been shown to possess more flexibility in which substrates bind to the active site. As stated earlier, in addition to AA binding, COX-2 is also capable of metabolizing the endocannabinoids (75-77). Purified COX-2 can bind and oxygenate AEA and 2-AG while COX-1 has much reduced activity (75-77)

COX-1 and COX-2 Structure and Substrate Binding - AA vs. 2-AG

Exploration into why COX-2 can bind a wide array of substrates while COX-1 is more restricted led to structural investigations of both enzymes bound to AA and 1-AG (major form of 2-AG at equilibrium). As mentioned previously, in both COX isoforms,

productive AA binding orients the ω-fatty acid tail into the top of the COX active site with the carboxylic acid group placed near the opening of the active site, known as the constriction site (63, 78), which positions the 13-*proS*-hydrogen of AA for radical extraction by Tyr-385 (Figure 10).

1-AG binding to COX-2 is similar to that of AA, with the ω-fatty acid tail of 1-AG placed in the hydrophobic binding pocket of COX-2 with the 13-*proS*-hydrogen oriented close to Tyr-385 (Figure 10) (79). The difference in substrate binding lies near the constriction site. To facilitate the glycerol group of 1-AG, a leucine-531 residue must flip out of the binding pocket. This creates the space necessary to bind 1-AG. Finally, the only hydrophilic interaction between 1-AG and COX-2 is between Tyr-355 and the carboxyl oxygen of 1-AG (79).

Unlike COX-2, COX-1 is not able to effectively metabolize the endocannabinoids. For AA to be turned over by COX-1, the substrate must form hydrogen bonds between the carboxyl group of AA and Tyr-355 and Arg-120 at the constriction site (63, 80). The position of Arg-120 is stabilized by interactions with Leu-531 (78, 80). With a lack of flexibility of Leu-531, the COX active site of COX-1 does not possess the volume necessary to accommodate larger substrates, including 2-AG and AEA (79). In COX-2, mutating the side chain of Leu-531 to alanine, phenylalanine, proline or threonine does not change substrate binding or decrease activity caused by a lack of Leu-531 and Arg-120 interaction, suggesting that Arg-120 binding in COX-2 is independent of Leu-531 involvement (79).

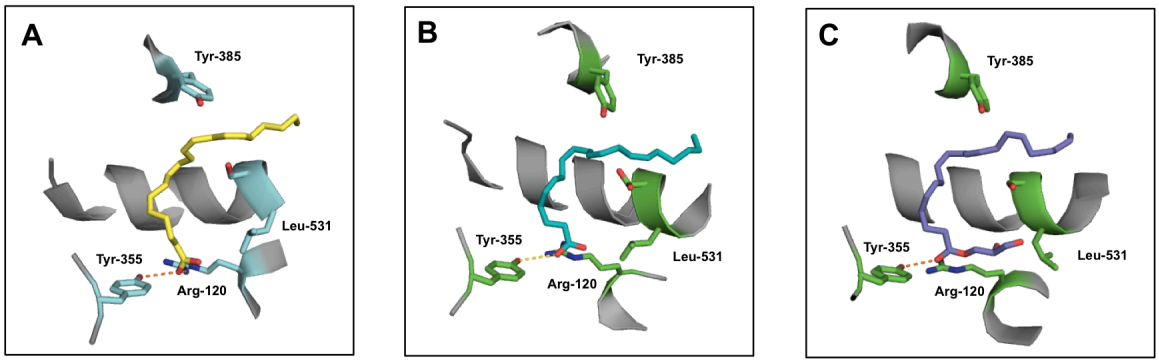

Figure 9: Crystal structures for AA and 1-AG binding to COX enzymes in the COX Active Site. A) Arachidonic acid binding to COX-1. The orientation of AA (yellow) places the carboxylate at the constriction site, with hydrogen bonding (orange) to both Tyr-355 and Arg 120 (blue). This places the 13-*proS*-hydrogen below Tyr-385 for radical extraction. B) AA binding to COX-2. AA (cyan) orients in the binding pocket similarly to COX-1 with the exception of missing hydrogen bond between Arg-120 (green) and the carboxylate. C) 1-AG binding to COX-2. Similar to AA, the 13-*proS*-hydrogen of 1-AG (blue) is positioned close to Tyr-385 (green) for hydrogen extraction. At the constriction site, Leu-531 inverts its orientation compared to AA binding in order to accommodate the glycerol group of 1-AG.

COX-2 Dependent Endocannabinoid Oxygenation

As mentioned previously, endocannabinoids are also substrates for cyclooxygenase. Yu et al. presented the first evidence of COX-mediated metabolism of endocannabinoids in 1997. They showed that COX-2, but not COX-1, metabolized AEA at a rate of oxidation comparable to arachidonic acid, but with a 4-fold higher K_m value for AEA (75). The products of AEA metabolism are similar to the products produced from AA, with the major products being PGH_2-EA, which is a substrate for the prostaglandin synthases, leading to production of a wide array of prostaglandin ethanolamide derivatives (81). However, unlike AA derived PGH_2, PGH_2-EA is a poor substrate for the thromboxane synthases (Figure 9) (77).

The rate of oxygenation of 2-AG by COX-2 is as efficient as AA oxygenation (42, 76). The products of 2-AG oxidation are virtually the same prostaglandin derivatives as those generated from AA, termed prostaglandin glycerol esters (PG-Gs). Similarly to PGH_2-EA, PGH_2-G is a poor substrate for thromboxane A_2 and only the products of prostaglandin synthases are made (Figure 9). Furthermore, 2-AG is a poor substrate for oxygenation by COX-1.

The physiological actions of PG-Gs are of growing interest because they have been shown to activate calcium mobilization in macrophages and tumor cells, modulate synaptic transmissions, and induce hyperalgesia (82-86). Investigation into the physiological relevance of these COX-2 products has been difficult because of instability in biological fluids due to an active, unique, and unidentified serine hydrolase (87). The identity of this hydrolase will be further examined later in this work.

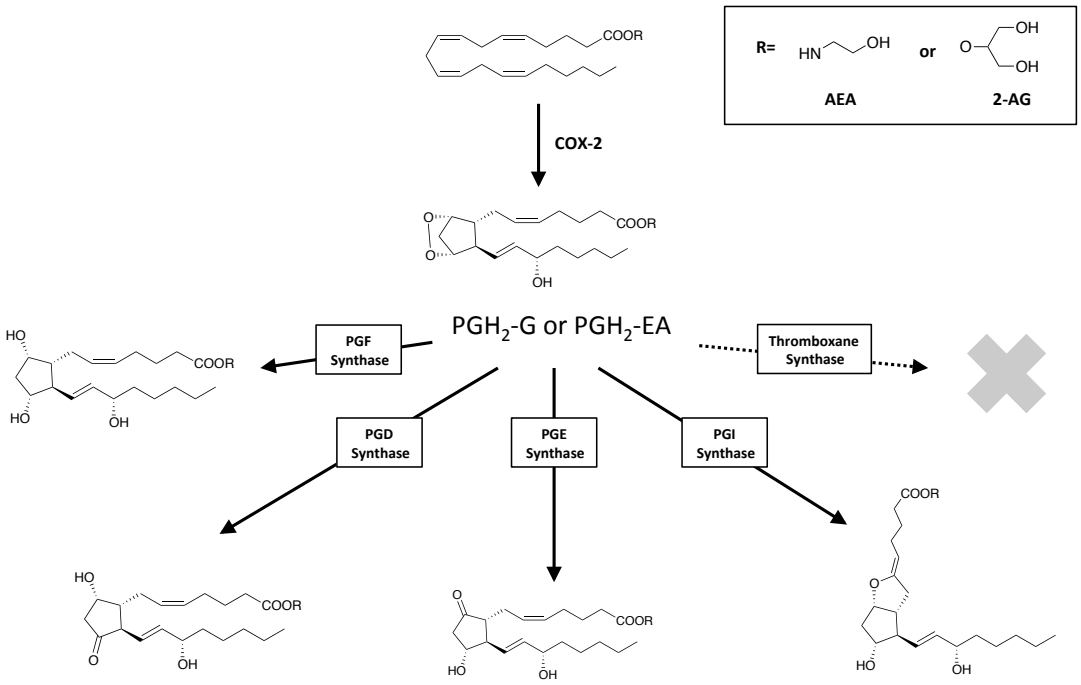

Figure 10: Endocannabinoid Oxidation by COX-2

Physiology of Oxygenation Products of Endocannabinoids

There is a growing interest in understanding the roles endocannabinoid derived COX-2 products play in physiological and pathophysiological settings. The first insights into the effects of these molecules came from the study of the synthetic $PGF_{2\alpha}$-EA analog, bimatoprost, and its use as an ocular hypotensive agent in the treatment of glaucoma and ocular hypertension (88). Bimatoproast and $PGF_{2\alpha}$-EA exert the same effect on intraocular pressure as $PGF_{2\alpha}$, however the fact that antagonists can block the effects of $PGF_{2\alpha}$-EA while having no effect on $PGF_{2\alpha}$ suggests a specific receptor for $PGF_{2\alpha}$-EA. This receptor was identified as a heterodimer of the FP receptor, comprised of one wild type FP receptor and one splice variant of the FP receptor with a shortened C-terminus (88).

$PGF_{2\alpha}$-EA has also been implicated in the process of inflammation. In rat inflammatory pain models, $PGF_{2\alpha}$-EA levels in the spine were significantly increased and showed a pro-algesic effect. COX inhibition in this model caused a decrease in $PGF_{2\alpha}$-EA levels upon stimulation (89). However, not all prostamides elicit negative responses during inflammation. PGE_2-EA has been reported to reduce the expression of IL-12p40 in activated macrophages and microglial cells, which leads to a reduction of the cytokines, IL-12 and IL-23 (90). PGE_2-EA also reduces the effects of lipopolysaccharide (LPS)-induced tumor necrosis factor (TNF-α) in whole blood and monocytes (91). All these effects are predominately elicited through the binding of PGE_2-EA to the EP_2 receptor. Additionally, it appears that PGE_2-EA binds to all the EP receptors (92).

In addition to the prostamides, PG-Gs have also shown a wide array of physiological responses. In RAW264.7 murine macrophages, PGE_2-G caused an increase

in Ca^{2+} mobilization that was independent of any known prostaglandin receptors. This increase triggered the synthesis of IP_3, activation of PKC, which leads to ERK phosphorylation. (82, 86). These effects of PGE_2-G were also mimicked in human non-small cell lung carcinoma cancer cell line, H1819, where administration of the substrate triggered the same Ca^{2+} mobilization (86). This increase in Ca^{2+} and increase in IP_3 production suggests the existence of PGE_2-G-specific G-protein coupled receptors.

Additionally, PGE_2-G can induce hyperalgesia and modulate NF-κB activation in carrageenan-induced inflammation in the rat hind paw (85), as well as induce proinflammatory and neurotoxic effects in a rat model for Huntington's disease (93). PGE_2-G and $PGF_{2\alpha}$-G also increase LPS-induced inflammation in macrophage activation. Interestingly, not all PG-Gs are proinflammatory. Specifically, PGD_2-G reduces macrophage activation and exerts anti-inflammatory effects in LPS-induced inflammation in mice (72). Also, the PGD_2-G metabolite 15-deoxy-$\Delta^{12,14}$ prostaglandin J_2-glycerol ester demonstrated PPAR-γ activation and reduction in T cell activation (94, 95).

In neuronal cells, PG-Gs were able to modulate GABAergic receptor-mediated inhibition of synaptic transmission. Specifically, PGE_2-G was able to increase the frequency of miniature inhibitory postsynaptic currents, which was independent of the CB receptors (84). Other prostaglandin glycerol esters and amides (specifically PGD_2-G, PGF_{2a}-G and PGD_2-EA) were also able to increase these frequencies while being mediated through novel receptors (84). Additionally, PGE_2-G enhanced excitatory glutamatergic synaptic transmission, which was independent of the CB receptors in hippocampal neuron cultures (83). Specifically, these prostaglandin glycerol esters induced injury, apoptosis and potentiated N-methyl-D-Aspartate (NMDA)-receptor

induced cell death, which is reversible by NMDA receptor antagonists, signifying neurodegeneration is due to the increased release of glutamate (83, 96).

Figure 11 shows a full summary of the COX-2 oxidative metabolism of arachidonic acid and endocannabinoids. Injury or stimulation causes an elevation in COX-2 expression and activity, which oxygenates AA, 2-AG and AEA to produce PGs, PG-Gs, and PG-EAs, respectively. As stated above, endocannabinoids activate CB receptors while COX-2 oxidative metabolites of 2-AG or AEA exert their role in modulating activity through novel, unidentified receptors (83, 84). Upon activation of these receptors, a number of different physiological effects occur, including many pro-inflammatory or anti-inflammatory responses.

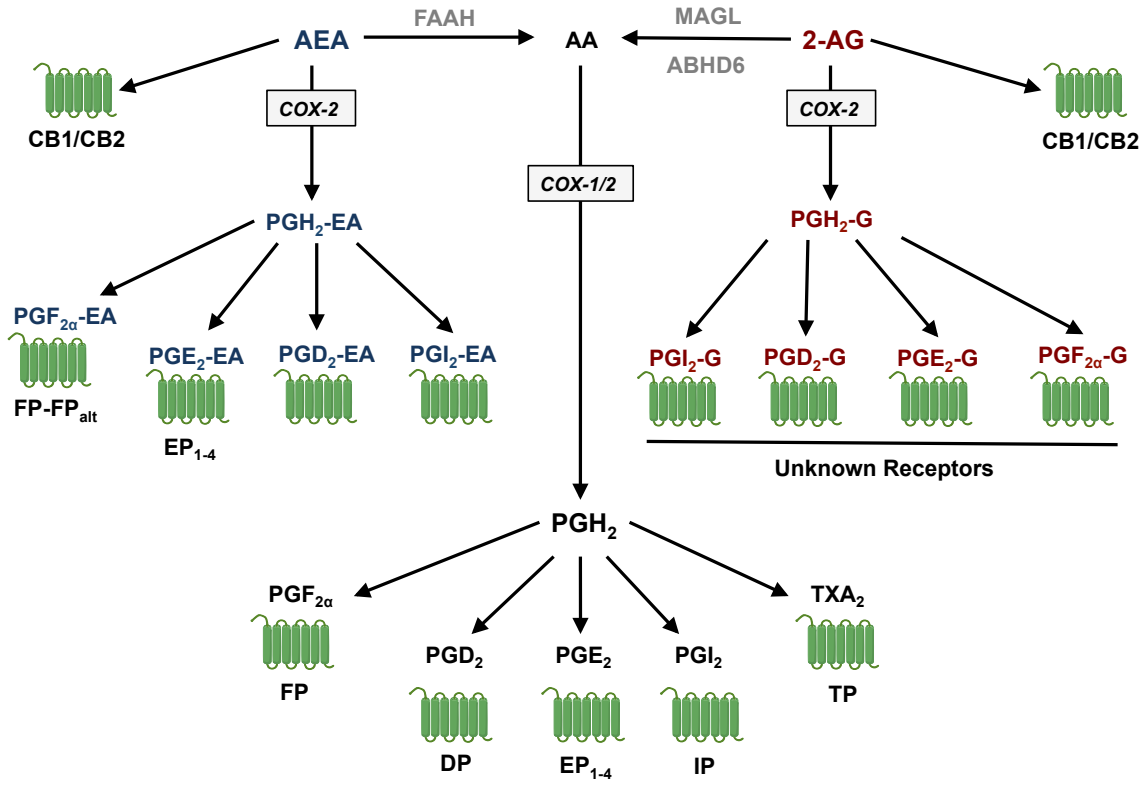

Figure 11: COX-2 at the interface of the eicosanoid and endocannabinoid systems. Enzymes responsible for 2-AG hydrolysis into AA and glycerol are mainly monoacylglycerol lipase (MAGL) and α/β hydrolase domain 6 (ABHD6). Fatty acid amide hydrolase (FAAH) hydrolyzes AEA into AA and ethanolamine. AA is metabolized by cyclooxygenases (COX-1/2) to give PGH_2, which is taken up by specific PG synthases to produce the PGs (PGD_2, PGE_2, $PGF_{2\alpha}$, PGI_2) or thromboxane synthase to from thromboxanes (TXA_2). PGs act through specific G protein-coupled receptors. During inflammation, COX-2 is upregulated leading to increased formation of PGs. Additionally, 2-AG and AEA can be metabolized by COX-2 to form PG-glycerol esters (PG-Gs) and PG-ethanolamides (PG-EAs), respectively. The molecular targets of PG-Gs and PG-EAs are not well known. However, it is known that PGE_2-EA is a ligand of the EP receptors, whereas $PGF_{2\alpha}$-EA activates a heterodimer of the FP receptor and one of its splicing variants. Abbreviations: DP, PGD_2 receptor; EP, PGE_2 receptor; FP, $PGF_{2\alpha}$ receptor; IP, PGI_2 receptor; TP, TXA_2 receptor.

Prostaglandin Glycerol Ester Hydrolytic Instability

As stated previously, PG-Gs elicit a wide array of biological responses in predominantly an *in vitro* setting. However, understanding the *in vivo* effects of these lipid metabolites has been difficult due to hydrolytic instability. Vila *et.al.* demonstrated that PGE_2-G is rapidly cleared from rat plasma post intravenous administration, with no detectable levels after 5 minutes. They attributed this instability to the presence of rat plasma esterases that hydrolyze the glycerol moiety of PG-Gs. The endocannabinoid hydrolyzing enzymes, FAAH and MAGL, were initially investigated as the responsible PG-G hydrolyzing enzymes (97). However, kinetic analysis of both enzymes showed that neither FAAH nor MAGL contributed to the hydrolysis of PG-Gs.

Further investigation let to the identification of carboxylesterase 1 (CES1) as an esterase capable of hydrolyzing PG-Gs, as well as the endocannabinoid, 2-AG (98). It was shown that CES1 was responsible for 40-50% of 2-AG hydrolysis and 80-95% of PG-G hydrolysis in THP1 human macrophages (98). Additionally, palmitoyl protein thioesterase 1 (PPT1) was identified as a PG-G hydrolyzing enzyme (99). Similar to CES1, PPT1 was able to hydrolyze both 2-AG and PG-Gs, though PPT1 was more efficient at hydrolyzing 2-AG (K_{cat}/K_m= 0.093 min^{-1} μM^{-1}) compared to PG-Gs (K_{cat}/K_m= 0.021 min^{-1} μM^{-1}). Beyond CES1 and PPT1, there is evidence to suggest the presence of other enzymes responsible for PG-G hydrolysis. These unknown enzymes will be discussed in depth later in this work.

Serine hydrolases

Overview

Serine hydrolases are one of the largest and most widely distributed enzyme classes and constitute ~1% of the proteome (100, 101). Serine hydrolases make up many of the proteases, esterases, lipases and amidises and can be organized into several distinct subfamilies based on three-dimensional structure and catalytic mechanism. The majority of serine hydrolases adopt the α/β-hydrolase fold and employ a conserved catalytic mechanism, which involves nucleophilic attack by an activated serine, which is embedded in the serine hydrolase consensus sequence, GXSXG, within the active site (101). Enhanced nucleophilicity of the serine arises from interactions in either a catalytic triad or dyad. The most common triad, present in most metabolic serine hydrolases, consists of a Ser-His-Asp triad, and allows for charge relay between the three residues. This triad will be discussed at length below. Other serine hydrolases utilize other triad combinations (Ser-Ser-Lys) or employ a dyad (Ser-Asp) (102, 103). In every case there is a basic residue, which extracts a proton from the hydroxyl of serine to increase the nucleophilicity of serine for attack of carboxylates in varies substrates, including proteins and lipids.

Ser-His-Asp Catalytic Triad

The first serine hydrolase catalytic site was discovered in the 1960s by David Blow *et. al.* upon investigation of the crystal structure of the serine protease, α-chymotrypsin (104). They observed two amino acid residues that were directly involved in the catalytic mechanism of the enzyme, serine and histidine (104). They showed that

the Ser and His residues resided close enough to form a hydrogen bond. Additionally, they observed the presence of aspartate residue hydrogen-bonded to the His in the catalytic site. The interaction of these three amino acids was dubbed the Ser-His-Asp catalytic triad (Figure 12). The importance of this catalytic triad was revealed when other protease structures, including trypsin and subtilisin, also contained this same catalytic triad. Interestingly, this catalytic triad exists in multiple hydrolase families, including proteases, esterases, and lipases, suggesting there is an independent evolutionary path for the formation of this important catalytic triad (105).

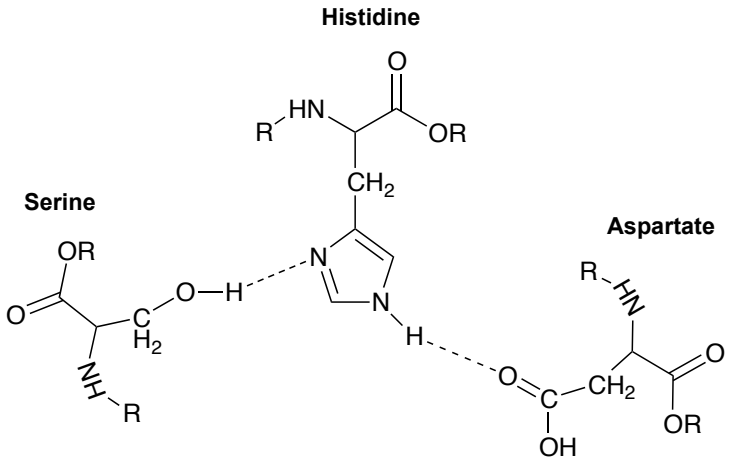

Figure 12: **The Ser-His-Asp catalytic triad**. Hydrogen bonding network between the three amino acids created the charged relay system

The components of the catalytic triad each play a specific role in generating the nucleophilic serine and completing the catalytic cycle. The orientation of His and Ser allow for hydrogen bonding between the hydroxyl of the Ser and the nitrogen of His. During hydrolysis, there is a transfer of the hydrogen from the oxygen of serine to the nitrogen of the imidazole of histidine, increasing the nucleophilicity of the serine and allowing for attack of carbon in the carbonyl of proteins and acyl-containing substrates

(e.g. 2-AG, AEA). The role of Asp in this process was originally suggested to accept hydrogen upon removal from Ser, though it was shown that proton relay from the Ser to the Asp is chemically unstable (104-106). Evidence suggests that hydrogen bonding between the Asp and His is important during catalysis, where Asp maintains orientation of the His and stabilizes the ion pairing between the negatively charged tetrahedral intermediate at Ser and the positively charged nitrogen of the His imidazole.

Interestingly, mutagenesis studies that replace the catalytic Asp with a neutral amino acid resulted in significant decreases in catalysis, supporting the role of Asp in orienting and stabilizing the His imidazole ion during catalysis (105). Additionally, the role of Ser and His during catalysis is extremely important, with any mutations of serine or histidine destroying catalytic activity (107, 108). This is not surprising because of the importance of both residues during catalysis, with the serine forming the acyl-enzyme intermediate and histidine transferring a proton from the serine to the substrate-leaving group. All these mutagenesis studies highlight the importance of each residue in the catalytic mechanism of serine hydrolases.

Catalytic Mechanism of Serine Hydrolases

Serine hydrolases all share a common catalytic mechanism, which involves nucleophilic attack of an activated serine within the active site of these enzymes (108). The enhanced nucleophilicity of the active site serine arises from the amino acid's interaction in a catalytic triad. Figure 13 shows the basic mechanism of catalysis by a lipid serine hydrolase, utilizing a Ser-His-Asp triad. Generally, nucleophilic attack by the serine hydroxyl group at the carbonyl carbon atom of a substrate is catalyzed by proton

transfer from the serine to the histidine imidazole group acting as a general base. This forms a tetrahedral intermediate of serine bound to substrate and an imidazole ion. The tetrahedral intermediate breaks down by acid catalysis to form the acyl bound serine, a basic imidazole, and the liberated alcohol or amine product (depending on substrate i.e. fatty acid or protein). The proton on the imidazole is transferred to the leaving product during this elimination. The acyl-serine is deacylated though proton extraction of water by the imidazole base, generating a newly formed imidazole ion and attack of the newly formed hydroxyl base at the carbon of the acyl group. This second tetrahedral intermediate breaks down through the same acid catalysis as before, to generate the hydroxylated substrate, and regenerate the serine and imidazole base for another round of hydrolysis (105).

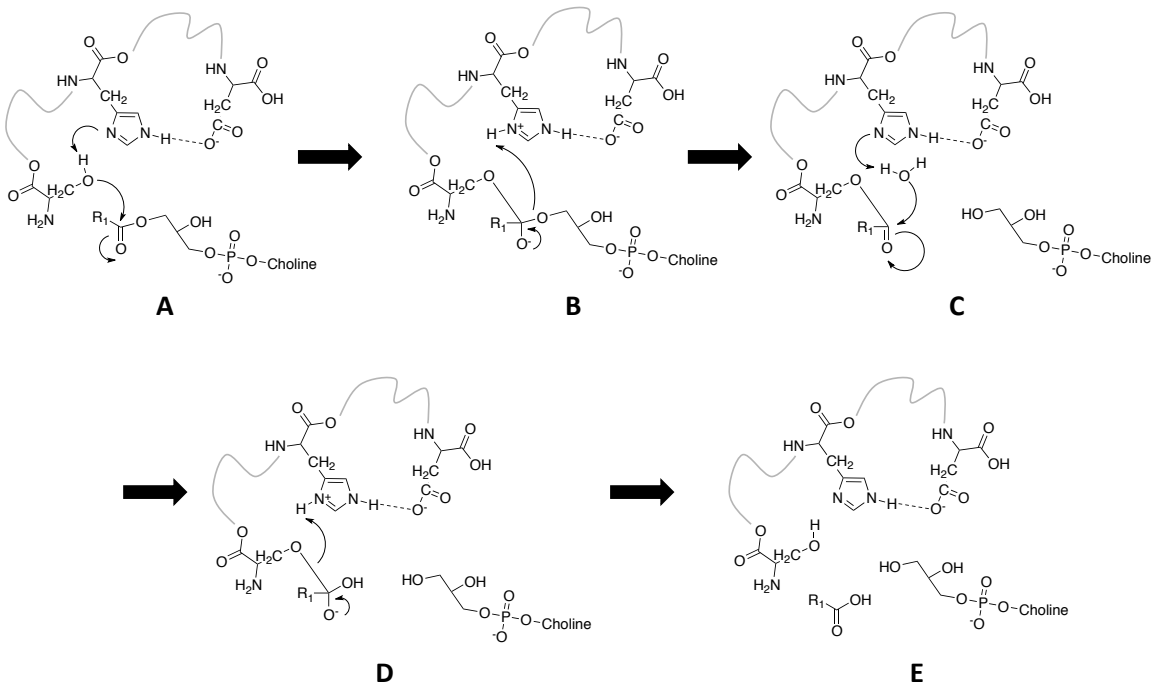

Figure 13: Catalytic Mechanism for Serine Hydrolases. (A) Nucleophilic attack by an activated serine leads to the formation of a serine tetrahedral intermediate. (B) The intermediate breaks down through acid catalysis to form the acyl serine intermediate and an alcohol product. (C) The serine is deacylated by proton extraction of water followed by nucleophilic attack of the generated hydroxyl. (D) This tetrahedral intermediate breaks down by acid catalysis to form (E) the free hydroxylated substrate and regeneration of serine and histidine.

Activity Based Protein Profiling

Serine hydrolases are an important enzyme class that are involved in numerous physiological; including inflammation, angiogenesis, hormone processing (109-111), and pathophysiological events; including cancer, emphysema and blood clotting disorders (112-114). As stated before, the class of serine hydrolases is expansive and understanding these enzymes' roles and functions in many of these pathogenic states may help in future treatments. Many of the serine hydrolases identified are completely uncharacterized with respect to their physiological functions making studying their physiological relevance difficult (114). Because all serine hydrolases utilize a similar catalytic mechanism, developing probes that can covalently interact with the activated serine of these enzymes has allowed for functional characterization, including substrate identification and physiological relevance of many of these uncharacterized proteins. Activity based protein profiling (ABPP) emerged as a technology that took advantage of the conserved catalytic mechanism of serine hydrolases (114, 115).

In general, the fundamental building blocks of ABPP are small-molecule probes that covalently label active site residues of a given enzyme class; including cysteine, serine, threonine hydrolases. The remainder of this work will focus on the serine hydrolases. Ideal probes target a large number of different enzymes within the serine hydrolase family by targeting the conserved catalytic mechanism. The serine hydrolase probes consist of electrophilic groups that modify the conserved active serine nucleophile leading to covalent tagging of the protein (115). These probes must also have a reporter tag allowing for visualization of targets. Reporter tags can range and include fluorophores, biotin and handles such as azides or alkynes with can be modified by click

chemistry [copper-catalyzed Huisgen's cycloaddition]. Unique to ABPP is the ability to assess the functional states of known and unknown enzymes within a proteome, due to the probes interaction with enzymatically active proteins only. Utilizing these probes allows for proteome wide comparisons of enzyme activity in a number of distinct biological states, e.g. healthy versus disease or untreated versus treated.

Historically, these probes were initially designed by protein chemists and enzymologists to try to understand mechanistic and structural characteristics of enzymes, and chemists utilized probes ranging from simple organic molecules to mechanism–based inhibitors. The work of Balls and Jensen in the 1950s on the stoichiometric inhibition of multiple serine proteases (trypsin, α-chymotrypsin, and cholinesterase) by the diisopropyl fluorophosphonate demonstrated irreversible inhibition by these compounds, which would become important for fluorophosphonate probe design in future ABPP work (116, 117). Additionally, in the 1970s, Tipper and Strominger proposed the β-lactam of penicillin was a structural analog of the D-ala-D-ala end of bacterial peptidoglycan and that the β-lactam covalently interacted with the catalytic serine of bacterial transpeptidases, the enzymes responsible for cell wall biosynthesis (118). Utilizing radiolabeled penicillin led to the identification of multiple binding partners for penicillin. They linked enzyme class function to biological function in determining specific enzymes involved in cell wall biosynthesis (119, 120). Much of this early work laid the foundation for later researchers to develop activity-based probes for multiple enzyme classes. In the case of serine hydrolases, many types of electrophile probes have been developed, including fluorophosphonates, aryl phosphonates, sulfonyl fluorides, and carbamates. Applications for ABPP will be discussed below.

Applications of ABPP

ABPP has been used to profile activity of serine hydrolases in a multitude of biological setting, including cancer, nervous system signaling, immune cell activities and atherosclerosis. There are a multitude of biological applications for ABPP in probing serine hydrolase activity. The first application for ABPP involves comparing proteomes to determine and identify changes in enzyme activity levels. For instance, many serine hydrolases play an important role in cancer and analysis of an array of different human cancer cells have identified numerous serine hydrolases that are specifically elevated in aggressive cancer types (121-123). For example, screens have identified increases in urokinase and tissue-type plasminogen activators, which are known to contribute to malignancy. Additionally, comparisons have identified changes in serine hydrolases previously not linked to cancer such as MAG lipase and other uncharacterized serine hydrolases (121-123). Interestingly, because ABPP monitors changed in activity and not gene expression, many of the aforementioned enzymes demonstrated changes in activity without having any changes in expression.

Changes in proteomes were monitored by fluorescence tagging of the serine hydrolases followed by SDS-PAGE fluorescence detection. Unfortunately, there are limits to the resolution of these gels, which limits the number of serine hydrolases that can be monitored in these studies. Because of this, new technologies coupling ABPP with LC-MS based platforms (termed multidimensional protein identification technology, ABPP-MudPIT) has allowed for deeper probing of the proteome (124). This has led to

the identification of hundreds of enzymes in proteomes and provides semi-quantitative information into the relative level of enzyme activities across varying proteomes.

Additionally, ABPP has been used to identify new inhibitors for serine hydrolases, including enzymes with known and unknown functions. Inhibitor identification is achieved though a process termed competitive ABPP (Figure 14).

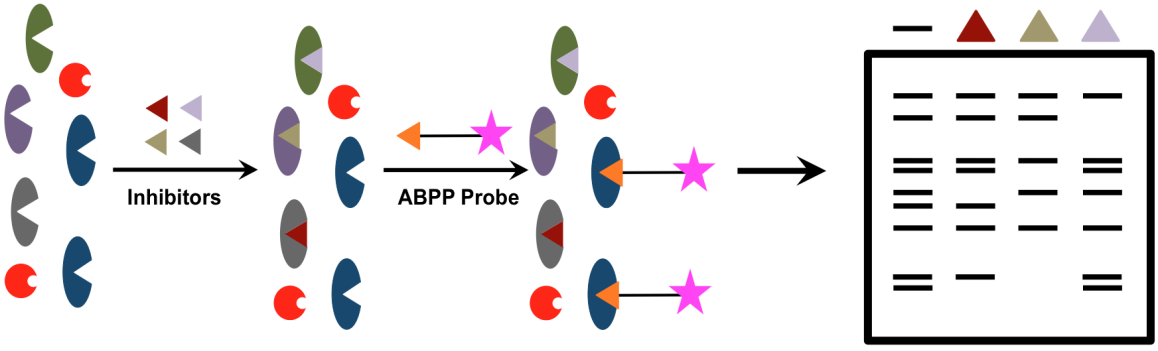

Figure 14: Competitive ABPP. Fluorescence probes allow for identification of inhibitors for multiple serine hydrolases in the proteome.

Competitive ABPP is possible because small molecules can compete against probes for binding in the active site of serine hydrolases, which causes a decrease in probe labeling. These changes in probe binding can be resolved by either gel-based methods or by LC-MS proteomic approaches (125-128). Because inhibitors are screened against entire proteomes, there is no need for purified protein for molecule screening. Additionally, since ABPP probes target a wide array of serine hydrolases, inhibitors can be developed for hydrolases with or without known substrates/function. Finally, because inhibitors are screened against an entire proteome, off-target effects of inhibitors can be assessed in one experiment and inhibitors can be developed and modified to selectively inhibit one enzyme compared to others.

This competitive ABPP was critical in developing inhibitors for a multitude of serine hydrolases, including FAAH, MAGL and lysophospholipases (125, 127, 129-131). Inhibitors have been used to confirm the role of FAAH and MAGL in endocannabinoid metabolism. Furthermore, development of lysophopholipase A1 and A2 (LYPLA1 and LYPLA2) inhibitors will allow for greater understanding of the function of these hydrolases beyond what little is know from present studies.

Dissertation Aims

The major goal of the research described herein was to determine the identity of the serine hydrolase responsible for PG-G hydrolysis in human cancer cells. Understanding the roles prostaglandin glycerol esters play in physiological and pathophysiological states in vivo has been difficult due to the hydrolytic instability of these lipids. A significant effort was made to identify the serine hydrolase responsible for PG-G hydrolysis through numerous techniques; including protein purification, ABPP proteomics, and serine hydrolase inventory and PG-G hydrolase activity comparisons. Chapter II presents a newly developed MALDI-MS method for the detection of prostaglandins and prostaglandin glycerol esters. This method facilitated speedier analysis of PG-Gs and PGs and allowed for high throughput methods for the development of COX-2 inhibitors. Chapter III details the initial steps taken to identify the PG-G hydrolase present in human breast cancer cells, MDA-MB-231. Protein purification was initially employed in combination with ABPP-driven proteomics to isolated and identify proteins with hydrolytic activity. Multiple serine hydrolases were identified and hydrolytic involvement was verified through cDNA overexpression in HEK293 cells and siRNA knockdown in MDA-MB-231 cells. Unfortunately, the approach employed in Chapter III did not yield the identity of the hydrolase. This lead to a computational analysis of all serine hydrolases inventoried across various cancer cell lines. This analysis led to the identification of lysophospholipase A2 (LYPLA2) as a serine hydrolase capable of metabolizing PG-Gs in human cancer cell lines. Chapter IV discusses the work that led to the identification and verification, through siRNA knockdown in multiple cell lines and cDNA overexpression in HEK293, which helped

solidify LYPLA2 as the hydrolase of interest. Additionally, recombinantly expressed LYPLA2 from *E.coli* was prepared. Kinetic analysis was performed on purified recombinant LYPLA2 against multiple substrates. Also, specific inhibitors for both LYPLA1 and LYPLA2 were evaluated against LYPLA2. Because LYPLA1 is closely related to LYPLA2, multiple studies were conducted to verify its involvement. Studies included, siRNA knockdown of LYPLA1 in MDA-MB-231, cDNA overexpression in HEK-293 and recombinant overexpression in *E.coli*. All studies verified that only LYPLA2 was responsible for PG-G hydrolysis. Lastly, preliminary analysis of LYPLA2 inhibition on lipid metabolism in cell culture was assessed in both RAW267.4 cells and 1483 human head and neck squamous cell carcinoma. In sum, the findings presented provide the first steps into the identification, characterization and importance of LYPLA2 in PG-G hydrolysis in both *in vitro* and in cells. Chapter V will contain a brief discussion of the implications of this research and any pressing questions that may exist.

Chapter II

HIGH-THROUGHPUT QUANTIFICATION OF BIOACTIVE LIPIDS BY MALDI MASS SPECTROMETRY: APPLICATION TO PROSTAGLANDINS

Introduction

Quantification of individual or multiple analytes in biological systems is a critical element of enzymology, metabolomics and biomonitoring. The most commonly used methods employ chromatographic separation followed by mass spectrometric analysis. Quantification is achieved by stable isotope dilution methods using isotopically labeled internal standards. These methods are highly sensitive and specific, but they require considerable time for sample preparation and chromatographic separation and utilize serial rather than parallel sample handling. Matrix-assisted laser desorption/ionization mass spectrometry (132) (MALDI MS) is a powerful analytical technique capable of parallel processing of hundreds of samples without the need for prior separation (133). MALDI MS is extremely sensitive (low attomole – femtomole sensitivity) and fast, with analysis times in large part dependent on the frequency of the irradiating laser. Solid-state lasers with repetition rates of 1 kHz allow multiple samples to be analyzed in under one second (since typically many fewer than 1000 laser shots are needed) (134). The fast analytical capability of MALDI MS is ideally suited for fast serial analysis of large numbers of samples. MALDI MS is widely used for characterization of protein samples but is not routinely employed in quantitative analyses.

We describe herein the development of a robust MALDI MS-based approach for the high-throughput analysis of an important class of bioactive lipids. Selective derivatization of ketone-containing prostaglandins (PGs) with positively charged hydrazines converted them to charged hydrazones that were readily quantified by MALDI MS. PGs are products of the cyclooxygenase (COX) pathway of arachidonic acid (AA) metabolism and PG-glycerol esters (PG-Gs) are products of oxygenation of the endocannabinoid, 2-arachidonoylglcyerol (2-AG) (Figure 1) (135).

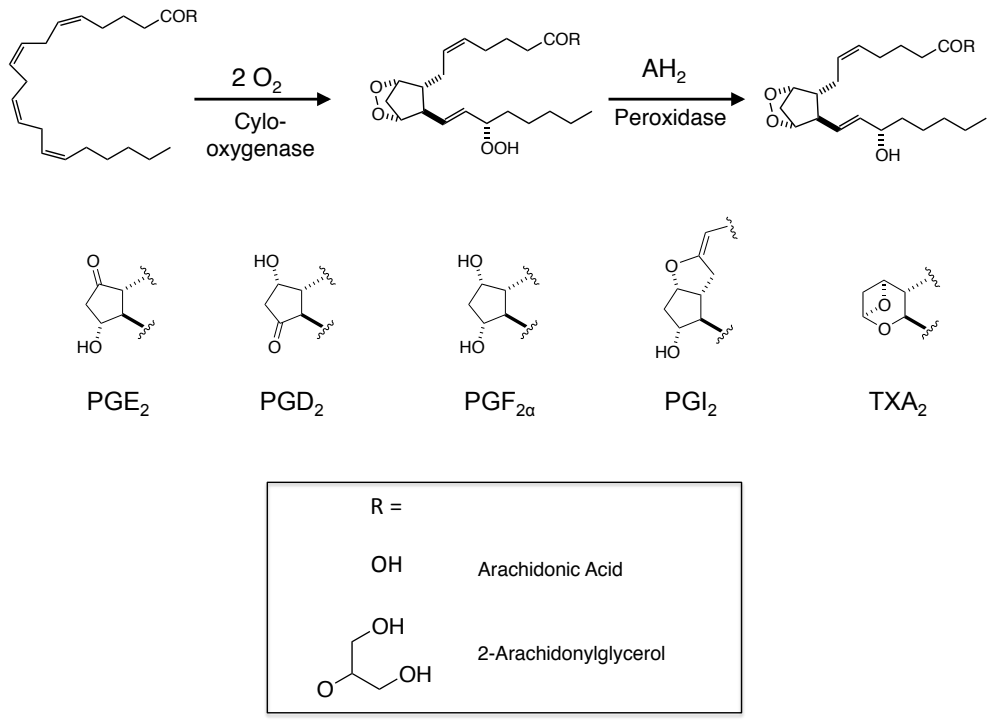

Figure 1. Conversion of AA and 2-AG to PGs and PG-Gs by COX-2. PGI_2 and TxA_2 are unstable and rapidly hydrolyze to 6-keto-$PGF_{1\alpha}$ and TxA_2, respectively.

As described, PGs and PG-Gs are potent lipid mediators that exert a broad range of biological responses through a series of membrane-bound G-protein-coupled receptors

(136). PGs have been implicated in diverse physiological and pathophysiological responses such as platelet aggregation, gastrointestinal integrity, wound healing, inflammation, hyperalgesia, and fever (137, 138). Many analytical methods have been described for their quantification based on mass spectrometry and they are widely applied in clinical and preclinical studies (139-142). All of the methods require extensive workup prior to analysis and/or time consuming HPLC separations followed by mass spectrometry. Because of the clinical importance of PG measurement, we developed a rapid high-throughput analytical method based on the derivatization of ketone-containing PGs followed by MALDI MS analysis. By using stable isotopically labeled internal standards, it was possible to develop quantitative mass spectrometric assays that displayed a large dynamic range. The assay was fully automated which enabled rapid liquid handling, high-throughput assay execution, and simultaneous deposition on a 384 well MALDI target. Multiple reaction monitoring for a particular PG and its internal standard allowed parallel quantification of samples with high sensitivity, specificity, and speed. This method should be applicable to an extraordinarily wide-range of biomolecules and to applications ranging from high-throughput enzyme assays to targeted metabolomics.

Materials and Methods

Reagents: AA was purchased from Nu-Chek Prep, Inc. (Elysian, MN, USA) Prostaglandin E_2, prostaglandin D_2, prostaglandin E_2-d4, prostaglandin E_2-1-glyceryl ester, 6-keto-prostaglandin $F_{1\alpha}$ and (*R*)-flurbiprofen ((*R*)-(-)-2-fluoro-α-methyl-4-biphenylacetic acid) were purchased from Cayman Chemicals (Ann Arbor, MI, USA). α-

Cyano-4-hydroxy-cinnamic acid (CHCA), Girard's reagent T, dimethyl sulfoxide (DMSO, Biotechnology performance certified), sulindac sulfide ((Z)-5-Fluoro-2-methyl-1-[p-(methylthio)benzylidene]indene-3-acetic acid), indomethacin (1-(4-chlorobenzoyl)-5-methoxy-2-methyl-3-indoleacetic acid) and (*S*)-flurbiprofen ((*S*)-(+)-2-fluoro-α-methyl-4-biphenylacetic acid) were purchased from Sigma-Aldrich (St. Louis, MO, USA). All organic solvents were HPLC grade. Water and ethyl acetate were purchased from Fisher Scientific (Pittsburgh, PA, USA). Acetonitrile was purchased from Acros (Morris Plains, NJ, USA). Ethanol was purchased from Pharmco-AAPER (Shelbyville, KY, USA). RAW264.7 (RAW) cells were obtained from the American Type Culture Collection (ATCC) and were maintained in Dulbecco's modified Eagle's medium (DMEM) supplemented with GlutaMax, high glucose, sodium pyruvate, and pyridoxine-HCl purchased from Gibco (Grand Island, NY, USA). Heat-inactivated fetal bovine serum (hi-FBS) was purchased from Summit Biotechnologies (Fort Collins, CO, USA). Lipopolysaccharide (LPS) was purchased from Calbiochem (San Diego, CA, USA).

Enzymes: The expression and purification of recombinant murine COX-2 (mCOX-2) from SF-9 cells was performed as previously described (143).

High-Throughput Screening Materials: Labcyte (Sunnyvale, CA, USA) 384-well flat bottom polypropylene plates were used for the stock and reaction plates. Tips for the 384-tip head of the Agilent (Santa Clara, CA, USA) Bravo used in the study were purchased from Biotix (San Diego, CA, USA).

Derivatization and Analysis of Prostaglandins: Prostaglandin standards were dissolved in a solution of 1:1-ethanol:water to a final concentration of 20 μM. Aliquots of this solution were mixed with an equivalent volume of Girard's reagent T (10 mg/mL

solution in 20% acetic acid). The mixture was allowed to react for 10 min at room temperature then added to an equivalent volume of a solution of 20 mg/mL CHCA in 60% acetonitrile in water. A one μL aliquot was spotted on a MALDI plate (5 pmol analyte on-plate) and analyzed with a Bruker UltrafleXtreme TOF/TOF MS, Bruker Autoflex Speed TOF MS (Billerica, MA, USA) or on a Thermo LTQ-XL linear ion trap equipped with a MALDI source (San Jose, CA, USA) for MS/MS analysis of derivatized prostaglandins (PGE_2 transition m/z 466.3→389.3, PGE_2-d4 m/z 470.3→393.3).

Mass Spectrometry Parameters: All mass spectra were analyzed in positive ion mode. Both the Bruker UltrafleXtreme and Autoflex Speed TOF MS instruments are equipped with a Nd:YAG (solid state) laser at 355 nm utilizing SmartBeam™ modulation. Both instruments were operated in reflector mode. The UltrafleXtreme was operated with the following settings: extraction voltage, 10 kV; delay time, 70 ns; mass range, 20-1000 m/z. The Autoflex Speed was operated with the following settings: extraction voltage, 19 kV; delay time, 40 ns; mass range, 160-1000 m/z. The LTQ-XL is equipped with a N_2 laser operating at 337 nm. MS/MS experiments for individual analytes utilized a collision energy of 50, activation Q of 0.300, activation time of 50 ms and a product ion mass range of 150-600 m/z.

COX-2 inhibitor assay: The ability of COX-2 to oxygenate AA or 2-AG was quantified by monitoring conversion to PGE_2 or PGE_2-G. A solution of COX-2 protein (200 nM) was made in 100 mM Tris/ 500 μM phenol solution, with a 2x molar equivalent of hematin, and was preincubated for 5 min at room temperature. A concentration range of inhibitors was added to aliquots of the enzyme solution and allowed to incubate at 37°C for 20 min. AA was added to this solution (50 μM) and reaction allowed to proceed for

30 sec. The solution was quenched with an equal volume of ethyl acetate (containing PGE_2-d4 internal standard), the organic layer was collected and placed in a clean glass tube, then dried down under nitrogen. Samples were reconstituted in 1:1-ethanol:water and derivatized with an equivalent volume of Girard's reagent T (10 mg/mL solution in 20% acetic acid) and analyzed by MALDI as described above. All inhibitor concentrations for 50% enzyme activity (IC_{50}) were calculated by nonlinear regression analysis using GraphPad Prism software.

High-Throughput Analysis: Modifications to the COX-2 inhibitor assay were made to adapt the standard assay to a high-throughput format. Two 384-well stock plates were prepared with AA and inhibitors in DMSO. Using a Labcyte Echo® Liquid Handling system, 50 nL of inhibitor was dispensed into a waiting 384-well reaction plate (DMSO was dispensed for no inhibitor control). Each inhibitor concentration was tested in quadruplicate. A solution of COX-2 (50 μL), containing 200 nM enzyme with appropriate cofactors as described above, was added to the reaction plate and allowed to incubate at 37°C for 20 min. Using the Echo® system again, 750 nL of AA was added to another 384-well plate and placed on an Agilent BRAVO 384-well liquid handler. To the waiting 750 nL of AA, 29.25 μL of the inhibitor/enzyme solution was added; samples were mixed using the BRAVO and allowed to react for 30 sec. Thirty μL of the reaction solution was aspirated and dispensed into a pre-dispensed 30 μL of quench solution (Girard's reagent T in 20% acetic acid in ethanol solution with PGE_2-d4 internal standard). These samples were allowed to react as described above. Ten μL of the derivatized solutions was added to 10 μL of a 20 mg/mL solution of CHCA and 1 μL of

the final solution was spotted on a MALDI plate using the BRAVO. All samples were analyzed using the Thermo LTQ ion trap mass spectrometer as described above (Chart 1).

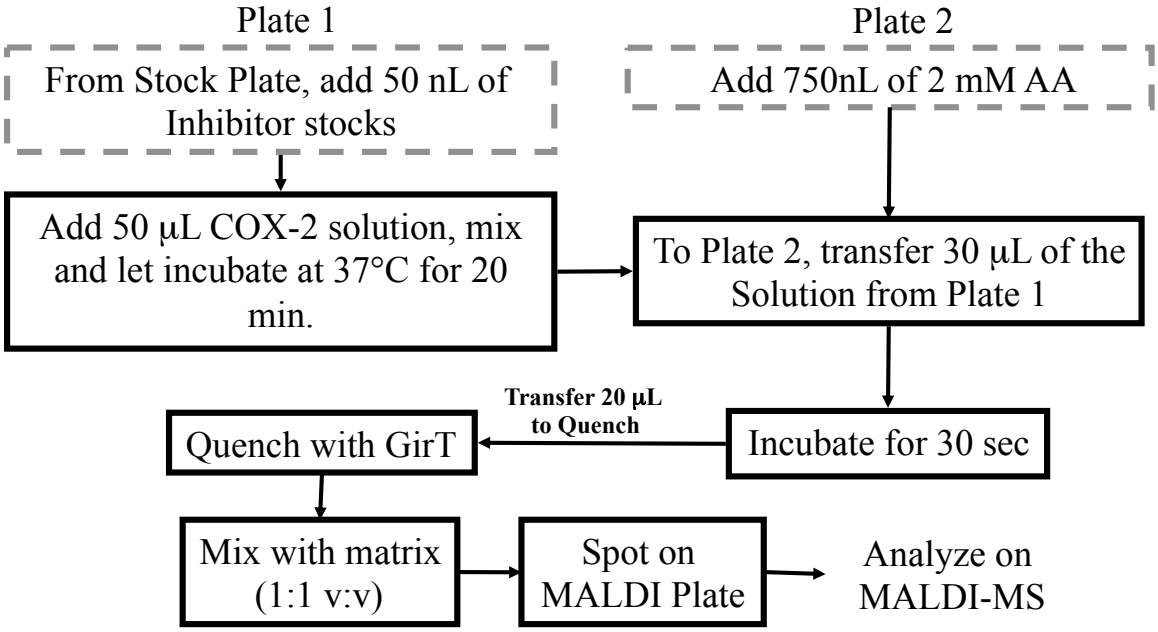

Chart 1. Flow chart representing the protocol used for the high throughput analysis. Liquid handling with the Bravo is represented in black boxes (—) whereas liquid handling with the Echo is indicated in grey, dashed boxes (- - -).

Activated Macrophage Eicosanoid Analysis: RAW cells were plated at 1.5 x 10^6 cells in a 30 mm dish in DMEM with 10% hi-FBS and 20 ng/mL of GM-CSF and allowed to incubate overnight. After the overnight incubation, the medium was removed and fresh DMEM with 10% hi-FBS was added. One set of cells was treated with only medium, the other set was treated with medium containing LPS (200 ng/mL) and IFNγ (20 U/mL) for 6 hr followed by addition of AA (20 μM). After 6 hr incubation, the medium was collected. A 2:1-ethyl acetate:0.1% acetic acid solution was added to the collected medium. Samples were vortexed, centrifuged (1000 x G for 5 min) and the organic layer was collected in clean glass tubes and dried down under nitrogen. Samples were reconstituted in ethanol, derivatized as described above and analyzed using the Bruker Autoflex Speed TOF-MS.

Results

Method Development and Validation

The ability to directly analyze prostaglandins using standard MALDI protocols and a number of different matrices in either positive or negative mode was assessed. Figure 2a shows the mass spectrum for 3 PGs and a PG-G. All spectra were dominated by peaks from the matrix (CHCA). It was determined that a charged moiety could be added to the analytes in order to improve detection by pre-ionizing the compounds. Girard's T reagent reacts with ketones to give hydrazone derivatives bearing charged moieties (144). Equation 1 displays the chemical reaction between PGE_2 and Girard's T reagent.

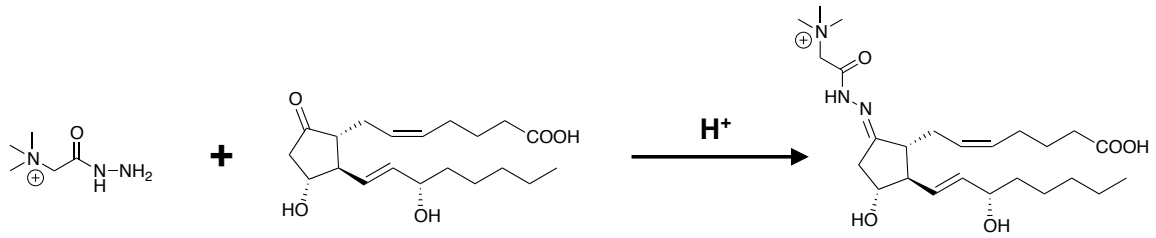

Equation 1: Derivatization of PGE_2 by Girard's T

Figure 2b represents the mass spectra obtained from the same prostaglandins derivatized with the Girard's T reagent. The mass spectra are dominated by the expected masses of the derivatized prostaglandins (PGE_2 m/z = 466.3, PGD_2 m/z = 466.3, PGE_2-G m/z = 540.3 and 6-keto-$PGF_{1\alpha}$ m/z = 484.3) and have a much higher signal to noise then their underivatized counterparts (Fig. 2a). Ions were observed at m/z = 448 in both PGE_2 and PGD_2 spectra corresponding to dehydration products likely formed by the acidic Girard's reagent T. A matrix ion was observed at m/z = 455.

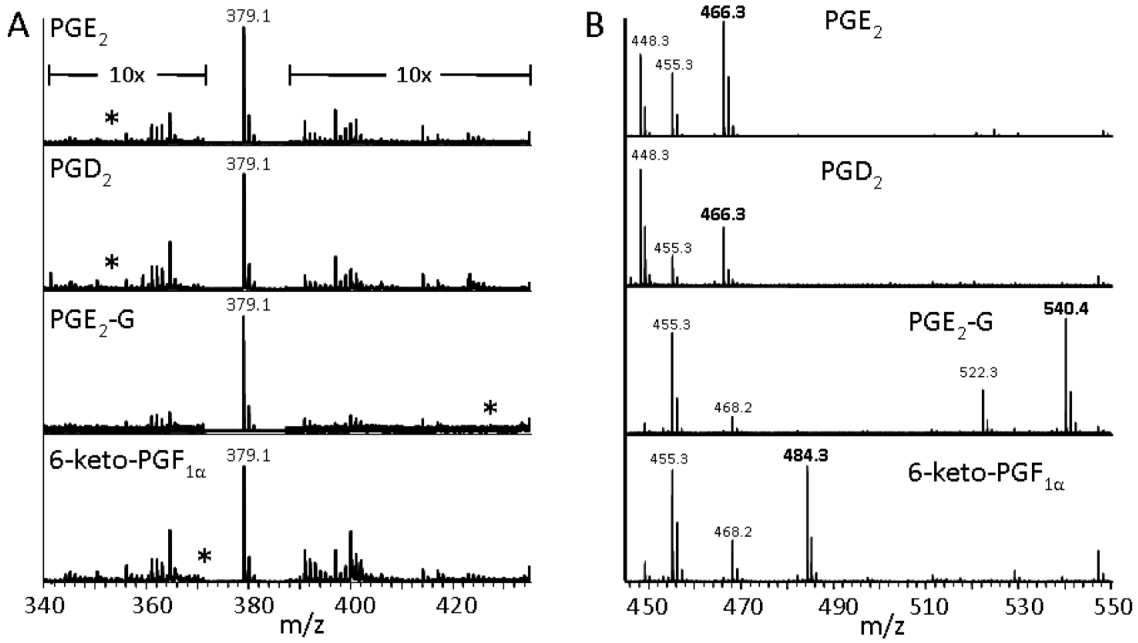

Figure 2. MALDI mass spectra of PGE_2, PGD_2, PGE_2-G, and 6-keto-$PGF_{1\alpha}$ before (A) and after (B) derivatization with Girard's T reagent. All mass spectra were obtained with CHCA matrix in the positive ion mode. The spectra in (A) are dominated by a protonated CHCA-dimer signal at m/z 379.1. The area surrounding this signal was increased 10x for all four spectra. The expected $[M+H]^+$ ions are indicated with asterisks in (A) at m/z 353.2, 353.2, 427.3, and 371.2 for PGE_2, PGD_2, PGE_2-G, and 6-keto-$PGF_{1\alpha}$, respectively. The expected Girard's T products are shown in (B) at m/z 466.3, 466.3, 540.4, and 484.3, respectively.

To assess linearity, the lower limit of detection, and the potential for signal interference, an 8-point concentration curve of PGE_2 and PGE_2 mixed with PGE_2-G (PGE_2-d4 was added as internal standard) was constructed in triplicate from 15 fmol on-plate to 2000 fmol on-plate. Quantification of PGE_2 and PGE_2-G was based on the MS^2 transitions: m/z 466.3→389.3 for PGE_2 and m/z 540.3→463.3 for PGE_2-G (Supplemental Figure 1). Figure 4 displays the concentration-response curves for PGE_2 alone and PGE_2 in solution with PGE_2-G.

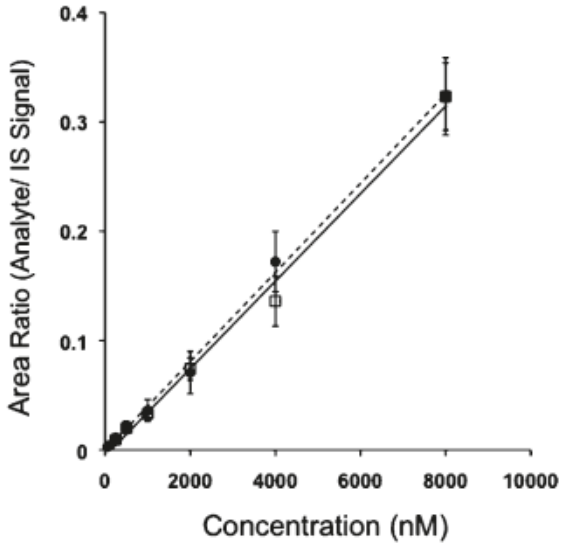

Figure 3. **Representation of standard curves for both PGE_2 in solution alone (●) and PGE_2 in solution with PGE_2-G (□).** The equations representing the depicted regression lines for PGE_2 alone was y = 4e-5x - 0.0008 and PGE_2 mixed with PGE_2-G was y = 4e-5x - 0.005 . The regression lines for either analyte did not differ significantly from unity (r^2=0.99).

The regression of the lines for PGE_2 alone and PGE_2 mixed with PGE_2-G are similar and neither slope differs significantly from unity (r^2=0.99). No signal interference was observed between the two curves demonstrating that neither prostaglandin affected

the analysis of the other on-plate. This signal response and sensitivity is comparable to that obtained from LC-MS/MS (data not shown).

COX-2 Inhibitor Assay: ^{14}C-TLC or Oxygen Consumption vs. MALDI MS/MS

Analysis of COX activity and inhibition is routinely assessed by monitoring AA metabolism, prostaglandin formation or oxygen consumption utilizing either a ^{14}C-thin layer chromatography (TLC) method or a polarographic electrode to monitor oxygen consumption (145, 146). Though both methods give accurate assessments for the analysis of COX activity, each has disadvantages. MALDI MS/MS analysis has the ability to analyze COX activity by using non-radioactively labeled material and has much faster analysis time compared to either ^{14}C-TLC or oxygen electrode-based analysis. In addition, the large dynamic range of the MALDI detection method enables the use of a wide range of enzyme, substrate, and inhibitor concentrations.

MALDI MS analysis was used to determine the IC_{50} value for inhibition of COX-2 by the known non-selective inhibitor, indomethacin. The results were compared with the IC_{50} values obtained from either ^{14}C-TLC or oxygen electrode assays. Figure 5 displays the IC_{50} curves obtained from MALDI MS analysis for indomethacin. The IC_{50} value for indomethacin obtained from the ^{14}C-TLC method was 210 nM (147) which is comparable to the IC_{50} of 200 nM obtained from MALDI MS/MS analysis. The IC50 value obtained using an oxygen consumption assay was 900 nM (148) (Figure 5).

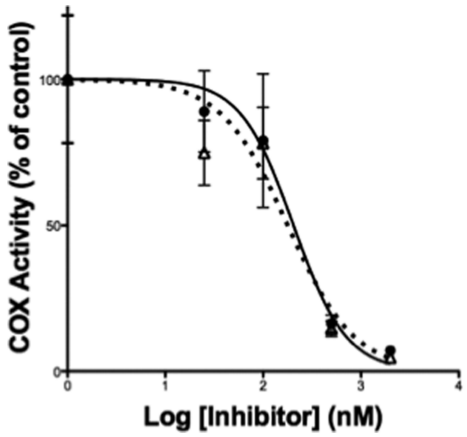

Figure 4. IC_{50} values for COX-2 inhibitor, indomethacin, determined by MALDI MS/MS; validation of Girard's reagent T as quench. The IC_{50} value of indomethacin inhibition of COX-2 was determined using either ethyl acetate as a quench (●) followed by Girard's T reagent or direct addition of Girard's reagent T in 20% acetic acid in ethanol as a quench (Δ),with similar IC_{50} values of 200 nM and 180 nM, respectively.

The oxygen electrode used for oxygen uptake method is relatively insensitive, which requires higher enzymes and substrate concentrations, which may account for the higher IC_{50} determined by this method. It is clear that by using MALDI MS analysis it is possible to obtain comparable results to either the ^{14}C-TLC or the oxygen uptake methods in dramatically shortened times.

COX-2 Inhibitor Assay - High Throughput Screening (HTS) Method Development

The rapidity of analysis by MALDI MS/MS makes it attractive to combine it with high-throughput liquid handling. We proceeded to develop a high-throughput assay for the analysis of inhibitors against either isoform of COX by analysis of PGE_2 formation. This was accomplished through a combination of ultra-low volume acoustic liquid

handling using a Labcyte Echo to produce the test compound plates and a Bravo liquid handler controlled by VWorks (Agilent, Santa Clara, CA, USA) using a 384-tip pipetting head. The highly accurate and rapid pipetting and mixing with the Bravo together with the precise timing of assay steps afforded by using VWorks allowed facile, rapid, and reproducible execution of 384 parallel enzyme reactions, derivatizations and spotting operations. We found that reactions could be quenched with Girard's T reagent, which eliminated the liquid-liquid extraction and sample evaporation steps. Figure 5 presents a comparison of the concentration-dependent inhibition curves obtained with indomethacin using ethyl acetate quench or direct addition of Girard's T as a quench. Both methods gave comparable results so it was determined that a high-throughput assay could be developed without the need for a liquid-liquid extraction.

Once the method was developed, we validated the assay by assessing the IC_{50} values obtained from four known COX-2 inhibitors. Figure 6A displays the results obtained from the analysis of the inhibition of COX-2 to metabolize AA by indomethacin and sulindac sulfide. The measured IC_{50} values (indomethacin IC_{50} = 65 nM, sulindac sulfide IC_{50} = 290 nM) are comparable to previously reported values, although there is some difference between the value of 65 nM for indomethacin and the value of 200 nM measured with manual pipetting and sample handling. In addition to potent COX-2 inhibitors, the ability to distinguish an inhibitor from a non-inhibitor was determined by assessing COX-2 inhibition by stereoisomers flurbiprofen. Figure 6B displays the results obtained from the analysis of inhibition of COX-2 to metabolize AA by (*S*)-flurbiporfen and (*R*)-flurbiporfen. The measured IC_{50} values ((*S*)-flurbiprofen, IC_{50} = 120 nM; and (*R*)-flurbiprofen, no inhibition) were comparable to previously reported values (147-149).

The HTS method is capable of assessing COX-2 inhibition of a number of different known COX-2 inhibitors as well as distinguish between compounds that do and do not inhibit COX-2.

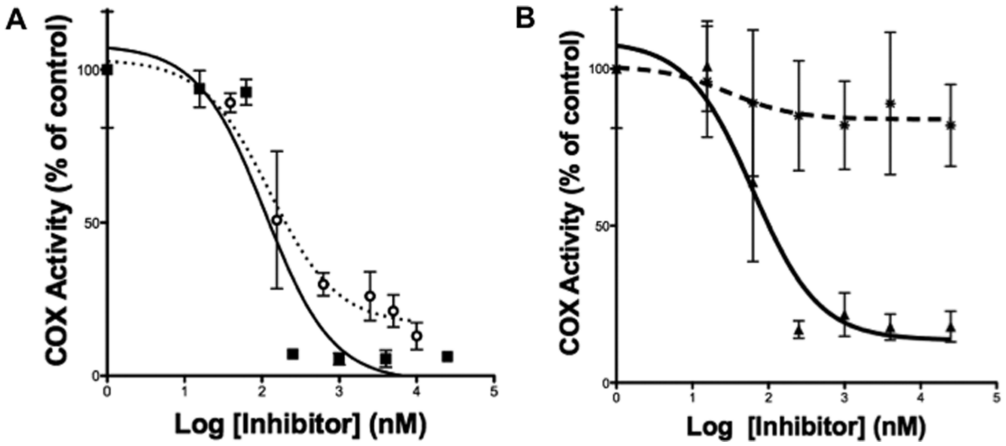

Figure 5. **IC_{50} values determined for COX-2 inhibitors using the high throughput assay**. (A) COX-2 inhibitors indomethacin (■) and sulindac sulfide(O) were assessed against COX-2 metabolism of AA. IC_{50} values determined were 65 nM and 290 nM, respectively. (B) Sterioisomers R-flurbiprofen (✱) and S- flurbiprofen (▲) were assessed against COX-2 metabolism of AA. IC_{50} values determined were no inhibition and 120 nM, respectively.

MALDI TOF analysis of Activated Macrophages

Analysis of AA metabolism in cultured cells has been performed mainly by LC-MS analysis (150). These methods have demonstrated the formation of a number of different prostaglandins, including PGE_2/D_2 and 15-keto-13,14-dihydro-PGE_2. Previous work also has shown that RAW cells treated with LPS/INF-γ have increased levels of COX-2, and addition of AA leads to increased production of PGD_2 (151). To assess whether this derivatization method could be applied to the analysis of cellular metabolism of AA, RAW cells were treated as described in *Materials and Methods*. Medium from

these cells was extracted and analyzed on a MALDI TOF MS. Figure 7 is a comparison between blank CHCA, Girard's T reagent only, untreated RAW cells and RAW cells treated with AA. When cells were treated with AA, increased levels of PGD_2 (m/z = 466.3) were detected which were similar to previous studies of LPS/INF-γ treated RAW cells (151). As seen from previous work in our lab, activation of RAW cells with LPS treatment stimulated the production of PGD2 compared to untreated samples (151). The utilization of the MALDI MS method allows us to quantify prostaglandins at levels similar to those quantified by LC-MS/MS analysis.

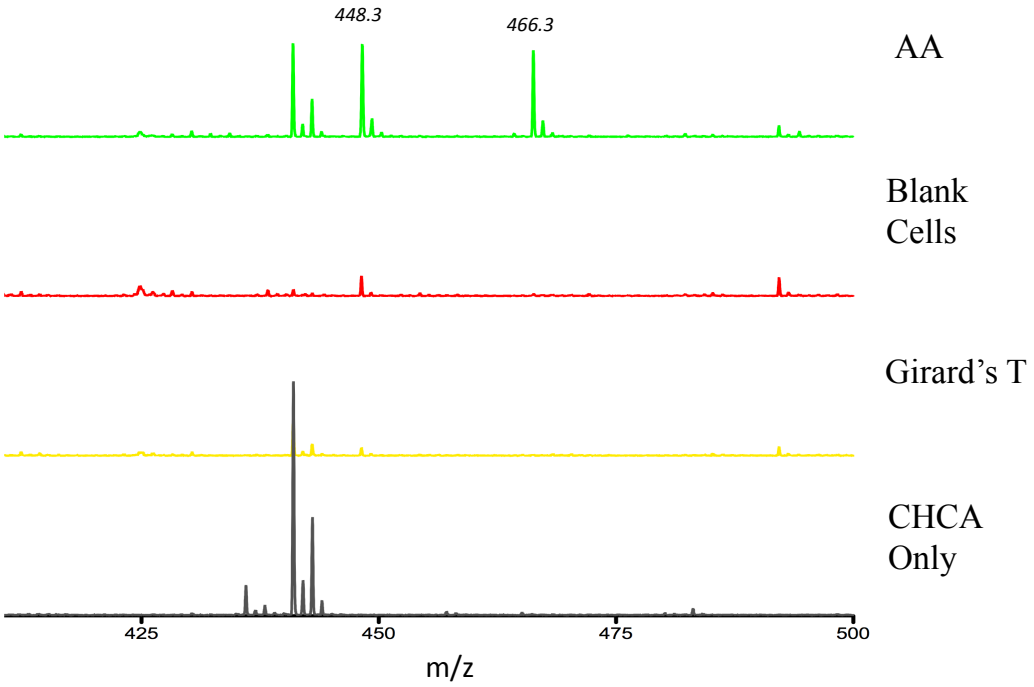

Figure 7. MALDI MS of media extracted from LPS-activated RAW cells. Cells dosed with AA (AA) showed increases in the formation of PGD_2 (m/z = 466.3)

Discussion

We have successfully analyzed ketone-containing prostaglandins after derivatization with Girard's T reagent by MALDI MS. We assessed the suitability of using MALDI to detect the production of prostaglandins in an endpoint assay for COX-2 inhibition. Initially MALDI MS was used as the analytical tool to detect derivatized prostaglandins, however we wanted to assess its suitability for high-throughput analyses. We determined that Girard's T reagent solution could be added as the quench for the assay, making it suitable for the automated process. We utilized state-of-the art liquid handling robotics to assay the biological activity of COX-2 in the presence of several inhibitors. The entire process was automated from substrate aliquoting, enzyme addition, reaction quenching, matrix mixing, and application to a 384-well MALDI plate and automated MS analysis. Three hundred eighty-four independent biochemical assays can be completed from initial incubation to final analysis in approximately 6 hr. This is a drastic improvement in time and number of samples analyzed compared to other analytical techniques.

Additionally, we wanted to assess the capability of this newly developed MALDI method to analyze more complex cellular samples. We showed that we are able to obtain comparable results to LC-MS, again in a fraction of the time. This was demonstrated from the analysis of extracted media from activated macrophages where we found increased production of PG's in AA-treated RAW cells compared to untreated cells. Individual data points were acquired in less than a second using no more than 1 uL of samples compared to ~15 min for a complete LC separation (142).

In the quarter of a century since MALDI was first described, it has been one of the prime technologies that has revolutionized the analysis of biological samples, especially the study of peptides and proteins. As the speed and resolution of mass spectrometry technology has advanced, it now holds great potential for high-throughput analysis. This report has demonstrated the efficacy of MALDI MS for the high-throughput, sensitive, and quantitative analysis of prostaglandins in complex samples including whole cells. This technology has wide application in many areas of biological and chemical analysis.

Supplemental Information

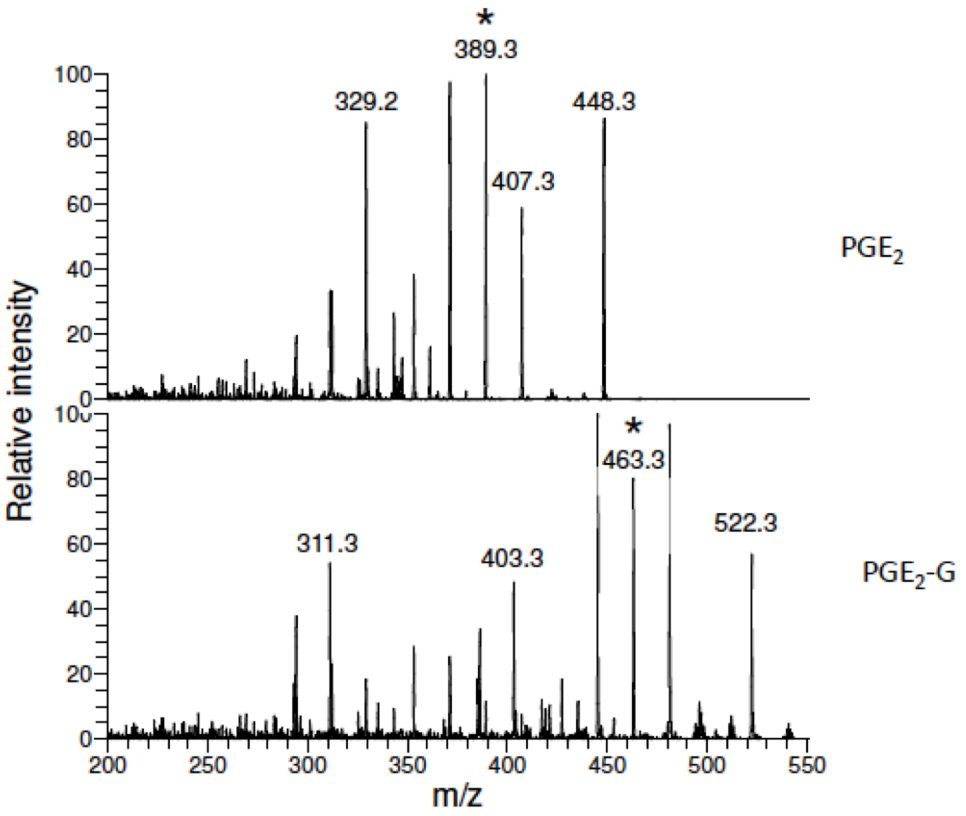

Supplemental Figure 1. MALDI MS/MS for PGE_2 and PGE_2-G. Derivatized PGE2 and PGE2-G ions were subjected to collisionally activated dissociation in a linear ion trap in order to determine the optimal transitions for SRM analysis. The fragments chosen for MS^2 of PGE_2 and PGE_2-G were m/z = 389.3 and 463.3 (indicated by ✶), respectively. These signals were chosen because they were unique and gave the largest intensity which allowed for accurate quantification and good sensitivity. Full scan and MS^2 spectra for PGE_2-d4 were also acquired (data not shown) and showed similar intensity and fragmentation as PGE_2.

Chapter III

IDENTIFICATION OF A PROSTAGLANDIN GLYCEROL ESTER HYDROLASE IN MDA-MB-231 CANCER CELLS BY PROTEIN PURIFICATION

Introduction

A growing field of interest in lipid metabolism has focused on the role of a group of oxidation products formed by cyclooxygenase 2. These metabolites are formed from the oxidation of endocannabinoids, 2-arachidonoylglycerol (2-AG) and N-arachidonylethanolamine (AEA), to form the prostaglandin derivatives, namely prostaglandin glycerol esters (PG-Gs) and ethanolamine (PG-EAs). Investigation into the physiological effects of these lipids began with insights into the effects the synthetic $PGF_{2\alpha}$-EA analog, bimatoprost, elicited during treatment of ocular hypertension (88). Bimatoprost and $PGF_{2\alpha}$-EA exerted the same effect on intraocular pressure as $PGF_{2\alpha}$, but through action on the heterodimer of the FP receptor, comprised of a wild type FP receptor and a splice variant of the FP receptor with a shortened C-terminus (88). PG-Gs also exert an array of physiological responses. PGE_2-G caused an increase in Ca^{2+} mobilization, which was independent of any known prostaglandin receptor activation and dependent on the synthesis of IP_3 and diacylglycerol. Ca^{2+} mobilization and diacylglycerol synthesis led to the activation of PKC and an increase in ERK phosphorylation. (82, 86). Additionally, PGE_2-G can induce hyperalgesia and modulate NF-κB activation (85), as well as induce pro-inflammatory and neurotoxic effects (93).

Interestingly, PGD_2-G and its metabolite 15-deoxy-$\Delta^{12,14}$ prostaglandin J_2-glycerol ester exert anti-inflammatory effects (94, 95).

Though PG-Gs can elicit a wide array of biological responses in an *in vitro* setting, understanding *in vivo* effects of these lipid metabolites has been difficult due to hydrolytic instability. Vila *et. al.* showed that PGE_2-G is rapidly hydrolyzed in rat plasma post intravenous administration, with no detectable levels after 5 minutes. They attributed this instability to the presence of plasma esterases that hydrolyze PG-Gs. Initially, endocannabinoid hydrolyzing enzymes, fatty acid amide hydrolase (FAAH) and monoacylglycerol lipase (MAGL), were examined as potential PG-G hydrolyzing enzymes (97). However, kinetic analysis showed that PG-Gs were very poor substrates for hydrolysis by these enzymes. Furthermore, use of the organophosphate pesticides lead to the identification of carboxylesterase 1 (CES1) and palmitoyl protein thioesterase 1 (PPT1) as esterases capable of hydrolyzing both 2-AG and PG-Gs (98). Beyond CES1 and PPT1, there is evidence to suggest the existence of other enzymes responsible for PG-G hydrolysis.

Utilizing protein purification techniques coupled with mass spectrometric analysis, we ventured to identify the enzyme responsible for PG-G hydrolysis in MDA-MB-231 cancer cells. These cancer cells were chosen for a multitude of reasons; they do not express CES1, PPT1 or MAGL, they are easy to maintain, and they exhibit significant PGE_2-G hydrolytic activity. Multiple purification techniques led to the identification of three enzymes by proteomics as potential PG-G hydrolase targets; namely 6-phosphoglucolactonase (PGLS), dimethylarginine dimethylaminohydrolase 2 (DDAH2), and platelet activating factor acetylhydrolase 1β3 subunit (PAFAH1β3).

Unfortunately, further validation did not support the involvement of these proteins in hydrolysis. Here we present the purification scheme utilized and the results obtained from purification, proteomics and validation of identified enzymes through gene silencing and protein overexpression.

Materials and Methods

Cells and Reagents. Prostaglandin glycerol esters (PGE_2-1 glycerol ester), deuterated prostaglandins and prostaglandin glycerol esters (PGE_2-d_4 and PGE_2-G-d_5) were purchased from Cayman Chemicals (Ann Arbor, MI). LC-MS solvents were purchased from Fisher Scientific (Chicago, Il). DharmaFECT 1 was purchased from Thermo Scientific (Pittsburgh, PA). Human breast cancer adenocarcinoma cell lines; MDA-MB-231, and human embryonic kidney cells; HEK293 were from American Type Culture Collection (ATCC, Manassas, VA). Recombinant cDNA and Turbofect were purchased from OriGene Technologies (Rockville, MD). FBS was purchased from Atlas Biologicals (Fort Collins, CO).

Culture Conditions. MDA-MB-231 and HEK293 were maintained as adherent cultures in RPMI (Gibco) media supplemented with 10% (v/v) fetal bovine serum (FBS, Atlas) at 37°C and 5% CO_2.

Serine Hydrolase Inhibition. The general serine hydrolase probe, methoxy fluorophosphonate coupled to tetramethylrhodamine (FP-TAMRA, purchased from Thermo), was used to determine the involvement of serine hydrolases in the metabolism of prostaglandin glycerol esters. FP-TAMRA (100 nM) or DMSO was added to 100 uL of MDA-MB-231 cytosol and allowed to incubate for 30 mins at 37°C. Samples were

treated as mentioned in *Prostaglandin Glycerol Ester Hydrolase Assay,* with the following changes. Samples were allowed to incubate from 0 to 60 mins to obtain a full hydrolysis time course.

Protein Purification of PGE_2-G Hydrolase(s): All steps were carried out at 4°C. All chromatographic steps were carried out using an AKTA FPLC protein purification system. All buffers were made the day prior to use and cooled to 4°C. All columns were from GE Healthcare.

(A) *Cytosolic Preparation*. Ten grams of MDA-MB-231 cells (GenScript) was taken and resuspended in 25 mM Tris (pH 7.4) supplemented with 0.5 mM of EDTA and DTT, no protease inhibitors could be used because many of these inhibitors inhibit PG-G hydrolysis. Cells were lysed by sonication (Virsonic Cell Disrupter model 16-850, 10 x 10 sec pulses at relative output of 0.5, on ice). Cell lysates were taken and cytosolic fractions were isolated by centrifugation (100,000 x g for 1 h).

(B) *Strong Cation Exchange*. Cytosol was passed over a HiTrap SP FF cation exchange column (5 mL column), preequilibrated with 200 mM phosphate buffer (pH 6) with 0.1 mM DTT and EDTA, flow rate 1mL/min; all flowthrough was collected. Utilizing a strong cation exchange column allowed for the removal of unwanted proteases.

(C) *Strong Anion Exchange - High Q*. Flow through was dialyzed overnight (2000 molecular weight cut off (MWCO) dialysis cassette, Thermo) against 20 mM Tris (pH 7.4) with 0.2 mM EDTA and 0.1 mM DTT (Q Buffer A). Sample was loaded onto a HiTrap Q FF anion exchange column (20 mL) preequilibrated with Q Buffer A. Column was washed with 4 column volumes of Q Buffer A and eluted with a linear gradient of 0-

100% elution buffer (20mM Tris (pH 7.4) with 500 mM NaCl, 0.1 mM EDTA and DTT, Q Buffer B). Fractions were tested for hydrolytic activity using the method mentioned in *Prostaglandin Glycerol Ester Hydrolysis* section below.

(D) *Size Exclusion*. Active fractions were pooled and concentrated to 3 mL using a 3000 MW cutoff centrifugal filter unit (Millipore). Sample was applied to a 120 mL size exclusion column packed with Sephacryl S-200 resin preequilibrated with 20 mM *bis*-Tris HCl (pH 7.1) supplemented with 0.1mM EDTA and DTT and fractions were collected and tested for hydrolytic activity.

(E) *Mono-P*. Active fractions were pooled and applied to a 4 mL MonoP column prequilibrated with 20mM Bis-Tris HCl (pH 7.1) supplemented with 0.1 mM EDTA and DTT. Proteins were eluted using a linear gradient from 0-100% of Polybuffer 74 (GE Healthcare) diluted in ultrapure water and pH adjusted to pH 4 using iminodiacetic acid. Fractions were collected and tested for hydrolytic activity.

(F) *Mono-Q*. Active fractions were pooled and dialyzed overnight against Q Buffer A. Samples were applied to a Mono-Q anion exchange column preequilibrated with Q Buffer A. Proteins were eluted using a linear gradient from 0-100% Q Buffer B. Eluted protein fractions were collected and tested for hydrolytic activity. Active fractions were pooled and taken for ABPP and proteomic analysis.

(G) *Polyacrylamide Gel Electrophoresis*. SDS-polyacrylamide gels (4-20% gradient gel) were run under reducing conditions and stained with colloidal Coomassie blue.

Competitive Activity Based Protein Profiling (ABPP). Figure 1 represents the scheme for competitive ABPP. Generally, samples from the final step of purification were taken and competitive activity based protein profiling was conducted.

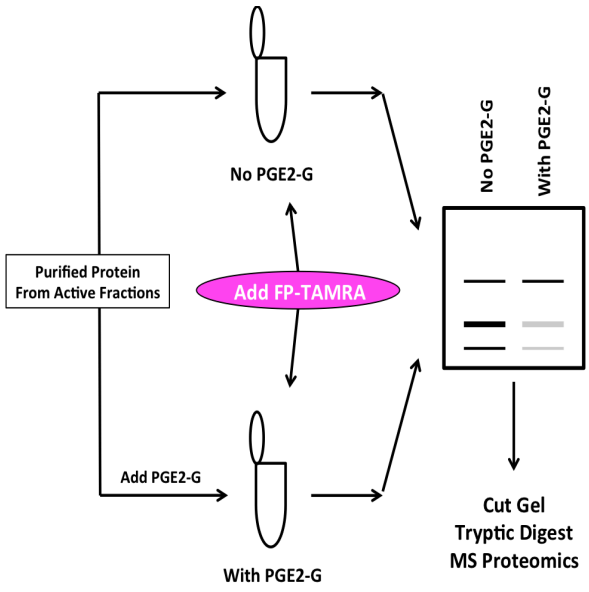

Figure 1: Scheme of Competitive ABPP

Aliquots were treated with either DMSO or 20 mM of PGE_2-G and allowed to interact for 5 minutes at room temperature. This ensures PGE_2-G binding into the catalytic pocket of the serine hydrolase of interest. 100 µM of fluorophosphonate (FP) bound to a tetramethylrhodamine (TAMRA), was added to each sample and allowed to incubate for an additional 30 mins. FP-TAMRA binds to the catalytically active serine in serine hydrolases. Adding an equal volume of Laemmli blue with SDS and boiling quenched binding. Denatured samples were run on a SDS-PAGE gel as mentioned above and FP-TAMRA bound proteins were visualized using a BioRad imager. Samples that showed decreased FP-TAMRA tagging in the presence of excess PGE_2-G were excised for tryptic digestion and proteomics.

*Proteomic Preparation and Analysis***.** Protein fractions were resolved by 4-20% SDS-PAGE, the gel was stained with colloidal Coomassie, and bands of interest were excised

from the gel and cut into $1mm^3$ pieces. The gel pieces were treated with 45 mM DTT for 45 minutes, and available Cys residues were carbamidomethylated with 100 mM iodoacetamide for 45 min. After destaining the gel pieces with 50% MeCN in 25 mM ammonium bicarbonate, proteins were digested with trypsin (10ng/uL) in 25 mM ammonium bicarbonate overnight at 37°C. Peptides were extracted by gel dehydration (60% MeCN, 0.1% TFA), the extract was dried by speed vac centrifugation, and peptides were reconstituted in 0.1% formic acid. The peptide extracts were then loaded onto a capillary reverse phase analytical column (360 μm O.D. x 100 μm I.D.) using an Eksigent NanoLC Ultra HPLC and autosampler. The analytical column was packed with 20 cm of C18 reverse phase material (Jupiter, 3 μm beads, 300Å, Phenomenox), directly into a laser-pulled emitter tip. Peptides were gradient-eluted at a flow rate of 500 nL/min, and the mobile phase solvents consisted of 0.1% formic acid, 99.9% water (solvent A) and 0.1% formic acid, 99.9% acetonitrile (solvent B). A 90-minute gradient was performed, consisting of the following: 0-10 min, 2% B; 10-50 min, 2-40% B; 50-60 min, 40-90% B; 60-65 min, 95% B; 65-70 min 95-2% B; 70-90 min, 2% B. Eluted peptides were mass analyzed on an LTQ Orbitrap XL mass spectrometer (Thermo Scientific), equipped with a nanoelectrospray ionization source. The instrument was operated using a data-dependent method with dynamic exclusion enabled. Full scan (m/z 400-2000) spectra were acquired with the Orbitrap (resolution 60,000), and the top 5 most abundant ions in each MS scan were selected for fragmentation via collision-induced dissociation (CID) in the LTQ. An isolation width of 2 m/z, activation time of 30 ms, and 35% normalized collision energy were used to generate MS2 spectra. Dynamic exclusion settings allowed for a repeat count of 1 within a repeat duration of 5 sec, and the exclusion duration time

was set to 15 sec. For identification of proteins, tandem mass spectra were searched with Sequest (Thermo Fisher Scientific) against a *Homo sapiens* subset database created from the UniprotKB protein database (www.uniprot.org). Variable modifications of +57.0214 on Cys (carbamidomethylation), and +15.9949 on Met (oxidation) were included for database searching. Search results were assembled using Scaffold 3.0 (Proteome Software), peptide and protein identifications were filtered to 95% and 99% probability, respectively, and proteins reported were required to have two or more peptides identified.

Prostaglandin Glycerol Ester Hydrolase Assay. Hydrolytic activity was determined by addition of 10 nmol of PGE_2-G to 100 µL of cytosol at 37°C. Reactions were quenched after 2 h by addition of 1mL of ethyl acetate containing deuterated internal standard (PGE_2-d_4). Quenched samples were placed on ice for 15 minutes before the organic layer was removed, evaporated to near dryness under nitrogen and reconstituted with 50% methanol. Samples were analyzed by LC-MS/MS analysis for the hydrolytic products PGE_2 and samples were quantified against the internal standard.

LC-MS/MS Analytical Procedures. Analysis of prostanoids was accomplished by reverse phase chromatography followed by mass spectrometric detection by selected reaction monitoring (SRM). The LC system used was a Shimadzu LC-20 and the mass spectrometer used was an Applied Biosystems 3200 QTrap. Resolution of PGs was done by gradient elution on a Phenomenex Luna C18 column (50 mm x 2.0 mm, 3 µm particle size). Solvent A was HPLC grade water with 0.1% formic acid and solvent B was acetonitrile (ACN) with 0.1% formic acid. Samples were injected onto the column with a starting condition of 80% solvent A and 20% solvent B at a flow rate of 0.5 mL/min. A linear gradient of increasing solvent B to 98% was run over 2 minutes and then held for

1.5 minutes.

Protein expression in HEK293 Cells. HEK293 cells were plated at a density of $3x10^5$ cells per well in a 6-well plate in RPMI medium supplemented with 10% FBS and were incubated for 24 h at 37°C. cDNA transfections were performed according to manufacturer's recommendations. Briefly, Turbofect and cDNA (1.5 μg) were added to serum free OPTIMEM medium and allowed to incubate at room temperature for 30 min. cDNA solution was added to each well drop wise and cells were incubated at 37°C for additional 48 h before harvesting.

siRNA Knockdown of Identified Proteins (PGLS and PAFAH1β3). siRNAs for PGLS and PAFAH1β3 were purchased from Life Technologies. MDA-MB-231 cells were plated at 1.0 x 10^6 cells per $100mm^2$ and allowed to incubate for 24 h to give 40-60% confluence. siRNA was introduced into the cells by complex formation with either siRNA and DharmaFECT 1 according to manufacturer's recommendations. Briefly, siRNA/DharmaFECT complexes were formed for 20 min in serum free OPTIMEM1 (Gibco). RPMI medium from each plate was removed and replaced with 5 mL of serum-free OPTIMEM1 medium followed by addition of 1 mL of transfection solution. Cells were cultured for 24 h at 37°C. Medium was subsequently replaced with RPMI containing 10% FBS and incubated at 37°C for an additional 48 h before harvesting.

Western Blot Analysis. Protein expression was determined in all cell lysates by western blot analysis. Cell lysates were all separated by sodium dodecyl sulfate (SDS) polyacrylamide gel electrophoresis (PAGE). Following SDS-PAGE separation, proteins were transferred onto a nitrocellulose membrane and probed with either anti PGLS, anti-DDAH2 or anti-PAFAH1β3 (1:500 v/v) and anti-GAPDH (1:1000, v/v) overnight

followed by incubation with IR visible secondary antibodies (1:5000, v/v). Blots were visualized using the Odyssey IR Imager.

Results

Characterization of PGE_2-G Hydrolysis in MDA-MB-231 Cancer Cells

MDA-MB-231 breast cancer cells were initially tested for hydrolytic activity by quantitatively monitoring the formation of PGE_2 by LC-MS/MS. Cytosolic fractions demonstrated PGE_2-G hydrolase activity that was linear with time and comparison to membrane fractions from the same cells revealed that virtually all of the activity was cytosolic (Figure 2). Importantly, serine esterases have been proposed as the hydrolases responsible for PG-G hydrolysis in rat plasma. Thus, we explored whether a member of the serine hydrolase family was responsible for PGE_2-G hydrolysis. MDA-MB-231 cytosol was preincubated with an irreversible serine hydrolase inhibitor, methoxy fluorophosphonate, and assessed for hydrolytic activity following incubation. As shown in Figure 2, fluorophosphonate treatment abolished hydrolysis of PGE_2-G. This supports the hypothesis that a serine hydrolase is responsible for PGE_2-G in MDA-MB-231 cells.

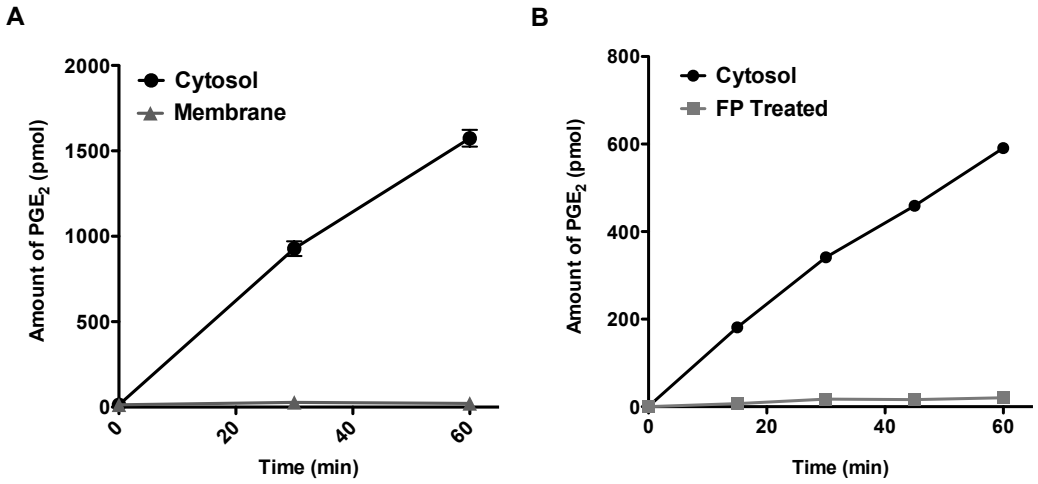

Figure 2: PGE_2-G hydrolase activities in MDA-MB-231. (A) Cellular fractionation of MDA-MB-231 cells displayed PGE_2-G hydrolase activity in the cytosolic fraction. Membrane fractions demonstrated no activity. (B) MDA-MB-231 cells displayed PGE_2-G hydrolase activity that was abolished by pretreatment with an irreversible fluorophosphonate inhibitor, FP-TAMRA.

Purification of unknown PG-G Serine Hydrolase

Cytosol was isolated from a 10 g pellet of MDA-MB-231 and applied to a strong cation exchange column to remove unwanted proteases. Protease inhibitors could not be used because many of these inhibitors are general serine hydrolase inhibitors, which caused complete inhibition of PGE_2-G hydrolysis in cytosol (data not shown). The dialyzed flow-through fraction was applied to a High-Q anion exchange column and eluted with a NaCl gradient. No hydrolytic activity was present in the void volume. A salt gradient was run and PGE_2-G hydrolase activity was eluted from the column at approximately 200 mM salt concentration. The active fractions were combined, concentrated and loaded onto a size exclusion column. The hydrolytic activity eluted from the size exclusion column at masses corresponding to a range of 75-25 kDa (Figure

3). The active fractions were pooled and applied to a chromatofocusing (Mono-P) column for further separation by pH. Interestingly, only 2 hydrolytically active fractions eluted from the chromatofocusing column at a pH of approximately 6 (Figure 3). Unfortunately, the levels of PGE_2-G hydrolysis from fractions isolated from the size exclusion column were significantly higher (top fraction produced ~10,000 ng/mL of PGE_2) compared to PGE_2-G hydrolysis from the Mono-P column (top fraction produced ~2500 ng/mL of PGE_2). This represents a decrease of 75% of the amount of PGE_2 produced in the most active fraction. Potentially, the enzyme was unstable through the Mono-P column due to drastic changes in pH. Many proteins have been reported that are unstable at lower pH.

Active fractions isolated from Mono-P column were combined, dialyzed and further purified using a Mono-Q anion exchange column to produce highly pure samples (Figure 3). Mono-Q columns are commonly used to refine the final step in purification because of the homogenous size of the beads in the packing material. The levels of PGE_2-G hydrolysis are not significantly changed through this column (top fraction produced 2400 ng/mL of PGE_2), which is comparable to the Mono-P column, suggesting that we did not lose much activity through this column.

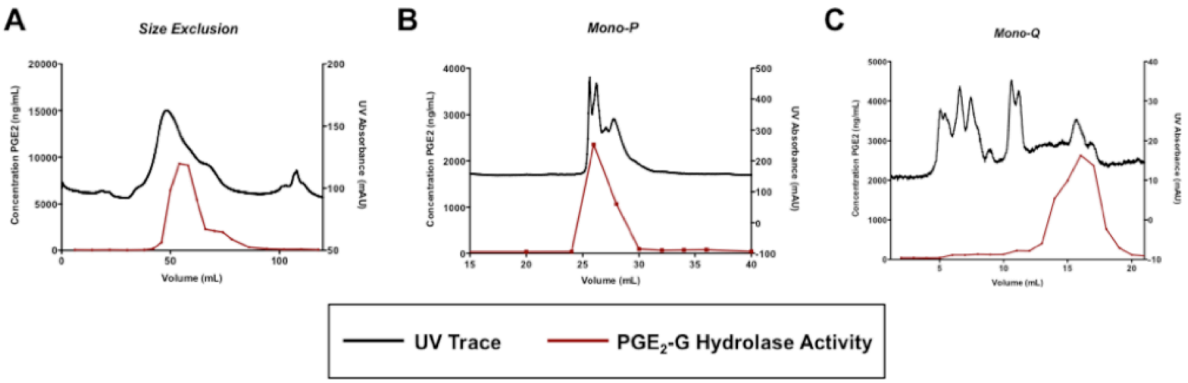

Figure 3: Elution and activity profiles for PG-G hydrolase purification on (A) Sephacryl S-200 size exclusion column, (B) Mono-P column eluted with Polybuffer 74, and (C) Mono-Q anion exchange column eluted with a NaCl salt gradient

Overall, hydrolytic activity was purified 138-fold compared to cytosolic extracts (Table 1). As stated above, there appears to be no significant increase in purity (~2-fold increase) between the size exclusion column and the Mono-Q column, implying the Mono-P column is either not contributing to purification, or may be detrimental to the purification due to significant decreases in PGE_2-G hydrolysis from the size exclusion column to the Mono-P column. Unfortunately specific activity was difficult to determine because the Polybuffer 74 required for the Mono-P chromatography interfered with protein determination, though it did not interfere with activity determinations.

Table1: Purification Table of PG-G Hydrolase from MDA-MB-231

Samples	Total Protein (mg)	Total Activity (units)	Specific Activity (Units/mg)	Fold Purification	% Yield
Cell Lysate	215	1248430	5804	1	100
Cytosol	219	1225410	5590	1	98
Strong Cation FT	87	713050	8242	1	57
HiTRAP Q Column	6	450814	78850	14	36
Size Exclusion	1	242648	394478	68	19
Mono-P	N/D	17179	N/D	N/D	N/D
Mono-Q	1>	26280	1600812	138	2

MonoP not determined (N/D) because Polybuffer 74 interfered with BCA protein determination

The yield is comparable to other purifications of serine hydrolases. However, the fold purification was significantly lower then those observed from other serine hydrolase purifications, which could also be associated with the loss in PGE_2-G hydrolysis between size exclusion chromatographic separation and Mono P chromatographic separation.

To determine the extent of purification, all steps from the purification were run on a 4-20% SDS-PAGE gel and stained by colloidal Coomassie blue. Figure 4 shows the

protein bands present in all the steps. The purification resulted in a significant decrease in the number of proteins in the samples, with intense bands present at 25kDa and 50kDa, and 4-5 minor protein bands throughout. Competitive ABPP was used to determine which proteins from the Mono-Q were capable of binding PGE_2-G.

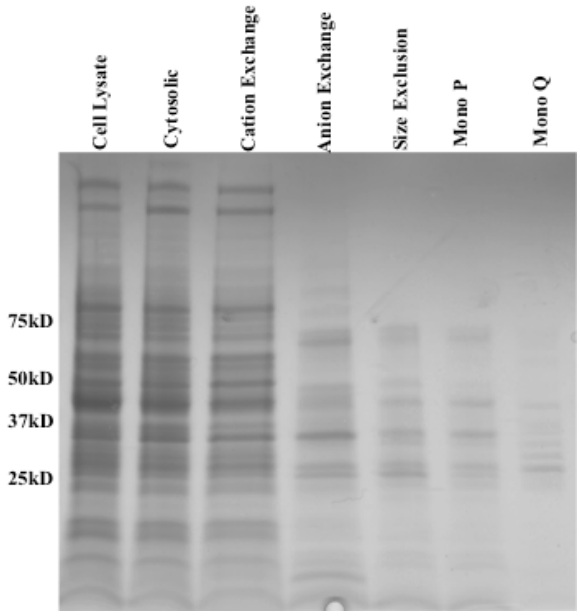

Figure 4: SDS-PAGE gel with Coomassie blue staining for each step in purification. The amount of protein present in the cell lysate and cytosol is significantly purified down to a few bands in the Mono-Q fractions. The most intense band present in the Mono-Q corresponds to a protein at 25kDa

Characterization of PG-G binding by Competitive ABPP

Competitive activity-based protein profiling was conducted to determine proteins corresponding to PGE_2-G binding. The assumption was that any serine hydrolase that can bind PGE_2-G in the active site may be responsible for hydrolysis. Samples from the Mono-Q column were treated with excess PGE_2-G or DMSO followed by FP-TAMRA tagging. Competitive ABPP yielded a protein with an apparent molecular weight of

25kDa that resulted in inhibition of FP-tagging in the presence of PGE_2-G (Figure 5). The ability of PGE_2-G to block FP binding demonstrated a serine hydrolase capable of binding PG-Gs at the active site serine. This protein band also correlated to the darkest band by colloidal Coomassie blue staining (Figure 5) and was excised for in-gel tryptic digestion and protein identification.

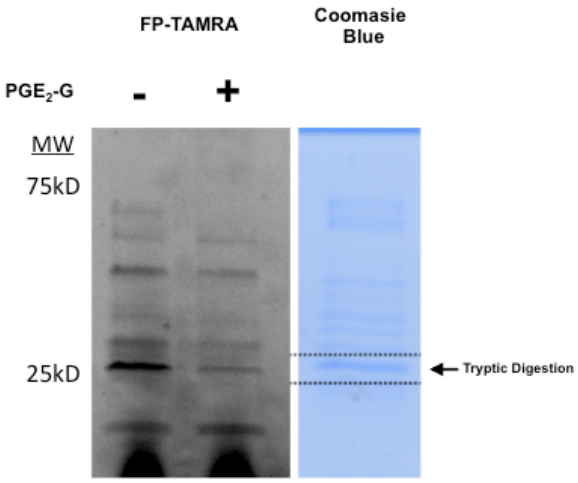

Figure 5: PGE_2-G Competitive ABPP. Excess PGE_2-G in purified fractions inhibited the labeling by FP-TAMRA probe compared to no PGE_2-G. Subsequent Coomassie blue staining showed a band at 25kDa that was excised for tryptic digestion and mass spectrometric identification.

Protein Identification and Validation

Three major serine hydrolases were identified from the 25kDa band. 6-Phosphoglucolactonase (PGLS), an enzyme involved in the pentose phosphate metabolism pathway; dimethylarginine dimethylaminohydrolase 2 (DDAH2), an enzyme responsible for hydrolysis of N(G),N(G)-dimethyl-L-arginine and N(G)-monomethyl-L-arginine; and platelet activating factor acetylhydrolase 1β3 subunit (PAFAH1β3), an enzyme responsible for platelet activating factor (PAF) hydrolysis.

Each enzyme is a member of the serine hydrolase family and all catalyze reactions that potentially mimic hydrolysis of PG-Gs. First, PGLS is important in pentose phosphate metabolism and catalyzes the second step of the pentose phosphate pathway, which is the hydrolysis of 6-phosphogluconolactone to form 6-phosphogluconate (Figure 6) (152). The hydrolysis catalyzed ring opening can potentially mimic components of the carboxylate and glycerol groups of PG-Gs. Second, PAFAH1β3 is a catalytic subunit of the PAFAH complex, which regulates the levels of platelet activating factor (PAF), a pro-inflammatory molecule (153). PAFAH1β3 hydrolyzes the carboxylic acid group off the glycerol backbone of PAF (Figure 6). PAF is very similar to lipids generated from hydrolysis of phospholipids in the bilayer. The PAF molecule contains multiple structural elements that are very similar to PG-Gs, including a glycerol moiety that is hydrolyzed from the carboxylic acid (153). Lastly, DDAH2 is important in nitric oxide synthase regulation. DDAH2 metabolizing N(G),N(G)-dimethyl-L-arginine and N(G)-monomethyl-L-arginine to L-citrulline and dimethylamine (Figure 6), which are both endogenous inhibitors of nitric oxide synthase (154, 155). Though not as likely as PGLS or PAFAH1β3, substrates of DDAH2 hydrolysis contain some elements that resemble PG-Gs.

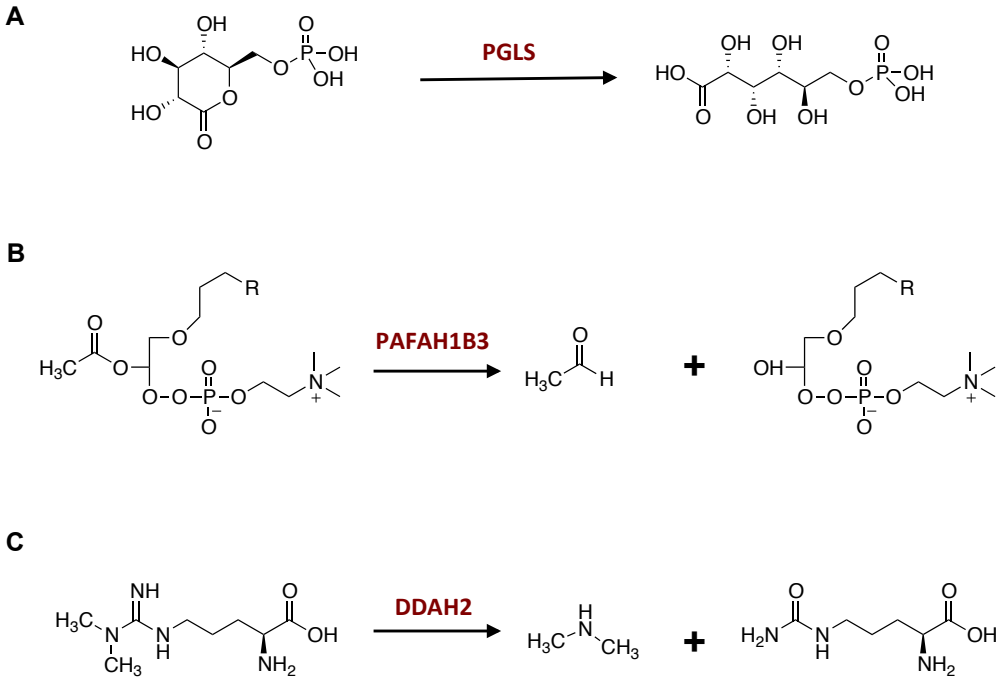

Figure 6: Known hydrolytic functions of PGLS, PAFAH1β3, and DDAH2. (A) PGLS catalyzes the pentose ring opening of 6-phosphogluconolactone at the ketone carbon to form 6-phosphogluconate. (B) PAFAH1β3 hydrolyzes PAF at the *sn*2 position of the glycerol backbone to release a lysophospholipid and a free acyl group. (C) DDAH2 metabolizes dimethylarginine to form dimethylamine and L-citrulline. R represents a long chain fatty acid.

To investigate the significance of PGLS, DDAH2 and PAFAH1β3 in PGE_2-G hydrolysis, cDNA for each protein was transfected and overexpressed in HEK293 cells. Importantly, these cells express no detectable levels of any of the proteins by western blot (Figure 7) and have low levels of hydrolase activity against PGE_2-G (Figure 7). All three proteins were successfully transfected into HEK293 and cytosolic fraction from the transfected cells demonstrated high expression of each protein by western blot (Figure 7) compared to control. Unfortunately, upon overexpression of DDAH2 and PAFAH1β3, HEK293 cytosolic fractions showed no significant increase in hydrolysis of PGE_2-G

compared to untransfected cells (Figure 7). Comparatively, PGLS overexpression showed a slight increase in activity, though this increase in activity did not correlate to the significant increase in protein expression. Further validation was necessary to verify PGLS as a PGE_2-G hydrolase.

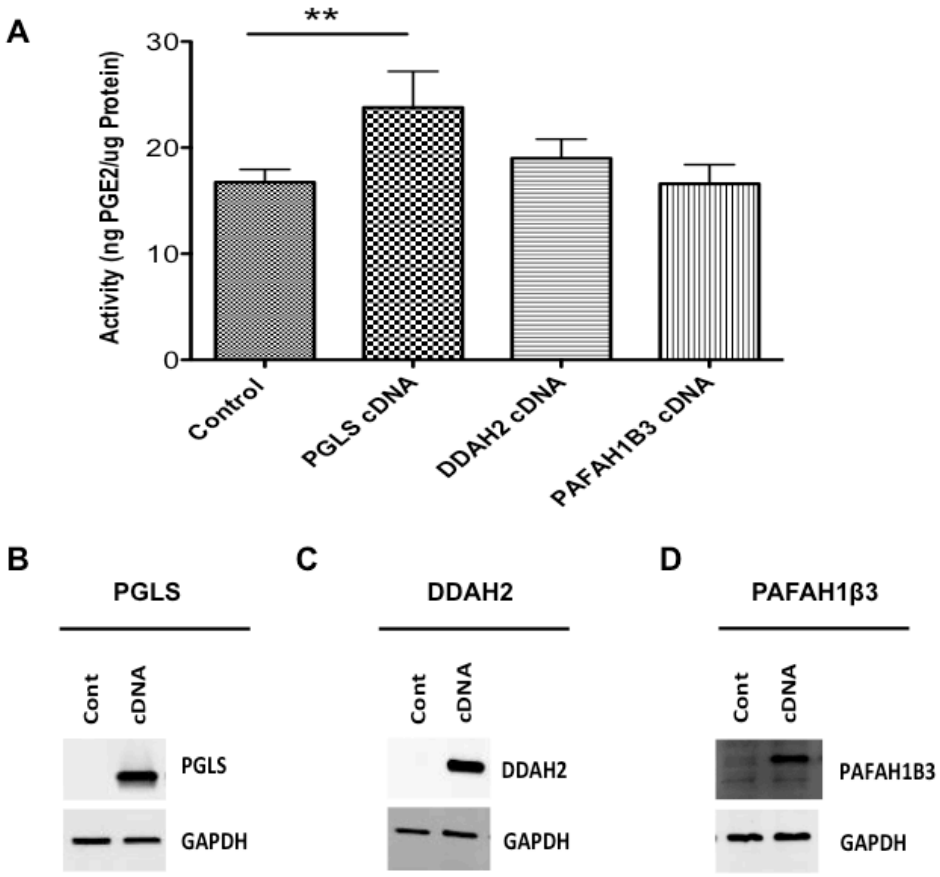

Figure 7: PGLS, DDAH2 and PAFAH1β3 overexpression in HEK293. (A) PGE_2-G hydrolytic activity of cell lysates obtained from HEK293 (control) or either PGLS, DDAH2, or PAFAH1β3 overexpressed HEK293 cells. Western blot analysis of overexpression in control HEK293 cells (control) and (B) PGLS, (C) DDAH2 or (D) PAFAH1β3 overexpressed HEK293 cells (cDNA). GAPDH Western blotting verified equaling protein loading (5μg per lane). Data represented as mean ± SD of n = 6 analysis. ** <0.01 by t-test.

siRNA knockdowns of PGLS and PAFAH1β3 were conducted in MDA-MB-231 cells. The levels of both PGLS and PAFAH1β3 were markedly reduced in MDA-MB-231 cells upon transfection as determined by western blot analysis (Figure 8). Unfortunately, hydrolysis of PGE_2-G by cytosolic fractions obtained from either knockdown demonstrated no reduction in hydrolysis compared to control cells (Figure 8). Taken together, cDNA overexpression in HEK293 and siRNA knockdown in MDA-MB-231 do not support the involvement of PGLS, DDAH2 or PAFAH1β3 in prostaglandin glycerol ester hydrolysis.

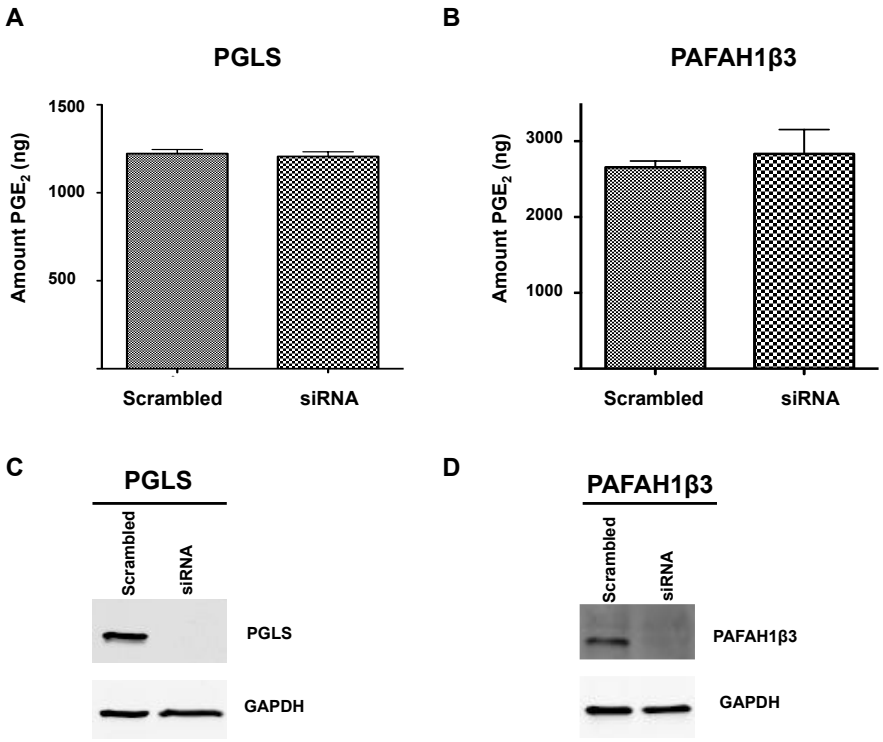

Figure 8: PGLS and PAFAH1β3 siRNA knockdown in MDA-MB-231 cells. PGE_2-G hydrolytic activity of cell lysate obtained from MDA-MB-231 control (scrambled) or (A) PGLS deficient MDA-MB-231 (siRNA) or (B) PAFAH1β3 deficient MDA-MB-231 (siRNA). (C) Western blot analysis of PGLS in control MDA-MB-231 (scrambled) and PGLS depleted cells (siRNA). (D) Western blot analysis of PAFAH1β3 in control MDA-MB-231 (scrambled) and PAFAH1β3 depleted cells (siRNA). GAPDH Western bloting verified protein loading (5μg per lane).

Discussion

Hydrolysis of prostaglandin glycerol esters has made investigation into the *in vivo* effects of these lipids difficult. Protein purification was employed in order to isolate the hydrolase responsible for prostaglandin glycerol ester hydrolysis from MDA-MB-231 cells. Competitive ABPP was utilized to determine the appropriate molecular weight of the serine hydrolase in the purified samples. PGE_2-G was able to inhibit the labeling of a protein with a molecular weight of 25kDa. In-gel tryptic digestion and proteomics identified three enzymes, PGLS, DDAH2, and PAFAH1β3, as potential candidates responsible for PG-G hydrolysis. However, cDNA overexpression and siRNA knockdown of these proteins determined that none were capable of hydrolyzing PG-Gs

Serine hydrolases have been purified from multiple sources with great success. A major issue that arose during the purification was the significant loss of activity due to the Mono-P column. As mentioned above, samples applied to the Mono-P column displayed activity significantly lower then the input for the column. This implied that the serine hydrolase of interest was not stable under the conditions used for this column. Secondly, the amount of starting material used in other purifications is usually much greater then 10 g. In most cases, tissue samples or large quantities of cells are utilized as raw materials, which provides higher amounts of protein for isolation. In terms of our purification, 10 g may not be sufficient to achieve the level of purity and stability necessary to isolate the major serine hydrolase of interest.

Protein purification is a technique that requires a number of important starting conditions that may be too difficult to achieve in our laboratory. Achieving the amount of cells required for purification would be too costly or too difficult to achieve. Utilizing

different approaches to identify the unknown serine hydrolase needs to be employed. One important characteristic of the PG-G hydrolase is that it belongs to the serine hydrolase superfamily. Understanding the nature of serine hydrolases has led to the development of new analytical and computational approaches to investigate the activity of this class of enzymes in complex biological samples (114). ABPP coupled with multi-dimension protein identification technology (MuDPIT) has allowed for the analysis, inventory, and characterization of serine hydrolases throughout multiple cancer cell lines (123, 156). By understanding the relationship between enzyme activity and PG-G hydrolase activity, there may be a way to relate the extent of PG-G hydrolysis across a number of different cancer cell types and compare that to the serine hydrolase activity levels determined by ABPP-MuDPIT.

Chapter IV

IDENTIFICATION OF THE MAJOR PROSTAGLANDIN GLYCEROL ESTER HYDROLASE IN HUMAN CANCER CELLS

Introduction

Endocannabinoids are a class of AA)-containing bioactive lipids that have a myriad of physiological functions (1, 157-162). This diverse class of signaling molecules includes 2-arachidonoylglycerol (2-AG) and arachidonoylethanolamide (AEA), which are produced from membrane phospholipids and initiate cellular responses through interactions with the cannabinoid receptors, CB1 and CB2 (1, 161, 162). Their effects are mitigated through metabolism by the endocannabinoid serine hydrolases, monoacylglycerol lipase (MAGL), α/β hydrolase domain-containing protein 6 and 12 (ABHD6 and ABHD12), and fatty acid amide hydrolase (FAAH) (28, 35, 51, 163, 164). In addition to these lipases, endocannabinoids have been shown to be selective substrates for cyclooxygenase enzymes, particularly cyclooxygenase-2 (COX-2). Oxidation of 2-AG by COX-2 results in the production of prostaglandin glycerol esters (PG-Gs, Figure 1). These lipids are of growing interest because they elicit a wide array of cellular responses, including activation of calcium mobilization, modulation of synaptic transmission, induction of hyperalgesia, exacerbation of neurotoxicity and neuroinflammation, and elicitation of anti-inflammatory effects upon lipopolysaccharide stimulation (82-86, 93, 165).

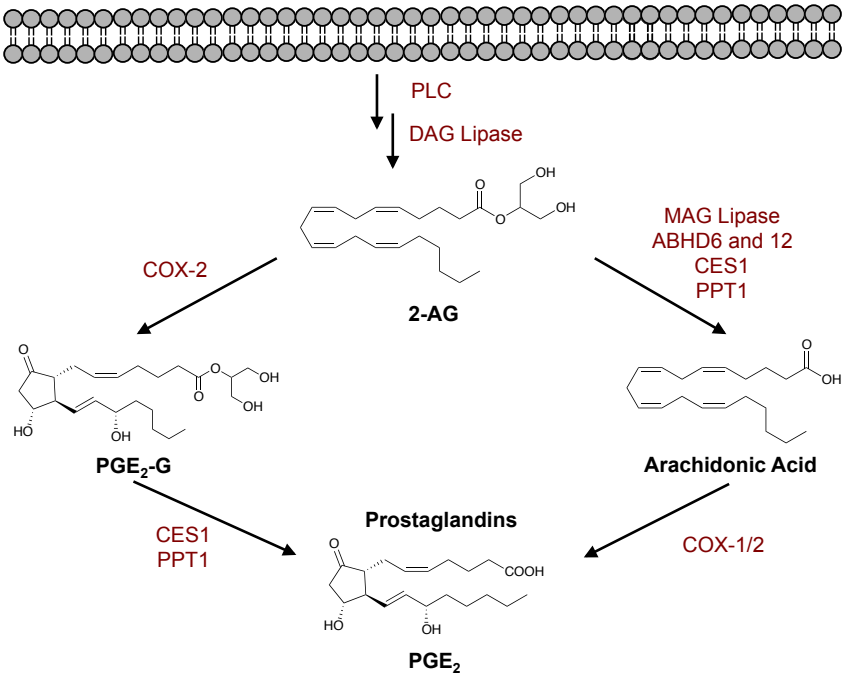

Figure 1: Biosynthesis and metabolism of 2-AG. Following production of 2-AG, lipases (MAG lipase, ABHD6 and 12, CES1, and PPT1) can hydrolyze 2-AG to AA, which can be oxidized to form prostaglandins (PGE_2 shown here). Additionally, 2-AG is oxidized by COX-2 to form PG-Gs (PGE_2-G shown here). PG-Gs can be hydrolyzed by CES1, PPT1, and/or other enzymes to form the corresponding free acid prostaglandins.

Investigation into the physiological relevance of PG-Gs in vivo has been a significant challenge due to their instability to hydrolysis in biological fluids (87). Two serine hydrolases have been shown to metabolize PG-Gs in human THP1 cells, carboxylesterase 1 (CES1) and palmitoyl-protein thioesterase 1 (PPT1). CES1, a xenobiotic-metabolizing enzyme that is expressed in high amounts in the liver, hydrolyzes a wide array of substrates, ranging from ester and amide-containing xenobiotics (166), to long chain fatty acid esters and thioesters (167), and cholesteryl esters from lipid droplets (167, 168). Similarly, PPT1, a lysosomal hydrolase, has

multiple substrates; however it is predominantly responsible for the depalmitoylation of a number of proteins as well as hydrolysis of palmitoyl-CoA and palmitoyl thioglucoside (169, 170). Consistent with the wide substrate diversity exhibited by CES1 and PPT1, both enzymes are capable of hydrolyzing PG-Gs and 2-AG (98, 99, 171). In THP1 monocytes, the hydrolysis of 2-AG was almost entirely attributed to CES1, with minor involvement of PPT1 (98, 99, 171). Kinetic analysis of both enzymes showed greater catalytic turnover for 2-AG than for PG-Gs, with both enzymes exhibiting almost 2-fold more activity for 2-AG than for PG-Gs (99).

We chose to investigate the hydrolase responsible for PG-G metabolism in cancer cell lines because of the high PGE_2-G hydrolytic activity detected in preliminary experiments, the ease of cell maintenance, and the potential for straightforward biochemical and genetic manipulation. The various enzymes described above are serine hydrolases, so we explored the possibility that the PGE_2-G hydrolase(s) in human cancer cells is(are) a member of this superfamily. Serine hydrolases are a diverse class of enzymes that include lipases, proteases, and esterases (100, 101), and many class members are involved in lipid biosynthesis and metabolism (35, 51, 163, 164). A unifying feature of the serine hydrolase family is a catalytic mechanism that involves the activation of a serine nucleophile for attack on substrates containing esters, amides, or thioester bonds (100). This conserved mechanism has enabled the development of irreversible fluorophosphonate probes that can covalently modify the active site serine and render the enzyme catalytically inactive (101). Nomura et al. (123, 156) coupled fluorophosphonate probe binding with mass spectrometric proteomics techniques, known as ABPP-MuDPIT, to determine the relative activity levels of serine hydrolases across

different cancer cell lines. Utilizing these inventories and comparing the relative activities of individual serine hydrolases to PGE_2-G hydrolase activities has allowed us to identify lysophospholipase A2 (LYPLA2) as the primary hydrolase responsible for PG-G metabolism.

Lysophospholipases are an important class of serine hydrolases which metabolize lysophospholipids to form free fatty acid and the glycerol phosphate-containing head group and will be discussed in detail below (172). Thus, we have identified a novel function and substrate for LYPLA2. Specifically, we identify LYPLA2 as the serine hydrolase responsible for hydrolysis of PG-Gs across a number of different cancer cell lines. siRNA knockdown and cDNA overexpression validated the involvement of LYPLA2 in PG-G hydrolysis. Active enzyme was expressed and purified in *E.coli,* which allowed for kinetic evaluation of an array of different substrates. In contrast to other PG-G hydrolyzing enzymes, we found that LYPLA2 exerted no action on 2-AG, or AEA. Thus, this is the first report of a hydrolase that preferentially hydrolyzes PG-Gs with no effects on the endocannabinoids. Identification and manipulation of LYPLA2 will lead to a better understanding of its involvement in lipid metabolism and signaling and facilitate the exploration of the effects of PG-Gs in both *in vitro* and *in vivo* settings.

Lysophospholipases

Lysophospholipid Production, Recycling and Metabolism

Phospholipids, originally thought to only be important in membrane formation in cells, have emerged as an important player in a wide array of physiological and pathological processes. The products of phospholipid metabolism have been shown to induce a wide array of different cellular responses; including signal transduction,

mediator formation and eicosanoid production in both normal and disease states. One class that has become increasingly interesting are lysophospholipids (lysoPLs). These molecules are a byproduct formed from the actions of phospholipases on phospholipids to generate polyunsaturated fatty acids. These lysoPLs consist of one long chain fatty acid and one hydrophilic head group (e.g. phosphocholine, phosphoethanolamine, etc..) attached to the glycerol backbone. Due to the presence of both a polar head group and a hydrophobic tail, these lysoPLs possess detergent like properties that cells need to process in order to prevent toxicity (173-177).

Two major routes of lysophospholipid detoxification have been identified in cells (Figure 2). One detoxification process is known as the Lands' cycle, which involves the recycling of lysoPLs by an acetyltransferase, lysophospholipid acetyltransferases (LPLAT), to regenerate phospholipids, which are reincorporated into the phospholipid bilayer (178-180). This process has been described as the main process that gives membranes their lipid diversity. By utilizing acetyl-CoAs as building blocks, a wide array of different lipids can be combined with these lysoPLs before being reincorporated into the lipid bilayer. The second route of detoxification involves degradation of the lysoPLs by hydrolysis of the acyl chain to liberate the remaining fatty acid chain and the glycerolphosphate head group by the serine hydrolases known as the lysophospholipases (172). By shifting the lysoPLs between the degradation and the recycling pathways, cells can control important cellular functions.

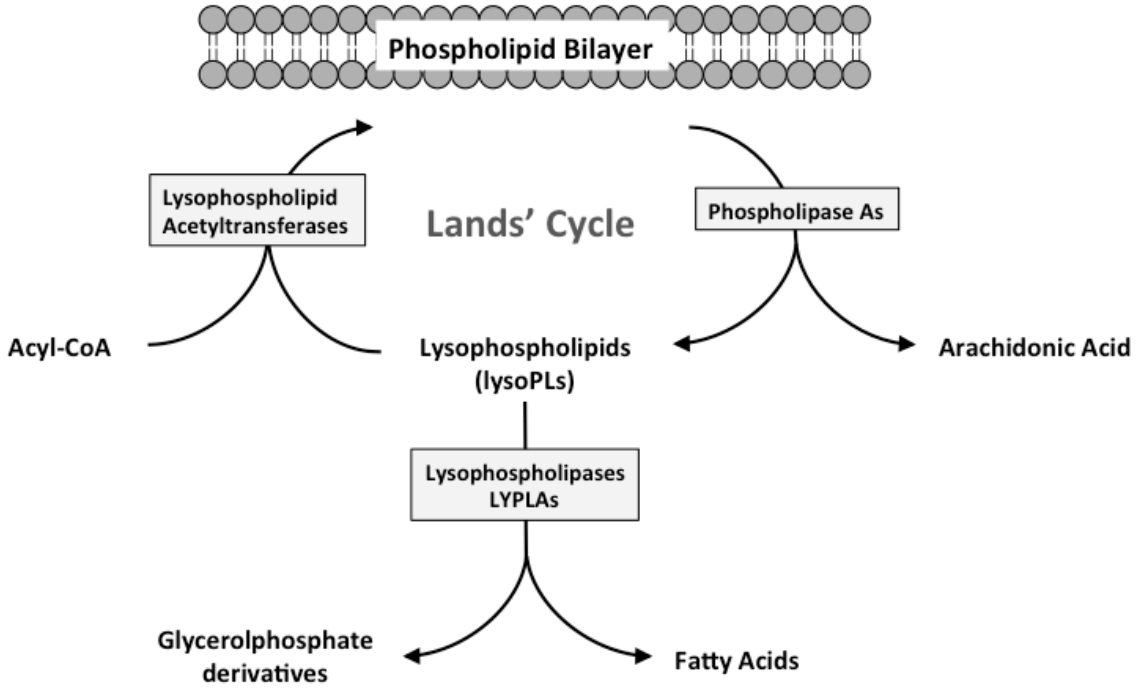

Figure 2: Lysophospholipid biosynthesis and processing. Lysophospholipids are produced from the hydrolysis of phospholipids from the lipid membrane by phospholipases to generat lysoPLs. LysoPLs are processed in two ways; one by entering the Land's Cycle which adds another fatty acid by an acetyltransferase and reincorporates the phospholipid into the lipid bilayer or two by further hydrolsis by lysophopholipases to produce a free fatty acid and a glycerolphosphate derivative

Lysophospholipase activity in mammalian systems and cells has been shown to be much higher as compared to the phospholipase and transacylase actitivties (181-184). This high activity allows cells to maintain safe levels of lipid metabolites needed for proper cellular function.

Lysophospholipase A1 and A2

As previously described, lysoPLs exhibit a wide array of diverse biological functions, because of this there are several enzymes that strictly maintain and metabolize

lysoPL levels, referred to as lysophospholipases, specifically lysophospholipase A1 and A2 (LYPLA1 and LYPLA2, respectively) (183). These low molecular weight LYPLAs have been reported and purified from a number of different tissues and cells, including rabbit heart (185), pig gastric mucosa (186), rat liver (187), murine macrophage $P388D_1$ (183, 188), and human HL60 cells (189). LYPLA1 and LYPLA2 are 25 kDa proteins that display similar properties; for example, both enzymes' metabolic activities are independent of Ca^{2+}, Mg^{2+}, and EDTA and neither show any PLA transacylase activity, acyltransferase activity or non-specific general esterase activity (183, 186, 187, 189). Additionally, kinetic evaluation of these enzymes demonstrated that they are specific towards lysophospholipids, with no detectable levels of phospholipase activity.

Despite the similarity between LYPLA1 and LYPLA2, there is evidence to suggest that the two are actually distinct enzymes instead of splice variants or posttranslational modifications of the same gene. First, antibodies that recognize LYPLA1 are not able to cross-react with LYPLA2, similarly LYPLA2 antibodies are not able to recognize LYPLA1 (183, 186, 187). Additionally, during purification, LYPLA1 is able to bind phosphorylcholine affinity columns while the LYPLA2 is not (183). Also, upon purification LYPLA2 is much less stable compared to LYPLA1. Furthermore, LYPLA1 is also able to turn over a larger variety of substrates; including lysophosphatidylcholine (lysoPC), lysophosphatidylethanolamine (lysoPE), lysophosphatidylglycerol, lysophosphatidylinositol, lysophosphatidylserine, while LYPLA2 prefers only the lysoPC and lysoPE containing lipids (186, 187, 189). Finally, the most striking evidence is that the two proteins only share about 64% sequence similarity, suggesting that the two enzymes are indeed independent proteins (189).

Lysophospholipases are members of the serine hydrolase family, which gives both enzymes very similar sequence motifs that are present across many of the serine proteases, lipases and esterases (172). Much of the structural work has been done on LYPLA1 due to difficulties in crystallization and stability of LYPLA2. Referring to the sequence of both enzymes, the serine hydrolase consensus sequence GXSXG is conserved in both enzymes active sites. This sequence was verified through site directed mutagenesis of Ser-119 of LYPLA1 within this GXSXG motif (190). The S119A mutant of this enzyme completely abolished the catalytic activity of the enzyme. Additionally, the other important residues for catalytic activity were identified as Asp-174 and His-208. These three residues complete the classic catalytic triad (Ser-Asp-His) of serine hydrolases (190-192).

Figure 3 shows the crystal structure of LYPLA1. Secondary structural elements of LYPLA1 resemble the α/β hydrolase fold, which places the catalytic triad in a similar position as other α/β hydrolases (191, 192)., Additionally, the catalytic residues; Ser-119, Asp-174, and His-208, are placed close enough to place the amino acids in the appropriate positions to form the charge-relay network necessary for serine hydrolase catalysis (191, 192). Sequence comparison of LYPLA2 and LYPLA1 show that the catalytic triad identified in LYPLA1 is conserved in LYPLA2, e.g. Ser-122, Asp-176, His-210. This verifies that the catalytic mechanism present in LYPLA2 is similar to LYPLA1 and resembles the classical serine hydrolases catalytic triad (191).

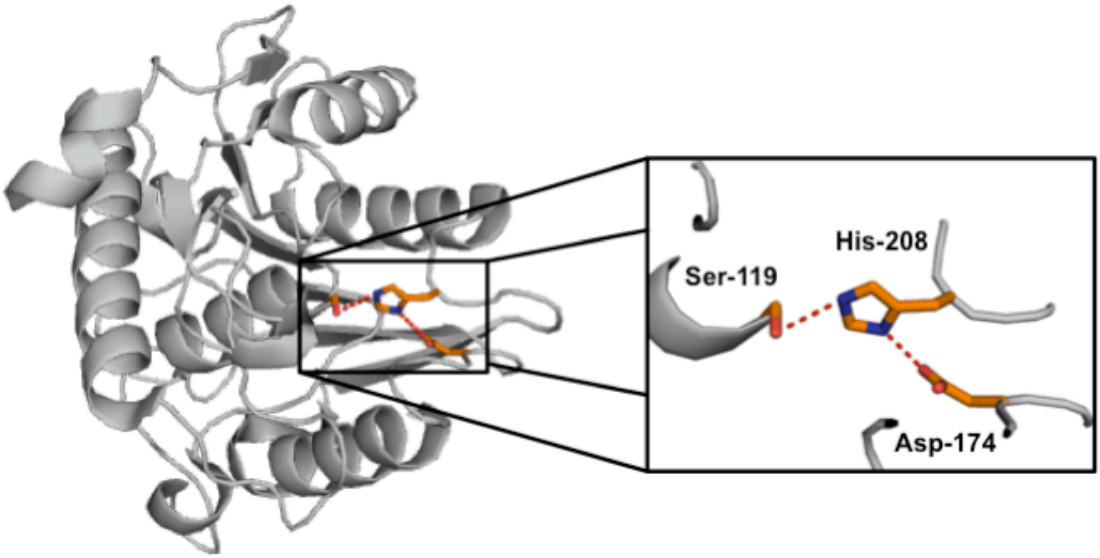

Figure 3: Crystal Structure of LYPLA1. The catalytic triad is highlighted (orange) to show the charge-relay network between the serine, histidine and aspartate

Tissue distribution studies demonstrated that LYPLAs are widely distributed throughout the body. mRNA levels demonstrated that LYPLAs are most abundant in heart, placenta, testis and skeletal muscle followed by liver, pancreas, kidney, brain, and lung. In contrast to the variable expression levels in adult, fetal distribution is more uniform throughout the tissues (193). The ubiquitous existence of LYPLA proteins correlates with its activity across a wide array of tissues and cells. LysoPls are implicated in a mulitude of biological processes as well as pathological states. Exploring the roles LYPLAs play will be essential in understanding their physiological function and demonstrates the essential function these enzymes play in maintaining lysoPL levels.

Materials and Methods

Chemicals, Cells and Reagents. 2-AG, AEA, PG-Gs (PGE_2-1 glycerol ester, PGD_2-1 glycerol ester, $PGF_{2\alpha}$-1 glycerol ester), prostaglandin serinol amide (PGE_2-SA), deuterated prostaglandins and PG-Gs (PGE_2-d_4 and PGE_2-G-d_5) and deuterated AA (AA-d_8) were purchased from Cayman Chemicals (Ann Arbor, MI). LC-MS solvents were from Fisher Scientific (Chicago, Il). DharmaFECT 1 and methoxy fluorophosphonate coupled to tetramethylrhodamine (FP-TAMRA) was acquired from Thermo Scientific (Pittsburgh, PA). All siRNA, Lipofactamine 2000 and Lipofectamine RNAiMAX were from Life Technologies (Carlsbad, CA). Human breast cancer adenocarcinoma cell lines; MDA-MB-231 and MCF7, prostate cancer cell lines; PC3 and LNCaP, human embryonic kidney cells, HEK293, 1483 human head and neck squamous cell carcinoma and mouse macrophage like RAW264.7 were obtained from the American Type Culture Collection (ATCC, Manassas, VA). All cell culture media was from Gibco (Carlsbad, CA). Recombinant LYPLA2 cDNA and Turbofect were purchased from OriGene Technologies (Rockville, MD). FBS was from Atlas Biologicals (Fort Collins, CO). HIS-Select Nickel Affinity beads are from Sigma (St. Louis, MO). 120 mL HiPREP 16/60 Sephacryl S-200 HR was from GE Healthcare (Piscataway, NJ). Luna liquid chromatography reverse phase C18 column was from Phenomenex (Torrance, CA).

Culture Conditions. MDA-MB-231, MCF7, LNCaP, and HEK293 cells were maintained as an adherent culture in RPMI medium supplemented with 10% (v/v) fetal bovine serum (FBS) at 37°C and 5% CO_2. PC3 cells were grown in DMEM/F12 supplemented with 10% (v/v) FBS. RAW 264.7 mouse macrophage cells were maintained in high glucose DMEM supplemented with 10% FBS. All cells were grown to no more than 75%

confluence.

siRNA Knockdown of LYPLA2 in Multiple Cancer Cell Types. MDA-MB-231 cells were plated at 1.0 x 10^6 cells per 100 mm^2 and allowed to incubate for 24 h to 40-60% confluence. siRNA was introduced into the cells as a complex with DharmaFECT 1 according to manufacturer's recommendations. Briefly, siRNA/DharmaFECT complexes were formed for 20 min in serum free OPTIMEM1. RPMI medium from each plate was removed and replaced with 5 mL of serum-free OPTIMEM1 medium followed by addition of 1 mL of transfection solution. Cells were cultured for 24 h at 37°C. Medium was subsequently replaced with RPMI containing 10% FBS and incubated at 37°C for an additional 48 h before harvesting.

PC3 cells were plated at 1.0 x 10^6 cells per 100 mm^2 and allowed to incubate for 24 h to give 40-60% confluence. Complex formation with siRNA and Lipofectamine 2000 was performed according to manufacturer's recommendations. Briefly, siRNA/Lipofectamine complexes were formed for 20 min in serum free OPTIMEM1. The medium in each plate was removed and replaced with serum-free OPTIMEM1 medium followed by addition of 1 mL of transfection solution. The cells were cultured for 8 h at 37°C. The medium was subsequently replaced with DMEM/F12 supplemented with 10% (v/v) FBS. Cells were incubated at 37°C for an additional 48 h before harvesting.

LNCaP cells were plated at 1.0 x 10^6 cells per 100mm^2 and allowed to incubate for 24 h to 40-60% confluence. Complex formation with siRNA and Lipofectamine RNAiMAX was performed according to manufacturer's recommendations. Briefly, siRNA/Lipofectamine complexes were formed for 5 min in serum-free OPTIMEM1.

One mL of transfection solution was added to each plate, and the cells were cultured for 72 h at 37°C before harvesting.

LYPLA2 cDNA Overexpression in HEK293 Cells. HEK293 cells were plated at a density of 3 x 10^5 cells per well in a 6 well plate in RPMI medium supplemented with 10% FBS and incubated for 24 h at 37°C. cDNA was prepared by adding 45 μL of Turbofect to 250 μL of OPTIMEM1 followed by 15 μL (1.5 μg) of cDNA. The cells were incubated at room temperature for 30 min. cDNA solution was added to each well drop-wise, and cells were incubated at 37°C for an additional 48 h before harvesting.

Preparation of Cell Lysates. Cells were harvested by scraping, pelleted by centrifugation, and washed once with phosphate-buffered saline. The cells were resuspended in 500 μL ice-cold 25 mM Tris buffer (pH 7.5) containing 0.1 mM of both EDTA and DTT. Cells were lysed by sonication (Virsonic Cell Disrupter model 16-850, 10 x 10 sec pulses at relative output of 0.5, on ice), and the cytosolic fractions were separated by centrifugation (100,000 x *g* for 1 h). Protein concentrations were determined using the BCA reagent kit according to the manufacturer's instruction (Pierce, Rockford Il).

PG-G Hydrolase Assay. Hydrolytic activity was determined by adding 10 nmol of PGE_2-G to 100μL cell lysates at 37°C. Reactions were quenched after 2 h by addition of 1 mL of ethyl acetate containing deuterated internal standard (PGE_2-d_4). The organic layer was removed, evaporated to near dryness under nitrogen, and reconstituted with 50% methanol. Samples were analyzed by LC-MS/MS for the hydrolytic product, PGE_2, which was quantified against the internal standard using stable isotope dilution.

Serine Hydrolase Inhibition. The general serine hydrolase probe, FP-TAMRA was used to determine the involvement of serine hydrolases in the metabolism of PG-Gs. FP-

TAMRA (100 nM) or DMSO was added to 100 uL of MDA-MB-231 cytosol and allowed to incubate for 30 min at 37°C. PG-G hydrolase activity was determined as described above, except that samples were incubated from 0 to 60 min to obtain a full hydrolysis time course.

Western Blot Analysis. Protein expression was determined by western blot analysis. Samples were separated by sodium dodecyl sulfate (SDS) polyacrylamide gel electrophoresis (PAGE). Then, proteins were transferred to a nitrocellulose membrane and probed with either rabbit anti-LYPLA2 (1:500 v/v), rabbit anti-LYPLA1 (1:500 v/v) or anti-COX-2 (1:1000 v/v) and goat anti-β-actin (1:5000, v/v) overnight at 4°C. Membranes were washed and incubated with IR-visible anti-rabbit or anti-goat secondary antibodies (1:5000, v/v). Blots were visualized using an Odyssey IR Imager.

Recombinant protein E.coli Expression. Full-length LYPLA2 or LYPLA1 was cloned into an untagged (pC6H) or a hexahistidine-tagged (p6Hb) vector using overlap PCR and isothermal assembly (194). These constructs were subsequently transformed into BL21 Rosetta *E. coli* cells (Catalog # 71402, EMD Millipore) for protein expression. Large-scale expression was carried out in 10 L of autoinduction medium (195) at 37°C overnight.

His-tagged LYPLA2 E.coli Purification. All purification was performed at 4°C. *E.coli* cell pellets were resuspended in 20 mM sodium phosphate buffer (pH 7.4) containing 500 mM NaCl, 20 mM imidazole, and 0.1mM DTT. Cells were lysed by sonication (10 x 10 sec pulses at relative output of 0.5, on ice) and the cytosolic fraction was separated by centrifugation (100,000 x *g* for 1 h). HIS-Select Nickel Affinity beads pre-equilibrated with Buffer A (20 mM sodium phosphate buffer (pH 7.4), 500 mM NaCl, 20mM

imidazole, and 0.1 mM DTT) were added to the cytosolic fraction, and protein was bound overnight. Beads were packed into a column and washed with 4 column volumes of Buffer A. His tagged protein was eluted by linear gradient from 0 to 100% Buffer B (20 mM sodium phosphate buffer (pH 7.4), 500 mM NaCl, and 500 mM imidazole). Eluted protein was collected and concentrated using a Millipore 3000 MWCO centrifugal filter. Protein was loaded onto a 120 mL HiPREP 16/60 Sephacryl S-200 HR size exclusion column pre-equilibrated with 2 column volumes of running buffer (Tris buffer (pH 7.5)), 0.1 mM EDTA, 0.1 mM DTT). The column was was eluted with 1 column volume of running buffer at a flow rate of 0.5 mL/min, protein was collected, and purity was validated by SDS-PAGE.

LYPLA2 Kinetic Analysis. Hydrolysis reactions with recombinant LYPLA2 (100 nM protein) were performed in 25 mM Tris buffer (pH 7.5) with 0.1 mM EDTA and 0.1 mM DTT. Substrates were added at varying concentrations, ranging from 0-200 μM. After preincubation of LYPLA2 for 5 min at 37°C, reactions were initiated with the addition of substrate. Reactions were quenched after 5 min with 1 mL of ethyl acetate containing 20 ng/mL of either PGE_2-d4 (for PGE_2-G and PGD_2-G), $PGF_{2\alpha}$-d4 (for $PGF_{2\alpha}$-G), AA-d_8 (for 2-AG and AEA) or l7:0 lysoPC (for stearoyl and palmitoyl lysoPC). 5 minutes was optimal for determining kinetic parameters for substrates analyzed. The organic layer was collected and dried to completion under nitrogen. Samples were reconstituted in 50% methanol and analyzed by LC-MS/MS. Kinetic parameters were determined by performing non-linear regression analysis using a Michaelis-Menton equation with Prism Graphpad version 5.0d.

Hydrolytic Activity of LYPLA2 Following Small Molecule Inhibition. Inhibition reactions

were conducted in 25 mM Tris buffer (pH 7.5) with 0.1 mM EDTA and 0.1 mM DTT containing 100 nM of recombinant LYPLA2. 100 μL of protein was preincubated with 0-100 μM of either Compound 1 or 21 (131), or the PGE_2-G structural analog (prostaglandin E_2 serinol amide, PGE_2-SA) for 5 min. Reactions were initiated by addition of 5 μM of PGE_2-G and then quenched after 5 min with 1 mL of ethyl acetate containing 20 ng/mL of PGE_2-d4. The organic layer was evaporated to dryness under nitrogen, reconstituted in 50% methanol, and analyzed by LC-MS/MS for PGE_2.

LYPLA2 inhibition in RAW 264.7 murine macrophage-like cells. The effects of LYPLA2 inhibition on PG-G production were tested by exposure of cells to Compound 1. RAW 264.7 cells were plated at 3 x 10^6 cells per 100 mm^2 plate and incubated for 24 h in DMEM supplemented with 10% FBS. Medium was replaced with serum-free DMEM containing either 1 μg/mL of lipopolysaccharide (LPS), 10 μM Compound 1, or a combination of both, and allowed to incubate for 6 h, Cells treated with LPS were then spiked with 5 μM of ionomycin (Calbiochem) for 45 min. Ionomycin stimulates the production of 2-AG and AA from endogenous sources (196). Lipids were extracted from the cell medium by addition of 2x volume of ethyl acetate containing PGE_2-d_4, PGE_2-G-d_5 and AA-d_8 internal standards. The organic layer was dried under nitrogen, and the residue was reconstituted in 50% methanol for analysis of PGs, PG-Gs, and AA by LC-MS/MS.

LYPLA2 inhibition in 1483 Human Squamous Cell Carcinoma. The effects of LYPLA2 inhibition on PG-G production were tested by exposure of cells to Compound 1. 1483 cells were plated at 3 x 10^6 cells per 100 mm^2 plate and incubated for 24 h in RPMI supplemented with 10% FBS. Medium was replaced with serum-free RPMI containing

10 μM Compound 1 and allowed to incubate for 2 h, Cells were then spiked with 5 μM of ionomycin for 45 min. Lipids were extracted from the cell medium by addition of 2x volume of ethyl acetate containing PGE_2-d_4, PGE_2-G-d_5 and AA-d_8 internal standards. The organic layer was dried under nitrogen, and the residue was reconstituted in 50% methanol for analysis of PGs, PG-Gs, and AA by LC-MS/MS.

LC-MS Analytical Procedures. Analysis of prostanoids was accomplished by reverse phase chromatography followed by mass spectrometric detection by selected reaction monitoring (SRM) using a Shimadzu LC-20 HPLC system coupled to an Applied Biosystems 3200 QTrap mass spectrometer. Separation of PGs and LysoPCs was achieved by gradient elution of a Phenomenex Luna C18 column (50mm x 2.0 mm, 3μm particle size). Solvent A was HPLC grade water with 0.1% formic acid, and solvent B was acetonitrile (ACN) with 0.1% formic acid. Samples were injected onto the column with a starting condition of 80% solvent A and 20% solvent B at a flow rate of 0.5 mL/min. A linear gradient of increasing solvent B to 98% was run over 2 min and then held for 1.5 min. SRM transitions were as follows; PGE_2 transition m/z 351.3→271.2, PGE_2-d4 m/z 355.3→275.2, 18:0 lysoPC m/z 524.3→184.3, 17:0 lysoPC m/z 510.3→184.3, 16:0 lysoPC m/z 496.3→184.3.

Resolution of PGs and PG-Gs was accomplished with a gradient formed between solvent A, HPLC grade water with 5mM ammonium acetate (pH 3.6), and solvent B, ACN supplemented with 6% (v/v) of solvent A. Samples were injected onto the column with a starting condition of 70% solvent A and 30% solvent B at a flow rate of 0.6 mL/min. A linear gradient of increasing solvent B to 100% was run over 3.1 min and then held for 1.8 min. SRM transitions were as follows; PGE_2-G transition m/z

444.3→391.3, PGE_2-G-d5 m/z 449.3→396.3, PGE_2 m/z 370.3→317.2, PGE_2-d4 m/z 374.3→321.2.

Resolution of AA was achieved by gradient elution. Solvent A was HPLC grade water with 80 μM silver acetate, and solvent B was methanol with 118 μM silver acetate. Samples were injected onto the column with a starting condition of 80% solvent A and 20% solvent B at a flow rate of 0.4 mL/min. A linear gradient of increasing solvent B to 100% was run over 1 min and then held for 2 min. SRM transition was as follows; AA m/z 518.9→411.1, AA-d8 m/z 526.9→419.1.

Results

Characterization of PGE_2-G Hydrolysis in Cancer Cells

MDA-MB-231 breast cancer cells were initially tested for hydrolytic activity by quantitatively monitoring the formation of PGE_2 from exogenously provided PGE_2-G by LC-MS/MS. As demonstrated in Chapter III, cytosolic fractions showed PGE_2-G hydrolase activity that was linear with time (Figure 2 in Chapter III,). It is important to note that MDA-MB-231 cells do not express detectable levels of MAGL (123). Initial studies demonstrated that the majority of hydrolytic activity was present in the cytosol, with no activity detectable in the membrane fraction (Figure 2 in Chapter III). Importantly, serine hydrolase inventories have been identified and published for multiple cancer cell lines, including MDA-MB-231. In Chapter III, we determined that the serine hydrolase family was responsible for PGE_2-G hydrolysis.

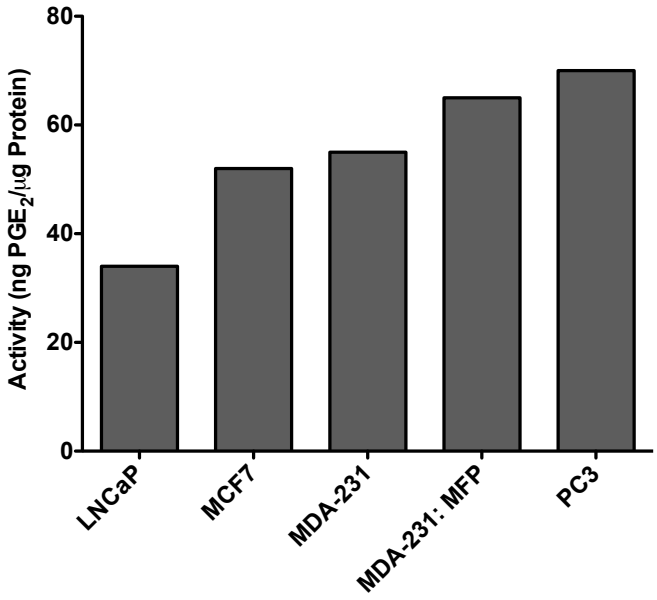

Figure 4: PGE_2-G hydrolase activities in human cancer cells. PGE_2-G hydrolytic activity was assessed across multiple human cancer cell types.

Nomura et al. recently profiled serine hydrolases in a series of human cancer cell lines (123, 156). The serine hydrolase proteome was enriched by covalently labeling the enzymes with fluorophosphonate molecules bound to biotin followed by avidin chromatography. The purified serine hydrolases were identified by multidimensional liquid chromatography mass spectrometry-based proteomic analysis of tryptic digests. Spectral counting, revealed the relative levels of serine hydrolases across a number of aggressive and non-aggressive cancer cell types (123, 156). Utilizing the cancer cell types investigated in these serine hydrolase inventories, we quantified PGE_2-G hydrolysis by the cytosolic fractions of two breast cancer cell lines, MDA-MB-231 and MCF7, and two prostate cancer cell lines, PC3 and LNCaP. Figure 4 demonstrates that LNCaP cells exhibited the lowest hydrolytic activity, while PC3 cells displayed the highest rate of PGE_2-G hydrolysis. All breast cancer cell lines tested, including MCF7, MDA-MB-231

and MDA-MB-231 cells passaged through a mouse fat pad (mfp), exhibited intermediate levels of activity. We compared both MDA-MB-231 cell types because MDA-MB-231 mfp cells express MAGL whereas the MDA-MB-231 do not (123). By comparing the PGE_2-G hydrolytic activity across the cell lines to published inventories of over 60 cytosolic serine hydrolases (Supplemental Table 1) (123, 156), we were able to identify one enzyme, acyl-protein thioesterase 2 (APT2), also referred to lysophospholipase A2 (LYPLA2), that correlated across all data sets.

LYPLA2 Involvement in PGE_2-G Hydrolysis

To investigate the role LYPLA2 plays in PGE_2-G hydrolysis, siRNA knockdown of enzyme expression was initially conducted in MDA-MB-231 cells. The level of LYPLA2 was markedly reduced in MDA-MB-231 cells upon transfection with siRNA as determined by western blot analysis (Figure 5A). Cytosolic fractions obtained from MDA-MB-231 cells following LYPLA2 knockdown displayed a 60% reduction in hydrolysis of PGE_2-G compared to control cells (Figure 5B). The effect of LYPLA2 on PGE_2-G hydrolysis was also reduced upon siRNA transfection in PC3 and LNCaP cell lines (Supplemental Figure 1). MDA-MB-231 cells were transfected with a second siRNA to account for potential off-target effects of the initial siRNA. PC3-, MDA-MB-231-, and LNCaP-transfected cell lines displayed significant decreases in the level of LYPLA2 as determined by western blot analysis (Supplemental Figure 1B). Comparisons of PGE_2-G hydrolytic activity from cytosol obtained from control and LYPLA2 knockdown cells (Supplemental Figure 1A) demonstrated a reduction in hydrolysis of 60% in PC3 cells and 50% in MDA-MB-231 cells, while siRNA

knockdown in LNCaP cells displayed a minor decrease of 25% in hydrolytic activity. This minor decrease in LNCaP hydrolytic activity may be due to lower expression levels of LYPLA2 (123, 156), which would correlate with smaller decreases in activity. However, cells that demonstrate high levels of hydrolytic activity are the most affected by siRNA knockdown of LYPLA2. For example, PC3 and MDA-MB-231 cells show the highest level of hydrolytic activity and upon LYPLA2 knockdown there is a 60% reduction in activity. Taken together, siRNA knockdown across multiple cell lines supports the involvement of LYPLA2 in the major PG-G hydrolysis enzyme in cells with high hydrolytic activity.

To further validate LYPLA2 involvement in PGE_2-G hydrolysis, cDNA for LYPLA2 was transfected and overexpressed in HEK293 cells. Importantly, these cells express no detectable levels of LYPLA2 by western blot (Figure 5C) and have low levels of hydrolase activity against PGE_2-G (Figure 5D). *LYPLA2* was successfully transfected into HEK293 cells, and the cytosolic fraction from the transfected cells demonstrated high expression of LYPLA2 by western blot (Figure 5C) compared to control cells. Importantly, upon overexpression of LYPLA2, HEK293 cytosolic fractions showed a significant increase in PGE_2-G hydrolytic activity compared to fractions from untransfected cells (Figure 5D). Combined with siRNA knockdown data, the overexpression data confirm LYPLA2 as the main serine hydrolase responsible for PGE_2-G hydrolysis in highly hydrolytically active multiple cancer cell lines.

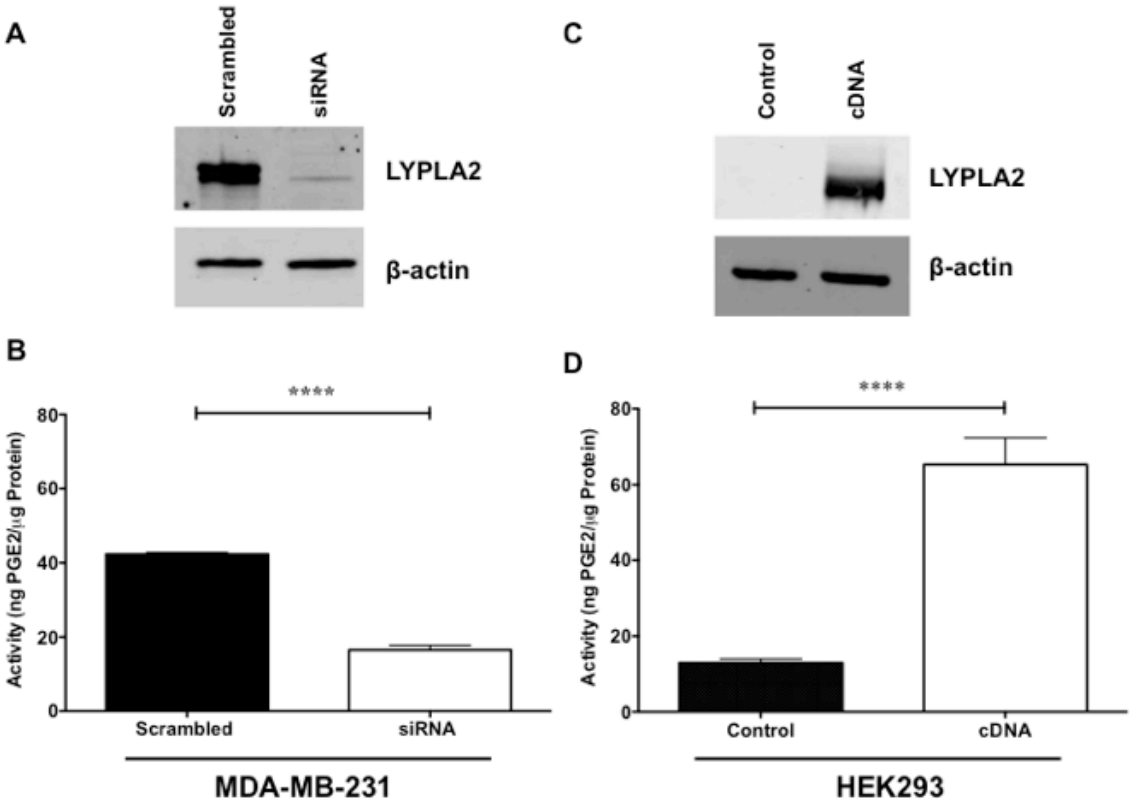

Figure 5: LYPLA2 siRNA knockdown in MDA-MB-231 cells and LYPLA2 overexpression in HEK293. (A) Western blot analysis of LYPLA2 in control MDA-MB-231 cells (scrambled) and LYPLA2-depleted cells (siRNA). β-actin Western blotting verified uniform protein loading (5 μg per lane). (B) PGE_2-G hydrolytic activity of cytosol obtained from MDA-MB-231 control cells (scrambled) or LYPLA2-deficient MDA-MB-231 cells (siRNA). (C) Western blot analysis of LYPLA2 in control HEK293 cells (control) and LYPLA2-overexpressing HEK293 cells (cDNA). β-actin Western blotting verified equaling protein loading (5 μg per lane). (D) PGE_2-G hydrolytic activity of cytosol obtained from HEK293 (control) or LYPLA2-overexpressing (cDNA) cells. Data are presented as the mean ± S.D. of triplicate analyses. **** indicates $p < 0.001$ by t-test.

LYPLA1 Involvement in PGE_2-G Hydrolysis

LYPLA2 is a member of the serine hydrolase family responsible for lysophospholipid metabolism. Additionally, there is a second isoform present in all tested cancer cell lines, named lysophospholipase A1 (LYPLA1). Like LYPLA2, this enzyme is responsible for hydrolysis of lysophospholipids. To investigate the role LYPLA1 plays in PGE_2-G hydrolysis, siRNA knockdown of LYPLA1, LYPLA2 and a combination of both enzymes was conducted in MDA-MB-231 cells. The levels of LYPLA1 and LYPLA2 were markedly reduced in MDA-MB-231 cells upon transfection with siRNA as determined by western blot analysis (Figure 6A and B). Cytosolic fractions obtained from MDA-MB-231 cells following LYPLA1 knockdown displayed a minor reduction in hydrolysis of PGE_2-G compared to control cells (Figure 6). Similar to above, cytosolic fractions from MDA-MB-231 cells following LYPLA2 knockdown displayed a significant reduction in hydrolysis of PGE_2-G compared to control cells. Additionally, cytosolic fractions from cells following knockdown of both LYPLA1 and LYPLA2 together displayed a significant reduction in hydrolysis of PGE_2-G compared to control cells, however there was no additive effects compared to LYPLA2 knockdown alone.

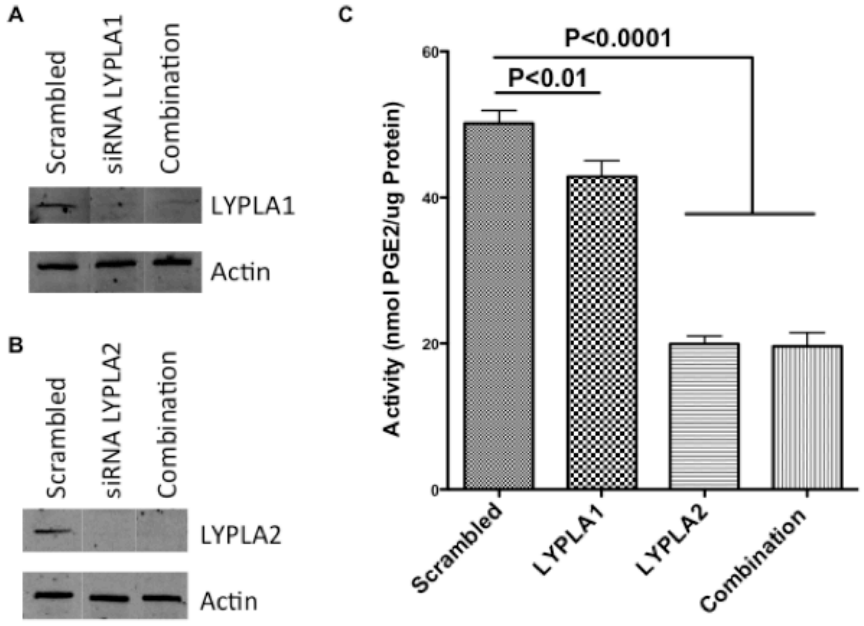

Figure 6: LYPLA1 and LYPLA2 siRNA knockdown in MDA-MB-231 cells. (A) Western blot analysis of LYPLA1 in control MDA-MB-231 cells (scrambled), LYPLA1-depleted cells (siRNA LYPLA1) and LYPLA1/LYPLA2-depleted cells (combination). β-actin Western blotting verified uniform protein loading (5 μg per lane). (B) Western blot analysis of LYPLA2 in control MDA-MB-231 cells (scrambled), LYPLA1-depleted cells (siRNA LYPLA1) and LYPLA1/LYPLA2-depleted cells (combination). β-actin Western blotting verified uniform protein loading (5 μg per lane). (C) PGE_2-G hydrolytic activity of cytosol obtained from MDA-MB-231 control cells (scrambled), LYPLA1-deficient (LYPLA1), LYPLA2-deficient (LYPLA2), or LYPLA1/LYPLA2-deficient MDA-MB-231 cells (combination). Data are presented as the mean ± S.D. of triplicate analyses.

To further validate whether LYPLA1 is involved in PGE_2-G hydrolysis, cDNA for LYPLA1 was transfected and overexpressed in HEK293 cells. *LYPLA1* was successfully transfected into HEK293 cells, and the cytosolic fraction from the transfected cells demonstrated high expression of LYPLA2 by western blot (Figure 7) compared to control cells.

Importantly, upon overexpression of LYPLA1, HEK293 cytosolic fractions showed no significant increase in PGE_2-G hydrolytic activity compared to fractions from

untransfected cells (Figure 5). Unlike the siRNA knockdown data, the overexpression data does not confirm LYPLA1 an additional serine hydrolase responsible for PGE_2-G hydrolysis in highly hydrolytically active cancer cell lines.

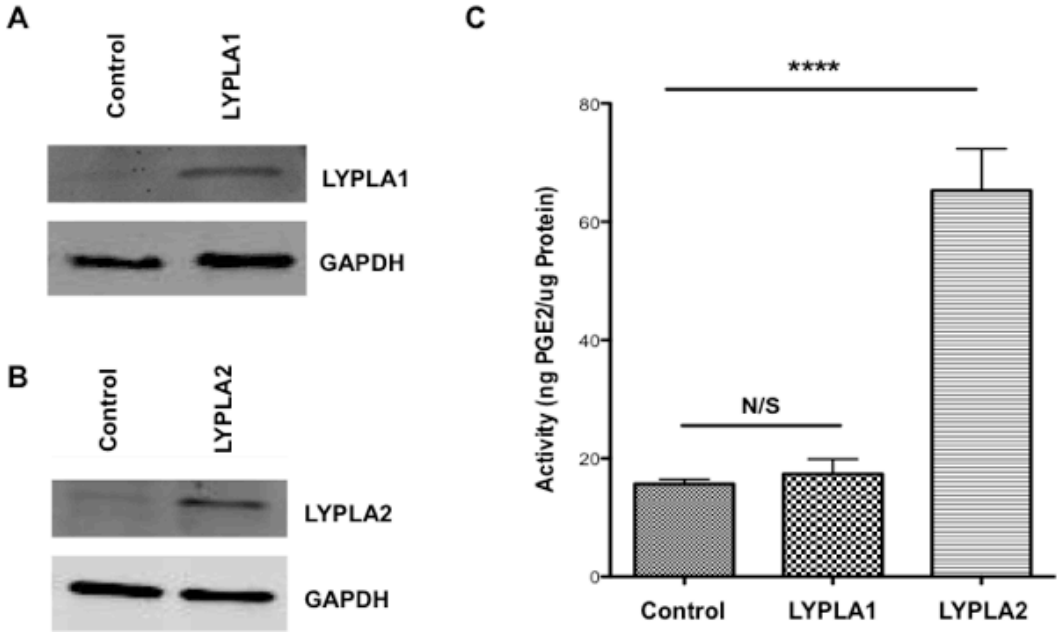

Figure 7: LYPLA1 and LYPLA2 overexpression in HEK293. Western blot analysis of (A) LYPLA1 and (B) LYPLA2 in control HEK293 cells (control), LYPLA1-overexpressing (LYPLA1) and LYPLA2-overexpressing HEK293 cells (LYPLA2). GAPDH Western blotting verified equaling protein loading (5 μg per lane). (B) PGE_2-G hydrolytic activity of cytosol obtained from HEK293 (control), LYPLA1-overexpressing (LYPLA1) or LYPLA2-overexpressing (LYPLA2) cells. Data are presented as the mean ± S.D. of n = 6 per analyses. **** indicates $p < 0.001$ by t-test. N/S = not significant

Expression of Recombinant Human LYPLA1 and LYPLA2

Further validation for LYPLA1 involvement was needed in order to determine whether it is a serine hydrolase involved in PG-G hydrolysis. Expression of human LYPLA1 in *E.coli* caused no significant increase in PGE_2-G hydrolysis while expression of human LYPLA2 in *E.coli* significantly increased PGE_2-G hydrolytic activity as

compared to the activity in wild-type cells (Figure 8). This data in combination with the siRNA knockdown and cDNA overexpression confirms that LYPLA1 is not responsible for PGE_2-G hydrolysis in cells. Importantly, siRNA knockdown, cDNA overexpression and expression in *E.coli* all confirm that LYPLA2 is the hydrolase responsible for hydrolysis in human cells.

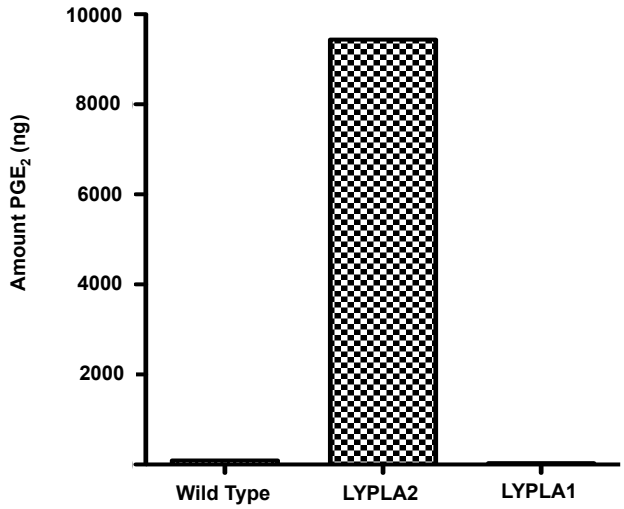

Figure 8: **Production of recombinant human LYPLA1 and LYPLA2 by overexpression in *E.coli***. PGE_2-G hydrolytic activity of cytosol obtained from wild-type *E. coli* and *E. coli* overexpressing recombinant human LYPLA1 or LYPLA2.

Expression, Isolation, and Activity of Recombinant Human LYPLA2

Having demonstrated that only LYPLA2 is involved in PGE_2-G hydrolysis, we next aimed to elucidate the biochemical activities of this serine hydrolase utilizing expressed and purified his-tagged recombinant hLYPLA2. Expression of LYPLA2 or his-tagged LYPLA2 in *E.coli*, significantly increased PGE_2-G hydrolytic activity as compared to the activity in wild-type cells (Figure 9), further confirming LYPLA2 is

capable of hydrolyzing PGE_2-G. Purification of the his-tagged hLYPLA2 (Figure 9), revealed a single band at 25kDa, on Coomassie blue-stained gels and Western blots, correlating to the predicted molecular weight of LYPLA2. On the basis of Coomassie blue staining, the expressed his-tagged hLYPLA2 was >95% pure.

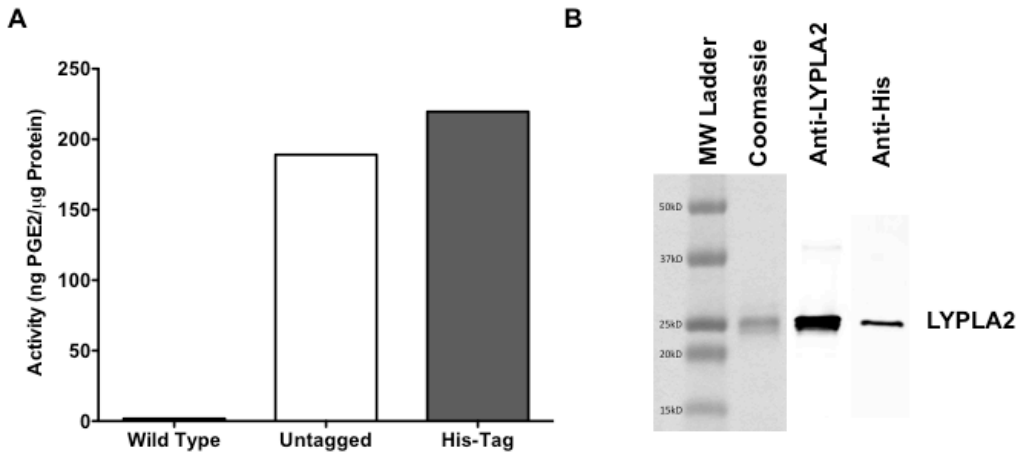

Figure 9: Production of recombinant his-tagged human LYPLA2 by overexpression in *E.coli*. (A) PGE_2-G hydrolytic activity of cytosol obtained from wild-type *E. coli* and *E. coli* overexpressing recombinant human LYPLA2, and recombinant his-tagged human LYPLA2. (B) Coomassie blue staining (left) and Western blot analysis of LYPLA2 (center) and His tag (right) of purified, recombinant his-tagged LYPLA2 produced by *E. coli*.

Lysophospholipids, Endocannabinoids, and Prostaglandin Glycerol Esters as Substrates of Recombinant LYPLA2: A Kinetic Analysis

Because recombinant human LYPLA2 could hydrolyze PGE_2-G to its free acid prostaglandin, we next evaluated kinetics of LYPLA2 hydrolysis against an array of substrates, including multiple PG-Gs (PGE_2-G, PGD_2-G, $PGF_{2\alpha}$-G), endocannabinoids

(2-AG and AEA), and lysophospholipids (palmitic (16:0) or stearic (18:0) lysophosphatidylcholine (lysoPC)). Analysis of substrate concentration-velocity plots (Figure 10) yielded steady-state Michaelis-Menton kinetic parameters (Table 1) for LYPLA2 hydrolytic activity against all substrates tested.

Table 1: Kinetic parameters for hydrolysis of multiple lipid substrates by recombinant human LYPLA2

Substrate	K_{cat} (min^{-1})	Km (μM)	K_{cat}/Km (min^{-1} μM^{-1})
PGE_2-G	**14.1 ± 0.4**	**13 ± 1.1**	**1.08**
$PGF_{2\alpha}$-G	**2.2 ± 0.3**	**5 ± 1.1**	**0.44**
PGD_2-G	**9.5 ± 1.6**	**67 ± 14**	**0.14**
LysoPC (16:0)	**33.3 ± 1.7**	**8.3 ± 1.0**	**4.0**
LysoPC (18:0)	**44.3 ± 10.2**	**7.8 ± 4.4**	**5.6**
2-AG	**N/A**	**N/A**	**N/A**
AEA	**N/A**	**N/A**	**N/A**

Initially, we determined activity towards lysophospholipid substrates and found that the catalytic efficiencies of LYPLA2 for palmitoyl and stearoyl lysoPC (K_{cat}/K_m = 4.0 and 5.6 $min^{-1}\mu M^{-1}$, respectively) were comparable to published values (172). Compared to its activity with lysophospholipids, LYPLA2 had lower hydrolytic efficiency towards PG-Gs. Interestingly, LYPLA2 showed a greater catalytic efficiency for PGE_2-G (K_{cat}/K_m = 1.1 $min^{-1}\mu M^{-1}$) than for $PGF_{2\alpha}$-G and PGD_2-G (K_{cat}/K_m = 0.44 and 0.14 $min^{-1}\mu M^{-1}$, respectively). Importantly, LYPLA2 did not display any catalytic activity against the endocannabinoids, 2-AG and AEA.

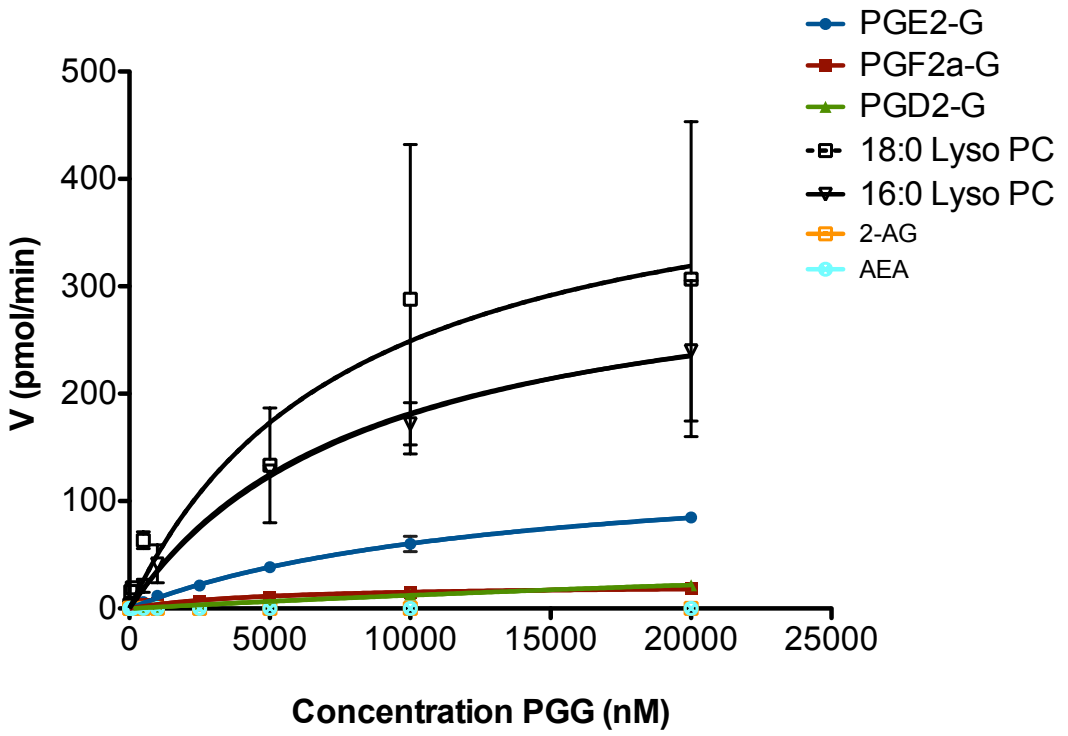

Figure 10: LYPLA2 hydrolytic activity against multiple lipid substrates. Substrate concentration (pmol) vs. reaction velocity (pmol/min) plots for recombinant his-tagged LYPLA2. Data are presented as the mean ± S.D. of triplicate analyses.

Inhibition of Recombinant LYPLA2 Results in Decreased Hydrolysis of PG-Gs

To understand the effect LYPLA2 has in a biological system requires LYPLA2-specific inhibitors. Fortunately, selective inhibitors for LYPLA2 have been discovered and evaluated by Abibekian *et al.* (131). Their inhibitors were identified by high-throughput competitive activity-based protein profiling and showed high specificity for LYPLA2 as compared to other lysophospholipases. In the same study, Abibekian *et al.* also discovered a lysophospholipase A1 specific inhibitor (131). As stated above, lysophospholipase A1 (LYPLA1) is a homologue which shares 60% sequence homology with LYPLA2 (172) but utilizes a wider array of substrates. Inhibitors were named Compound 1 (LYPLA2-specific inhibitor) and Compound 21 (LYPLA1-specific inhibitor). We assessed their effects (Figure 9), on the hydrolytic activity of LYPLA2. Demonstrated in Figure 11, Compound 1 (the selective LYPLA2 inhibitor) has an IC_{50} of 904 nM for the inhibition of PGE_2-G hydrolysis, comparable to previously reported values (510 nM) for the inhibition of hydrolysis of a fluorescence substrate, resorufin acetate (131); Compound 21 (a selective LYPLA1 inhibitor), however, did not affect LYPLA2 activity. A PGE_2-G structural analog, PGE_2-SA, was also assessed for LYPLA2 inhibition. Interestingly, PGE_2-SA had no effect on the hydrolysis of PGE_2-G, indicating the enzyme may have a very tight requirement for substrate binding.

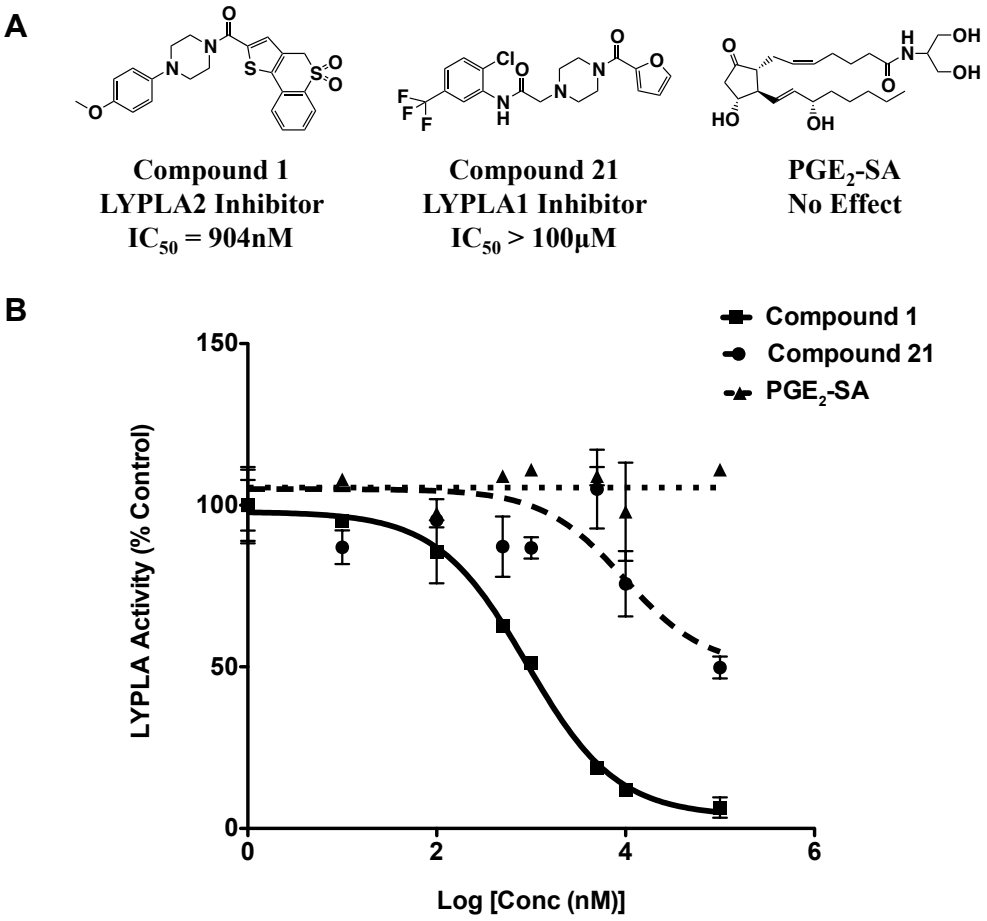

Figure 11: Inhibition of LYPLA2 by small molecule inhibitors. (A) Chemical structures and IC_{50} values for Compound 1(LYPLA2 specific inhibitor), Compound 21 (LYPLA1 specific inhibitor), and PGE_2-SA (structural analog of PGE_2-G). (B) Inhibition curves of LYPLA2-mediated hydrolysis of PGE_2-G by Compound 1 (■), Compound 21 (●), and PGE_2-SA (▲). Data are presented as the mean ± S.D. of triplicate analyses.

LYPLA2 Inhibition Reduced PG-G Hydrolysis in RAW 264.7 Murine Macrophage-Like Cells

To assess the physiological relevance of PG-G hydrolysis by LYPLA2, murine RAW264.7 macrophage-like cells were stimulated to produce PGE_2-G and PGD_2-G by priming cells with LPS (1 μg/mL) to induce expression of COX-2 (Figure 12) followed by treatment with the calcium ionophore ionomycin (5μM) to promote release of 2-AG/AA. We determined whether inhibition of LYPLA2 by Compound 1 could affect the amount of PG-Gs produced in stimulated RAW264.7 cells. Upon simulation, RAW264.7 cells produced high levels of PGD_2 and PGE_2 and much lower levels of PGD_2-G and PGE_2-G, as previously reported (Figure 12). Pretreatment of stimulated RAW264.7 cells with 10 μM of the LYPLA2-specific inhibitor prior to addition of ionomycin, increased the levels of PGD_2/PGE_2-G in the medium compared to those in the medium of uninhibited cells (40 vs 26 pmol). A concomitant decrease in PGD_2/PGE_2 was not observable because of the large excess of prostaglandins to PG-Gs in stimulated RAW cells.

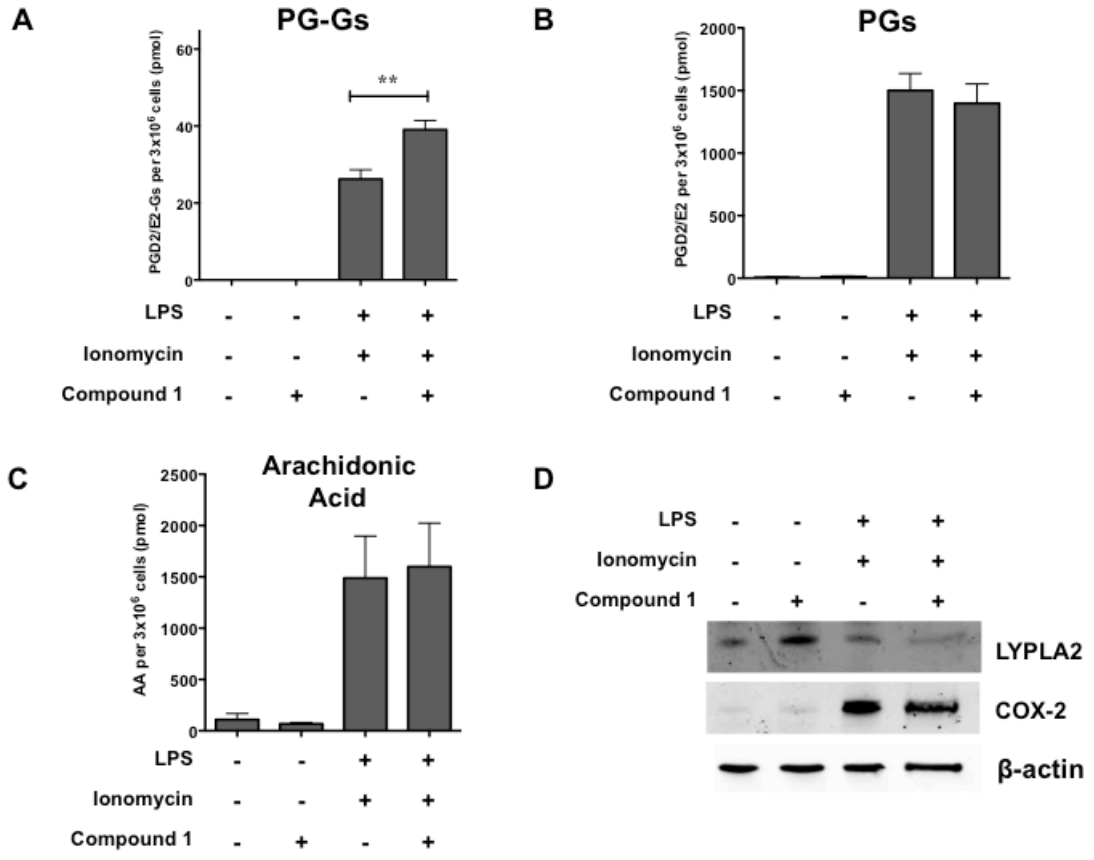

Figure 12: LYPLA2 inhibition significantly increases endogenous levels of PGE_2-G/PGD_2-G formed in RAW264.7 murine macrophage-like cells. Cells were treated with LPS (1 μg/mL) in the presence of absence of a LYPLA2-specific inhibitor (10 μM) for 6 h in serum free medium followed by treatment with ionomycin (5 μM) for 45 min. The culture medium was removed and lipids extracted for LC-MS/MS analysis for PGE_2-G/PGD_2-G (A), PGE_2/PGD_2 (B) and AA (C). (D) Western blot analysis of untreated and treated RAW264.7 macrophages confirmed the expression of COX-2 and LYPLA2 in cells. β-actin western blot verified protein loading (10 μg per lane). Data are presented as the mean ± S.D. of triplicate analyses. ** indicates $p < 0.01$

LYPLA2 Inhibition Reduced PG-G Hydrolysis in 1483 Human Squamous Cell Carcinoma Cells

To assess the physiological relevance of PG-G hydrolysis by LYPLA2 in a human cell setting, 1483 cancer cells were utilized because they constitutively express COX-2 (Figure 13). Ionophore ionomycin (5μM) was added to promote release of 2-AG/AA. We determined whether inhibition of LYPLA2 by Compound 1 could affect the amount of PG-Gs produced in 1483 cancer cells. Upon release of 2-AG and AA, 1483 cancer cells produced levels of PGD_2 and PGE_2 (70 pmol), but at significantly lower levels then those observed in RAW264.7 cells (1500 pmol). Interestingly, comparable levels of $PGF_{2\alpha}$ were also produced (30 pmol) implying that 1483 express high levels of both EP and FP synthases. Additionally, no detectable levels of PGD_2-G and PGE_2-G were observed (data not shown), however there are observable levels of $PGF_{2\alpha}$-G. Pretreatment of 1483 cancer cells with 10 μM of the LYPLA2-specific inhibitor prior to addition of ionomycin, increased the levels $PGF_{2\alpha}$-G in the medium compared to those in the medium of uninhibited cells (7 vs. 4 pmol). A concomitant decrease in $PGF_{2\alpha}$ was not observable because of the large excess of prostaglandins to PG-Gs in these cells. Finally, no change in detectable levels of PGD_2-G and PGE_2-G was observed, implying that there may be a need to understand the relationship between PGH_2 and PGH_2-G and these lipids' interactions with prostaglandin synthases.

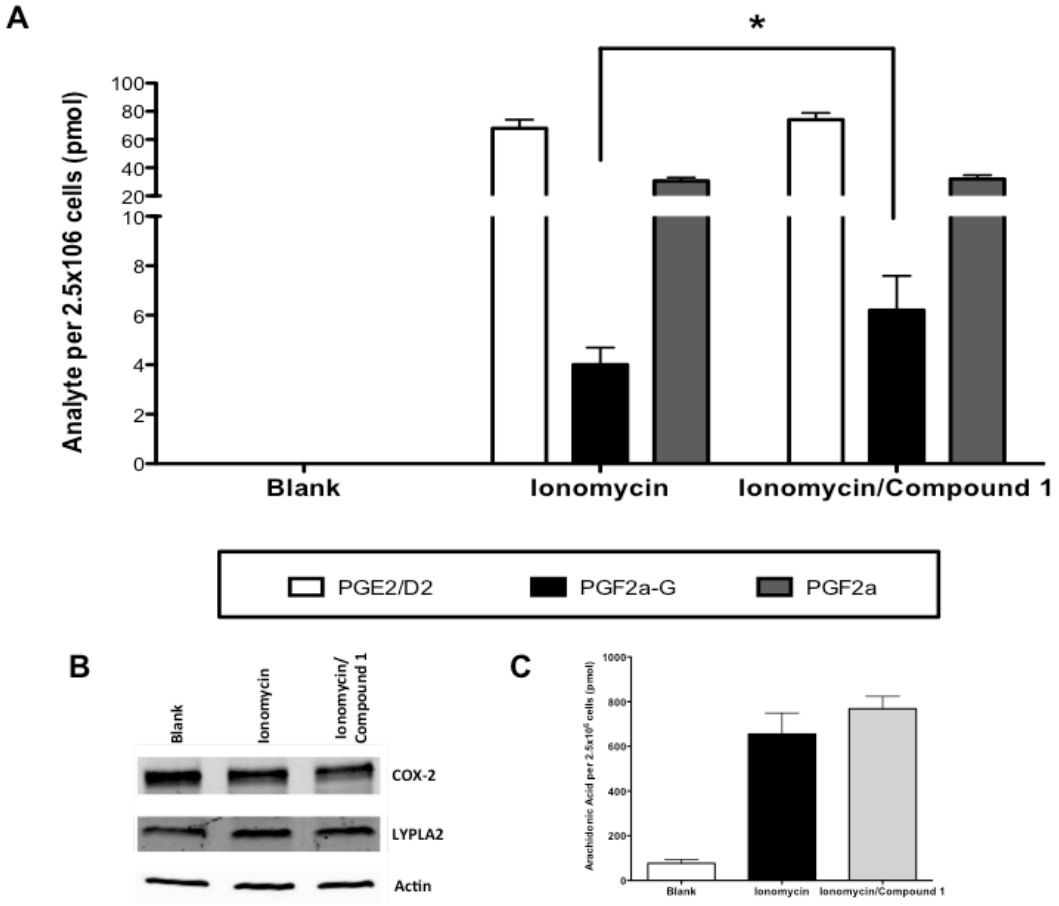

Figure 13: LYPLA2 inhibition significantly increases endogenous levels of $PGF_{2\alpha}$-G formed in 1483 human squamous cell carcinomas. Cells were treated with LYPLA2-specific inhibitor (10 μM) for 2 h in serum free medium followed by treatment with ionomycin (5 μM) for 45 min. The culture medium was removed and lipids extracted for LC-MS/MS analysis PGE_2/PGD_2 (A), $PGF_{2\alpha}$-G (A), $PGF_{2\alpha}$ (A) and AA (C). (B) Western blot analysis of untreated and treated 1483 human caner cells confirmed the constitutive expressionion of COX-2 and LYPLA2 in cells. β-actin western blot verified protein loading (10 μg per lane). Data are presented as the mean ± S.D. of quadruplicate analyses. * indicates $p < 0.01$

Discussion

Endocannabinoids are lipid mediators that elicit a variety of physiological effects, including analgesia and suppression of inflammation (1, 162, 197). COX-2 oxygenates 2-AG to form PG-Gs, which display effects that are frequently opposite those of endocannabinoids, e.g., hyperalgesia and neuroinflammation (82-86, 93, 165). However, complete elucidation of the effects of PG-Gs *in vivo* has been challenging due to their hydrolytic instability (87). The present studies have identified a serine hydrolase, LYPLA2, as a major enzyme responsible for PGE_2-G hydrolysis in human cancer cells.

LYPLA2 was expressed in *E. coli* and purified to apparent homogeneity in order to determine its specific activity against a range of substrates. LYPLA2 exhibited higher catalytic efficiency against lysophospholipids than against PG-Gs. Among the PG-Gs tested, PGE_2-G was the preferred substrate, followed by $PGF_{2\alpha}$-G and PGD_2-G. Remarkably, LYPLA2 displayed no activity against 2-AG or AEA. Thus, LYPLA2 is the first enzyme known to hydrolyze PG-Gs but not their endocannabinoid precursors. LYPLA2 is more active against PG-Gs than the two enzymes previously reported to exhibit PGE_2-G hydrolase activity. LYPLA2's catalytic activity for PGE_2-G is 2 times and 52 times greater than those of CES1 and PPT1, respectively (99). Furthermore, unlike LYPLA2, CES1 and PPT1 are both more active against 2-AG than against PGE_2-G (98, 99, 171). Interestingly, neither CES1 nor PPT1 are present in any of the cancer cell lines used, demonstrating that the majority of PG-G hydrolytic activity in highly enzymatically active cells is LYPLA2.

In human tissues, LYPLAs are widely distributed in multiple tissue types (193). Interestingly, LYPLA2 has a narrower range of lysophospholipid substrates than

LYPLA1. The latter enzyme, which is 60% identical to LYPLA2 in sequence, hydrolyzes a range of lysophospholipids; including lysophosphatidylcholine, lysophosphathidylethanolamine, lysophosphatidylglycerol, lysophosphatidylinositol, and lysophosphatidylserine. Additionally, LYPLA1 displays acyl-protein thioesterase activity, and has the ability to remove the palmitate group from G protein α subunits (198). In contrast, LYPLA2 hydrolyzes only lysophosphatidylcholine and lysophosphathidylethanolamine (186, 187, 189), and exhibits no acyl-protein thioesterase activity. Interestingly, LYPLA2 hydrolyzes PGE_2-G and other PG-Gs while LYPLA1 does not.

A previously reported inhibitor of LYPLA2 effectively reduced PGE_2-G hydrolysis in vitro and increased endogenous levels of PGD_2-G/E_2-G in RAW264.7 cell and $PGF_{2\alpha}$-G in 1483 cell cultures. Optimization of this scaffold may increase the potency of inhibition of PG-G hydrolysis, and it will be interesting to attempt to identify molecules that inhibit PG-G hydrolysis without inhibiting lysophospholipid hydrolysis. Such compounds should be very useful probes of PG-G biology. Furthermore, differential production of $PGF_{2\alpha}$-G or PGD_2-G/E_2-G demonstrates that there may be a larger picture in relation to how PGH_2 and PGH_2-G interact with the prostaglandin synthases. Further understanding into the relationship of prostaglandin precursors and prostaglandin synthases needs to be investigated.

Figure 14 presents an updated metabolic pathway for endocannabinoid metabolism.

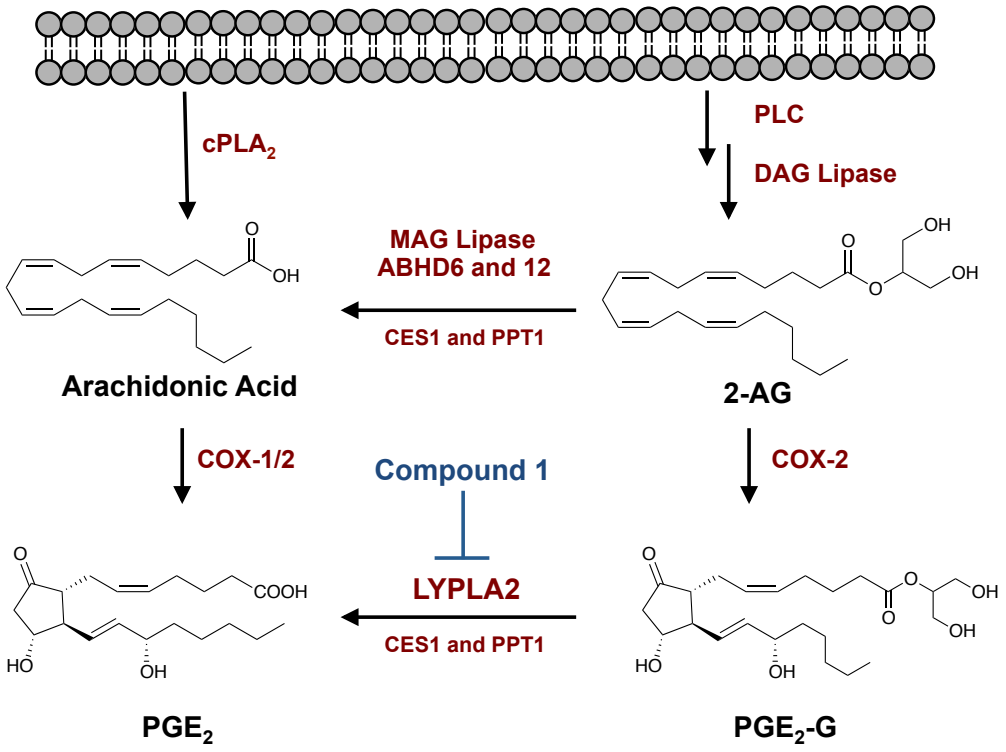

Figure 14: LYPLA2 involvement in the hydrolysis of glycerol prostaglandins in the endocannabinoid metabolism network. Abbreviations: cPLA2, cytosolic phospholipase A2; PLC, phospholipase C; DAGL, diacylglycerol lipase; COX, cyclooxygenase; CES, carboxyesterase; PTT1, Palmitoyl-protein thioesterase; LYPLA2, lysophospholipase A2.

Once 2-AG is released from the membrane by the actions of phospholipase C (PLC) and diacylglycerol lipase (DAGL) (197, 199), 2-AG can either be hydrolyzed by MAGL, ABHD6, or ABHD12 (200, 201), to form AA, or oxidized by COX-2 to form PG-Gs. In human normal and cancer cells, PG-Gs can be hydrolyzed to form free acid prostaglandins by LYPLA2. Inhibition of LYPLA2 can thereby cause an increase in the production of PG-Gs without having an effect on endocannabinoid hydrolysis.

Acknowledgements

We would like to thank the Vanderbilt Antibody and Protein Resource Core, and especially Erin Gribben, for all their help with *E.coli* expression and growth.

Supplemental Information

Activity (ng PGE2/µg protein)	LNCaP	MCF7	231MFP	PC3
Hydrolytic Acitity	**34**	**52**	**65**	**70**
Serine Hydrolases (Spectral Counting)	**LNCaP**	**MCF7**	**231MFP**	**PC3**
FASN Fatty acid synthase	1850	425	348	1324
MGLL monoglyceride lipase	11	7	37	54
FAAH2 Fatty-acid amide hydrolase 2	6	0	0	0
PREP prolyl endopeptidase	455	407	312	423
KIAA1363 (AADACL1 arylacetamide deacetylase-like 1)	58	1	26	373
APEH Acylamino-acid-releasing enzyme	571	145	165	642
PAFAH1B2 Platelet-activating factor acetylhydrolase IB subunit beta	19	84	105	22
PAFAH1B3 Platelet-activating factor acetylhydrolase IB subunit gamma	72	165	154	0
PAFAH2 Platelet-activating factor acetylhydrolase 2, cytoplasmic	19	9	5	22
ABHD2 Abhydrolase domain-containing protein 2	22	0	0	0
ABHD3 Abhydrolase domain-containing protein 3	2	0	0	7
ABHD4 Abhydrolase domain-containing protein 4	27	0	0	5
ABHD6 Abhydrolase domain-containing protein 6	55	0	1	62
ABHD10 Abhydrolase domain-containing protein 10	622	112	274	534
ABHD11 Abhydrolase domain-containing protein 11	258	169	64	136
ABHD12 Abhydrolase domain-containing protein 12	109	0	1	107
ABHD13 Abhydrolase domain-containing protein 13	2	0	0	1
LYPLA1 Acyl-protein thioesterase 1	81	92	42	21
LYPLA2 Acyl-protein thioesterase 2	31	95	97	138
LYPLAL1 Lysophospholipase-like protein 1	73	44	40	25
DPP4 Dipeptidyl peptidase 4	38	0	0	89
DPP7 similar to Dipeptidyl-peptidase 2	170	3	1	14
DPP8 Dipeptidyl peptidase 8	9	15	12	16
DPP9 Dipeptidyl peptidase 9	50	57	84	445
CES1 Liver carboxylesterase 1	0	0	0	0
CES2 carboxylesterase 2	18	11	12	8
CES3 esterase 3	2	0	0	0
PPT1 Palmitoyl-protein thioesterase 1	1	0	0	0
PPT2 palmitoyl-protein thioesterase 2	3	4	21	22
PRCP prolylcarboxypeptidase isoform 2 preproprotein	77	25	19	49
PREPL prolyl endopeptidase-like isoform C	63	33	30	98
RBBP9 Retinoblastoma-binding protein 9	9	23	29	10
PNPLA8 Patatin-like phospholipase domain-containing protein 8	15	0	0	11
PNPLA6 Neuropathy target esterase	46	0	1	211
PNPLA4 Patatin-like phospholipase domain-containing protein 4	49	3	6	42
SIAE Sialate O-acetylesterase	94	19	26	10
CTSA cathepsin A precursor	12	25	11	8
PPME1 Protein phosphatase methylesterase 1	63	20	17	48
Abhydrolase domain-containing protein FAM108A1	7	0	0	8
Abhydrolase domain-containing protein FAM108B1	12	0	0	31
PARL Presenilins-associated rhomboid-like protein	8	0	0	8
CPVL Probable serine carboxypeptidase	0	0	7	27
DAGLB Sn1-specific diacylglycerol lipase beta	6	0	0	20
PLAT Tissue-type plasminogen activator precursor	0	0	1	9
LIPA, highly similar to lysosomal acid lipase/cholesteryl ester hydrolase	0	0	5	0
HTRA1 Serine protease HTRA1	0	0	0	0
PGAP1 GPI inositol-deacylase	0	0	0	2
SCPEP Retinoid-inducible serine carboxypeptidase	121	0	0	47
PLAU urokinase plasminogen activator	0	0	0	1
PLA2G4A Cytosolic phospholipase A2	0	0	0	1
IAH1 Isoamyl acetate-hydrolyzing esterase 1	2	6	5	5
QRSL1 Glutaminyl-tRNA synthase-like protein 1	1	1	1	0
BCHE Cholinesterase precursor	10	0	0	0
BAT5	28	0	0	20
LACTB	2	0	0	2

Supplemental Data 1. Activity-based protein profiling, multidimensional protein identification technology (ABPP-MuDPIT) analysis of serine hydrolases in human cancer cell lines (123, 156). PGE_2-G hydrolase activity was compared to known serine hydrolase inventories.

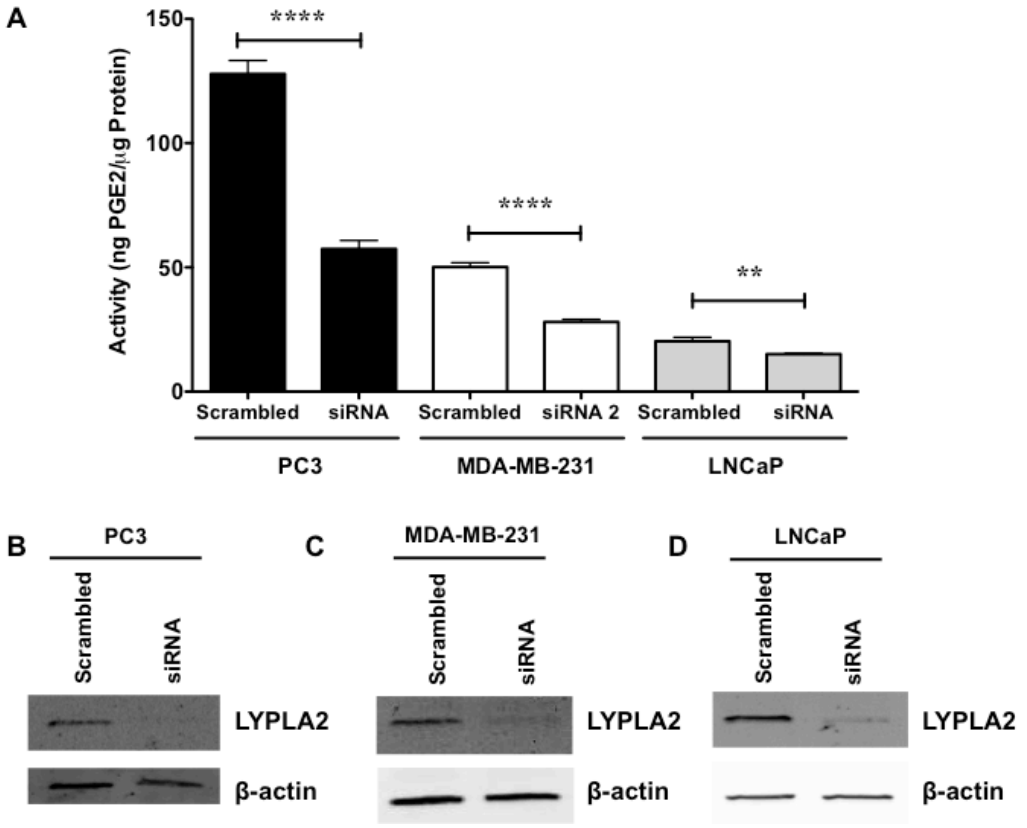

Supplemental Data 2: LYPLA2 siRNA knockdown in PC3, MDA-MB-231, and LNCaP cells. (A) PGE_2-G hydrolytic activity of cytosol obtained from PC3, MDA-MB-231, and LNCaP control (scrambled) or LYPLA2-deficient (siRNA) cells. Western blot analysis of LYPLA2 in control (scrambled) and LYPLA2-depleted (siRNA) PC3 (B), MDA-MB-231 (C), or LNCaP (D) cells. β-actin Western blotting verified equaling protein loading (5 μg per lane). Data are presented as the mean ± S.D. of triplicate analyses. **** indicates $p < 0.001$. ** indicates $p < 0.01$.

Chapter V

SUMMARY

COX-2 catalyzes the oxidation of free fatty acids such as arachidonic acid during pathogenic states, including pain and inflammation. This leads to the production of pro-inflammatory lipid molecules known as prostaglandins. These prostaglandins mediate a wide array of physiological and pathophysiological effects, including pain, inflammation, and fever. Additionally, COX-2 can oxidize the endocannabinoids, 2-arachidonoyl glycerol (2-AG) and arachidonylethanolamine (AEA), to form the prostaglandin derivatives, prostaglandin glycerol esters (PG-Gs) and prostaglandin ethanolamines (PG-EA). These prostaglandin derivatives have been shown to play unique roles on yet unidentified receptors throughout the body; eliciting pro-inflammatory responses, anti-inflammatory responses, hyperalgesia and neurotoxicity.

Though PG-G can elicit a wide array of biological responses in an *in vitro* setting, understanding *in vivo* effects of these lipid metabolites has been difficult due to hydrolytic instability. It has been shown that PGE_2-G is rapidly hydrolyzed in rat plasma post intravenous administration. This instability was attributed to the presence of plasma esterases that hydrolyze PG-Gs. Initially, the endocannabinoid hydrolyzing enzymes, FAAH and MAGL, were examined as potential PG-G hydrolyzing enzymes but kinetic analysis showed that neither enzyme efficiently hydrolysis. Inhibitor studies lead to the identification of CES1 and PPT1 as serine hydrolases capable of hydrolyzing both 2-G

and PG-Gs, though with both enzymes having higher affinity for 2-AG. Multiple human cancer cells possess high activity levels for PG-G hydrolysis and do not express CES1 and/or PPT1. The goal of my work was to identify the hydrolase responsible for PG-G hydrolysis in human cancer cell lines.

Firstly, we developed a high-throughput analytical method in order to facilitate analysis during purification of the active enzyme. The most widely used methods for PG and PG-G analysis employ chromatographic separation followed by mass spectrometric analysis, which requires significant time for sample preparation and sequential chromatography. We developed a high-throughput, separation-free methodology based on MALDI mass spectrometry that allowed for the parallel analysis of prostaglandins and prostaglandin glycerol esters. Utilizing derivatization techniques with Girard's reagent T we were able to incorporate a charged moiety into ketone-containing prostaglandins causing a dramatic increase in the signal-to-noise ratio relative to underivatized samples. This derivatization resulted in an increased dynamic range and improved linearity. Additionally, this method was adapted for high-throughput screening methods for enzymology and drug discovery.

Initially, MDA-MB-231 cellular fractionation studies demonstrated that the protein of interest was a cytosolic protein, with no major activity present in the membrane. Furthermore, because many of the lipid-hydrolyzing enzymes are serine hydrolases, we utilized a fluorophosphonate serine hydrolase inhibitor to verify that the unknown hydrolase was a member of the serine hydrolase superfamily. Understanding the cellular location and enzyme superfamily made purification simpler for two reasons: first, membrane protein purification requires the use of detergents, which can hinder

some forms of purification and second, because it allowed us to use very well developed ABPP techniques to identify the hydrolase. Utilizing protein purification techniques coupled with mass spectrometric proteomics, we ventured to identify the hydrolase responsible for PG-G hydrolysis in MDA-MB-231 cancer cells. Multiple purification steps led to the identification of three serine hydrolases as potential PG-G hydrolase targets; namely 6-phosphoglucolatonase (PGLS), dimethylarginine dimethylaminohydrolase 2 (DDAH2), and platelet activating factor acetylhydrolase 1β3 subunit (PAFAH1β3). All identified proteins were heterologously expressed in HEK293 cells, with only PGLS demonstrating a minor increase in hydrolytic activity compared to untransfected cells. Unfortunately, upon siRNA knockdown of PGLS in MDA-MB-231 cancer cells, no change in hydrolytic activity was observed. These results caused us to reevaluate how we went about identifying the unknown PG-G serine hydrolase.

A data comparison between serine hydrolase inventories/activities and PG-G hydrolase activity was utilized to determine the serine hydrolase of interest. By comparing PG-G hydrolytic activity across a number of human cancer cell types to serine hydrolase activity levels determined by activity-based protein profiling, we were able to identify the cytosolic lysophospholipid-metabolizing enzyme, lysophospholipase A2 (LYPLA2), as the major hydrolase responsible for PG-G hydrolysis. The importance of LYPLA2 in PGE_2-G hydrolysis was confirmed by siRNA knockdown across various cancer cell types. Heterologous expression of LYPLA2 in HEK293 cells also increased PGE_2-G hydrolysis. The LYPLA2 isoform, lysophophospholipase A1 (LYPLA1), was also assessed for hydrolytic activity. It was hypothesized that LYPLA1 may also play a role in PG-G hydrolysis because the enzyme shares 60% sequence homology with

LYPLA2 and also catalyzes the same lysophospholipid metabolism. However, upon siRNA knockdown of LYPLA1 in MDA-MB-231 cancer cells, heterologous expression of LYPLA1 in HEK293 cells, or recombinant expression of LYPLA1 in *E.coli*, no change in PGE_2-G hydrolytic activity was observed. These results confirmed that LYPLA2 was the major serine hydrolase responsible for PG-G hydrolysis in highly hydrolytically active cell lines.

Identification of LYPLA2 helped us understand why there was a significant decrease in hydrolytic activity during the MDA-MB-231 purification. It has been reported that during purification of LYPLA2, steps must be taken in order to ensure the stability of the protein. Addition of stabilizing agents such as 60-70% glycerol or exogenously added protein, such as cytochrome c, must be made in order to stabilize LYPLA2 during and after purification. Additionally, work has shown that LYPLA2 is only stable at pH range 6 to 7.5. Since the Mono P column was run from pH range 7 to 4, LYPLA2 may have been destabilized/degraded during this step in the purification.

Expression of LYPLA2 in *E.coli* led to the isolation and purification of active enzyme. Substrate kinetics were determined with the relative activities against a series of PG-Gs being PGE_2-G > $PGF_{2\alpha}$-G > PGD_2-G. Interestingly, LYPLA2 did not hydrolyze the endocannabinoids, 2-AG or AEA. Unlike CES1 and PPT1, LYPLA2 is the first PG-G hydrolyzing enzyme that is not capable of hydrolyzing the endocannabinoids. LYPLA2 has a narrower range of lysophospholipid substrates than LYPLA1, which hydrolyzes the majority of lysophospholipids, including lysophosphatidylcholine, lysophosphatidylethanolamine, lysophosphatidylglycerol, lysophosphatidylinositol, and lysophosphatidylserine. In contrast, LYPLA2 hydrolyzes only lysophosphatidylcholine

and lysophosphatidylethanolamine. There is very little known about LYPLA2, particularly why this isoform has much greater specificity compared to LYPLA1. Further investigation is needed to understand what residues are important for LYPLA2 specificity. Site-directed mutagenesis should be performed in order to identify these important residues. Since LYPLA1 and LYPLA2 share 60% sequence homology and LYPLA1 has a crystal structure, selection of residues for mutation can be accomplished by comparing the LYPLA2 sequence to LYPLA1. Based on the crystal structure of LYPLA1, determining what residues are different between the two enzymes within the active site will help explain substrate differences between LYPLA1 and LYPLA2. Finally, obtaining a crystal structure, as well as structures with both lysophospholipids and PG-Gs bounds, will also help elucidate important residues for binding.

Chemical inhibition of LYPLA2 in the RAW264.7 murine macrophage-like cell line and the 1483 human head-and-neck squamous cell carcinoma elicited an increase in PG-G production. These were the first examples in cell culture of increases in endogenously produced PG-Gs following inhibitor treatment. Interestingly, in human cancer cells the predominant PG-G produced was $PGF_{2\alpha}$-G and not PGD_2-G/E_2-G. Differential production of $PGF_{2\alpha}$-G compared to PGD_2-G/E_2-G potentially demonstrates that there may be a relation between PGH_2 and PGH_2-G interactions with the prostaglandin synthases. Further investigations into the relationship of prostaglandin precursors and prostaglandin synthases needs to be undertaken. Moreover, cancer cells may need to hydrolyze $PGF_{2\alpha}$-G over other PG-Gs because they may be detrimental to the survival and growth of the cancer cells. Additional studies need to be conducted to understand the effects various PG-Gs play on cancer cell survival and growth.

Identification of LYPLA2 as a major PG-G hydrolase will enable modulation of its activity to evaluate its importance as a regulator of cell signaling by this unique class of bioactive lipids. There are a number of different approaches that can be taken in order to investigate LYPLA2's importance *in vivo*. By having inhibitor compounds developed, and potentially expanded upon, we can further understand LYPLA2 and its role in living systems. Additionally, genetic knockout of LYPLA2 may allow for *in vivo* increases in PG-G, which will expand our understanding of PG-G function in physiological and pathophysiological settings.

REFERENCES

1. Piomelli D. The molecular logic of endocannabinoid signalling. Nat Rev Neurosci. 2003;4(11):873-84.

2. Zias J, Stark H, Sellgman J, Levy R, Werker E, Breuer A, et al. Early medical use of cannabis. Nature. 1993;363(6426):215.

3. Matsuda LA, Lolait SJ, Brownstein MJ, Young AC, Bonner TI. Structure of a cannabinoid receptor and functional expression of the cloned cDNA. Nature. 1990;346(6284):561-4.

4. Munro S, Thomas KL, Abu-Shaar M. Molecular characterization of a peripheral receptor for cannabinoids. Nature. 1993;365(6441):61-5.

5. Devane WA, Hanus L, Breuer A, Pertwee RG, Stevenson LA, Griffin G, et al. Isolation and structure of a brain constituent that binds to the cannabinoid receptor. Science. 1992;258(5090):1946-9.

6. Sugiura T, Kondo S, Sukagawa A, Nakane S, Shinoda A, Itoh K, et al. 2-Arachidonoylglycerol: a possible endogenous cannabinoid receptor ligand in brain. Biochemical and biophysical research communications. 1995;215(1):89-97.

7. Devane WA, Dysarz FA, 3rd, Johnson MR, Melvin LS, Howlett AC. Determination and characterization of a cannabinoid receptor in rat brain. Mol Pharmacol. 1988;34(5):605-13.

8. Herkenham M, Lynn AB, Johnson MR, Melvin LS, de Costa BR, Rice KC. Characterization and localization of cannabinoid receptors in rat brain: a quantitative in vitro autoradiographic study. J Neurosci. 1991;11(2):563-83.

9. Howlett AC, Bidaut-Russell M, Devane WA, Melvin LS, Johnson MR, Herkenham M. The cannabinoid receptor: biochemical, anatomical and behavioral characterization. Trends Neurosci. 1990;13(10):420-3.

10. Rodriguez de Fonseca F, Del Arco I, Bermudez-Silva FJ, Bilbao A, Cippitelli A, Navarro M. The endocannabinoid system: physiology and pharmacology. Alcohol Alcohol. 2005;40(1):2-14.

11. Galiegue S, Mary S, Marchand J, Dussossoy D, Carriere D, Carayon P, et al. Expression of central and peripheral cannabinoid receptors in human immune tissues and leukocyte subpopulations. Eur J Biochem. 1995;232(1):54-61.

12. Rueda D, Navarro B, Martinez-Serrano A, Guzman M, Galve-Roperh I. The endocannabinoid anandamide inhibits neuronal progenitor cell differentiation through attenuation of the Rap1/B-Raf/ERK pathway. J Biol Chem. 2002;277(48):46645-50.

13. Felder CC, Joyce KE, Briley EM, Glass M, Mackie KP, Fahey KJ, et al. LY320135, a novel cannabinoid CB1 receptor antagonist, unmasks coupling of the CB1 receptor to stimulation of cAMP accumulation. J Pharmacol Exp Ther. 1998;284(1):291-7.

14. Gebremedhin D, Lange AR, Campbell WB, Hillard CJ, Harder DR. Cannabinoid CB1 receptor of cat cerebral arterial muscle functions to inhibit L-type Ca2+ channel current. Am J Physiol. 1999;276(6 Pt 2):H2085-93.

15. Twitchell W, Brown S, Mackie K. Cannabinoids inhibit N- and P/Q-type calcium channels in cultured rat hippocampal neurons. J Neurophysiol. 1997;78(1):43-50.

16. Mackie K, Hille B. Cannabinoids inhibit N-type calcium channels in neuroblastoma-glioma cells. Proc Natl Acad Sci U S A. 1992;89(9):3825-9. PMCID: 525583.

17. Schlicker E, Kathmann M. Modulation of transmitter release via presynaptic cannabinoid receptors. Trends Pharmacol Sci. 2001;22(11):565-72.

18. Wilson RI, Nicoll RA. Endogenous cannabinoids mediate retrograde signalling at hippocampal synapses. Nature. 2001;410(6828):588-92.

19. Bouaboula M, Perrachon S, Milligan L, Canat X, Rinaldi-Carmona M, Portier M, et al. A selective inverse agonist for central cannabinoid receptor inhibits mitogen-activated protein kinase activation stimulated by insulin or insulin-like growth factor 1. Evidence for a new model of receptor/ligand interactions. J Biol Chem. 1997;272(35):22330-9.

20. Derkinderen P, Toutant M, Burgaya F, Le Bert M, Siciliano JC, de Franciscis V, et al. Regulation of a neuronal form of focal adhesion kinase by anandamide. Science. 1996;273(5282):1719-22.

21. Howlett AC, Barth F, Bonner TI, Cabral G, Casellas P, Devane WA, et al. International Union of Pharmacology. XXVII. Classification of cannabinoid receptors. Pharmacol Rev. 2002;54(2):161-202.

22. Hillard CJ, Manna S, Greenberg MJ, DiCamelli R, Ross RA, Stevenson LA, et al. Synthesis and characterization of potent and selective agonists of the neuronal cannabinoid receptor (CB1). J Pharmacol Exp Ther. 1999;289(3):1427-33.

23. Stella N, Schweitzer P, Piomelli D. A second endogenous cannabinoid that modulates long-term potentiation. Nature. 1997;388(6644):773-8.

24. Di Marzo V, Fontana A, Cadas H, Schinelli S, Cimino G, Schwartz JC, et al. Formation and inactivation of endogenous cannabinoid anandamide in central neurons. Nature. 1994;372(6507):686-91.

25. Sugiura T, Kondo S, Sukagawa A, Tonegawa T, Nakane S, Yamashita A, et al. Transacylase-mediated and phosphodiesterase-mediated synthesis of N-arachidonoylethanolamine, an endogenous cannabinoid-receptor ligand, in rat brain microsomes. Comparison with synthesis from free arachidonic acid and ethanolamine. Eur J Biochem. 1996;240(1):53-62.

26. Cadas H, di Tomaso E, Piomelli D. Occurrence and biosynthesis of endogenous cannabinoid precursor, N-arachidonoyl phosphatidylethanolamine, in rat brain. J Neurosci. 1997;17(4):1226-42.

27. Cadas H, Gaillet S, Beltramo M, Venance L, Piomelli D. Biosynthesis of an endogenous cannabinoid precursor in neurons and its control by calcium and cAMP. J Neurosci. 1996;16(12):3934-42.

28. Natarajan V, Schmid PC, Reddy PV, Schmid HH. Catabolism of N-acylethanolamine phospholipids by dog brain preparations. J Neurochem. 1984;42(6):1613-9.

29. Sun YX, Tsuboi K, Okamoto Y, Tonai T, Murakami M, Kudo I, et al. Biosynthesis of anandamide and N-palmitoylethanolamine by sequential actions of phospholipase A2 and lysophospholipase D. Biochem J. 2004;380(Pt 3):749-56. PMCID: 1224205.

30. Wang J, Okamoto Y, Morishita J, Tsuboi K, Miyatake A, Ueda N. Functional analysis of the purified anandamide-generating phospholipase D as a member of the metallo-beta-lactamase family. J Biol Chem. 2006;281(18):12325-35.

31. Simon GM, Cravatt BF. Endocannabinoid biosynthesis proceeding through glycerophospho-N-acyl ethanolamine and a role for alpha/beta-hydrolase 4 in this pathway. J Biol Chem. 2006;281(36):26465-72.

32. Simon GM, Cravatt BF. Characterization of mice lacking candidate N-acyl ethanolamine biosynthetic enzymes provides evidence for multiple pathways that contribute to endocannabinoid production in vivo. Mol Biosyst. 2010;6(8):1411-8. PMCID: 2946841.

33. Hillard CJ, Jarrahian A. The movement of N-arachidonoylethanolamine (anandamide) across cellular membranes. Chemistry and physics of lipids. 2000;108(1-2):123-34.

34. Beltramo M, Stella N, Calignano A, Lin SY, Makriyannis A, Piomelli D. Functional role of high-affinity anandamide transport, as revealed by selective inhibition. Science. 1997;277(5329):1094-7.

35. Schmid PC, Zuzarte-Augustin ML, Schmid HH. Properties of rat liver N-acylethanolamine amidohydrolase. J Biol Chem. 1985;260(26):14145-9.

36. Hillard CJ, Wilkison DM, Edgemond WS, Campbell WB. Characterization of the kinetics and distribution of N-arachidonylethanolamine (anandamide) hydrolysis by rat brain. Biochim Biophys Acta. 1995;1257(3):249-56.

37. Ueda N, Kurahashi Y, Yamamoto S, Tokunaga T. Partial purification and characterization of the porcine brain enzyme hydrolyzing and synthesizing anandamide. J Biol Chem. 1995;270(40):23823-7.

38. Cravatt BF, Giang DK, Mayfield SP, Boger DL, Lerner RA, Gilula NB. Molecular characterization of an enzyme that degrades neuromodulatory fatty-acid amides. Nature. 1996;384(6604):83-7.

39. Fu J, Gaetani S, Oveisi F, Lo Verme J, Serrano A, Rodriguez De Fonseca F, et al. Oleylethanolamide regulates feeding and body weight through activation of the nuclear receptor PPAR-alpha. Nature. 2003;425(6953):90-3.

40. Mazzari S, Canella R, Petrelli L, Marcolongo G, Leon A. N-(2-hydroxyethyl)hexadecanamide is orally active in reducing edema formation and inflammatory hyperalgesia by down-modulating mast cell activation. European journal of pharmacology. 1996;300(3):227-36.

41. Calignano A, La Rana G, Giuffrida A, Piomelli D. Control of pain initiation by endogenous cannabinoids. Nature. 1998;394(6690):277-81.

42. Kozak KR, Marnett LJ. Oxidative metabolism of endocannabinoids. Prostaglandins, leukotrienes, and essential fatty acids. 2002;66(2-3):211-20.

43. Prescott SM, Majerus PW. Characterization of 1,2-diacylglycerol hydrolysis in human platelets. Demonstration of an arachidonoyl-monoacylglycerol intermediate. J Biol Chem. 1983;258(2):764-9.

44. Sugiura T, Waku K. 2-Arachidonoylglycerol and the cannabinoid receptors. Chemistry and physics of lipids. 2000;108(1-2):89-106.

45. Wang J, Ueda N. Biology of endocannabinoid synthesis system. Prostaglandins Other Lipid Mediat. 2009;89(3-4):112-9.

46. Farooqui AA, Rammohan KW, Horrocks LA. Isolation, characterization, and regulation of diacylglycerol lipases from the bovine brain. Annals of the New York Academy of Sciences. 1989;559:25-36.

47. Tsutsumi T, Kobayashi T, Ueda H, Yamauchi E, Watanabe S, Okuyama H. Lysophosphoinositide-specific phospholipase C in rat brain synaptic plasma membranes. Neurochem Res. 1994;19(4):399-406.

48. Ueda H, Kobayashi T, Kishimoto M, Tsutsumi T, Okuyama H. A possible pathway of phosphoinositide metabolism through EDTA-insensitive phospholipase A1 followed by lysophosphoinositide-specific phospholipase C in rat brain. J Neurochem. 1993;61(5):1874-81.

49. Dinh TP, Carpenter D, Leslie FM, Freund TF, Katona I, Sensi SL, et al. Brain monoglyceride lipase participating in endocannabinoid inactivation. Proc Natl Acad Sci U S A. 2002;99(16):10819-24. PMCID: 125056.

50. Goparaju SK, Ueda N, Yamaguchi H, Yamamoto S. Anandamide amidohydrolase reacting with 2-arachidonoylglycerol, another cannabinoid receptor ligand. FEBS letters. 1998;422(1):69-73.

51. Lichtman AH, Hawkins EG, Griffin G, Cravatt BF. Pharmacological activity of fatty acid amides is regulated, but not mediated, by fatty acid amide hydrolase in vivo. J Pharmacol Exp Ther. 2002;302(1):73-9.

52. Dinh TP, Freund TF, Piomelli D. A role for monoglyceride lipase in 2-arachidonoylglycerol inactivation. Chemistry and physics of lipids. 2002;121(1-2):149-58.

53. Gulyas AI, Cravatt BF, Bracey MH, Dinh TP, Piomelli D, Boscia F, et al. Segregation of two endocannabinoid-hydrolyzing enzymes into pre- and postsynaptic compartments in the rat hippocampus, cerebellum and amygdala. The European journal of neuroscience. 2004;20(2):441-58.

54. Stone E. An account of the success of the bark of the willow in the cure of agues. Philos Trans R Soc Lond1753. p. 195-200.

55. 100 Years of Aspirin. Leverkusen: Bayer AG Consumer Care Business Group.

56. Hawkey CJ. COX-2 chronology. Gut. 2005;54(11):1509-14. PMCID: 1774747.

57. Jack DB. One hundred years of aspirin. Lancet. 1997;350(9075):437-9.

58. Botting RM. Vane's discovery of the mechanism of action of aspirin changed our understanding of its clinical pharmacology. Pharmacol Rep. 2010;62(3):518-25.

59. Vane JR. Inhibition of prostaglandin synthesis as a mechanism of action for aspirin-like drugs. Nat New Biol. 1971;231(25):232-5.

60. Smith JB, Willis AL. Aspirin selectively inhibits prostaglandin production in human platelets. Nat New Biol. 1971;231(25):235-7.

61. Smith WL, DeWitt DL, Garavito RM. Cyclooxygenases: structural, cellular, and molecular biology. Annu Rev Biochem. 2000;69:145-82.

62. Rouzer CA, Marnett LJ. Mechanism of free radical oxygenation of polyunsaturated fatty acids by cyclooxygenases. Chem Rev. 2003;103(6):2239-304.

63. Garavito RM, Malkowski MG, DeWitt DL. The structures of prostaglandin endoperoxide H synthases-1 and -2. Prostaglandins Other Lipid Mediat. 2002;68-69:129-52.

64. Rouzer CA, Marnett LJ. Cyclooxygenases: structural and functional insights. J Lipid Res. 2009;50 Suppl:S29-34.

65. Kulmacz RJ, Lands WE. Prostaglandin H synthase. Stoichiometry of heme cofactor. J Biol Chem. 1984;259(10):6358-63.

66. Kulmacz RJ, Lands WE. Stoichiometry and kinetics of the interaction of prostaglandin H synthase with anti-inflammatory agents. J Biol Chem. 1985;260(23):12572-8.

67. Yuan C, Rieke CJ, Rimon G, Wingerd BA, Smith WL. Partnering between monomers of cyclooxygenase-2 homodimers. Proc Natl Acad Sci U S A. 2006;103(16):6142-7. PMCID: 1458845.

68. Rimon G, Sidhu RS, Lauver DA, Lee JY, Sharma NP, Yuan C, et al. Coxibs interfere with the action of aspirin by binding tightly to one monomer of cyclooxygenase-1. Proc Natl Acad Sci U S A. 2010;107(1):28-33. PMCID: 2806742.

69. Sharma NP, Dong L, Yuan C, Noon KR, Smith WL. Asymmetric acetylation of the cyclooxygenase-2 homodimer by aspirin and its effects on the oxygenation of arachidonic, eicosapentaenoic, and docosahexaenoic acids. Mol Pharmacol. 2010;77(6):979-86.

70. Prusakiewicz JJ, Duggan KC, Rouzer CA, Marnett LJ. Differential sensitivity and mechanism of inhibition of COX-2 oxygenation of arachidonic acid and 2-arachidonoylglycerol by ibuprofen and mefenamic acid. Biochemistry. 2009;48(31):7353-5.

71. van der Donk WA, Tsai AL, Kulmacz RJ. The cyclooxygenase reaction mechanism. Biochemistry. 2002;41(52):15451-8.

72. Xie WL, Chipman JG, Robertson DL, Erikson RL, Simmons DL. Expression of a mitogen-responsive gene encoding prostaglandin synthase is regulated by mRNA splicing. Proc Natl Acad Sci U S A. 1991;88(7):2692-6.

73. Tanabe T, Tohnai N. Cyclooxygenase isozymes and their gene structures and expression. Prostaglandins Other Lipid Mediat. 2002;68-69:95-114.

74. Smyth EM, Grosser T, Wang M, Yu Y, FitzGerald GA. Prostanoids in health and disease. J Lipid Res. 2009;50 Suppl:S423-8.

75. Yu M, Ives D, Ramesha CS. Synthesis of prostaglandin E2 ethanolamide from anandamide by cyclooxygenase-2. J Biol Chem. 1997;272(34):21181-6.

76. Kozak KR, Rowlinson SW, Marnett LJ. Oxygenation of the endocannabinoid, 2-arachidonylglycerol, to glyceryl prostaglandins by cyclooxygenase-2. J Biol Chem. 2000;275(43):33744-9.

77. Kozak KR, Crews BC, Morrow JD, Wang LH, Ma YH, Weinander R, et al. Metabolism of the endocannabinoids, 2-arachidonylglycerol and anandamide, into prostaglandin, thromboxane, and prostacyclin glycerol esters and ethanolamides. J Biol Chem. 2002;277(47):44877-85.

78. Vecchio AJ, Simmons DM, Malkowski MG. Structural basis of fatty acid substrate binding to cyclooxygenase-2. J Biol Chem. 2010;285(29):22152-63.

79. Vecchio AJ, Malkowski MG. The structural basis of endocannabinoid oxygenation by cyclooxygenase-2. J Biol Chem. 2011;286(23):20736-45.

80. Malkowski MG, Ginell SL, Smith WL, Garavito RM. The productive conformation of arachidonic acid bound to prostaglandin synthase. Science. 2000;289(5486):1933-7.

81. Kozak KR, Prusakiewicz JJ, Rowlinson SW, Prudhomme DR, Marnett LJ. Amino acid determinants in cyclooxygenase-2 oxygenation of the endocannabinoid anandamide. Biochemistry. 2003;42(30):9041-9.

82. Nirodi CS, Crews BC, Kozak KR, Morrow JD, Marnett LJ. The glyceryl ester of prostaglandin E2 mobilizes calcium and activates signal transduction in RAW264.7 cells. Proc Natl Acad Sci U S A. 2004;101(7):1840-5.

83. Sang N, Zhang J, Chen C. PGE2 glycerol ester, a COX-2 oxidative metabolite of 2-arachidonoyl glycerol, modulates inhibitory synaptic transmission in mouse hippocampal neurons. The Journal of physiology. 2006;572(Pt 3):735-45.

84. Sang N, Zhang J, Chen C. COX-2 oxidative metabolite of endocannabinoid 2-AG enhances excitatory glutamatergic synaptic transmission and induces neurotoxicity. J Neurochem. 2007;102(6):1966-77.

85. Hu SS, Bradshaw HB, Chen JS, Tan B, Walker JM. Prostaglandin E2 glycerol ester, an endogenous COX-2 metabolite of 2-arachidonoylglycerol, induces hyperalgesia and modulates NFkappaB activity. Br J Pharmacol. 2008;153(7):1538-49.

86. Richie-Jannetta R, Nirodi CS, Crews BC, Woodward DF, Wang JW, Duff PT, et al. Structural determinants for calcium mobilization by prostaglandin E2 and prostaglandin F2alpha glyceryl esters in RAW 264.7 cells and H1819 cells. Prostaglandins Other Lipid Mediat. 2010;92(1-4):19-24.

87. Kozak KR, Crews BC, Ray JL, Tai HH, Morrow JD, Marnett LJ. Metabolism of prostaglandin glycerol esters and prostaglandin ethanolamides in vitro and in vivo. J Biol Chem. 2001;276(40):36993-8.

88. Woodward DF, Wang JW, Poloso NJ. Recent progress in prostaglandin F2alpha ethanolamide (prostamide F2alpha) research and therapeutics. Pharmacol Rev. 2013;65(4):1135-47.

89. Gatta L, Piscitelli F, Giordano C, Boccella S, Lichtman A, Maione S, et al. Discovery of prostamide F2alpha and its role in inflammatory pain and dorsal horn nociceptive neuron hyperexcitability. PLoS One. 2012;7(2):e31111.

90. Correa F, Docagne F, Clemente D, Mestre L, Becker C, Guaza C. Anandamide inhibits IL-12p40 production by acting on the promoter repressor element GA-12: possible involvement of the COX-2 metabolite prostamide E(2). Biochem J. 2008;409(3):761-70.

91. Brown KL, Davidson J, Rotondo D. Characterisation of the prostaglandin E2-ethanolamide suppression of tumour necrosis factor-alpha production in human monocytic cells. Biochim Biophys Acta. 2013;1831(6):1098-107.

92. Ross RA, Craib SJ, Stevenson LA, Pertwee RG, Henderson A, Toole J, et al. Pharmacological characterization of the anandamide cyclooxygenase metabolite: prostaglandin E2 ethanolamide. J Pharmacol Exp Ther. 2002;301(3):900-7.

93. Valdeolivas S, Pazos MR, Bisogno T, Piscitelli F, Iannotti FA, Allara M, et al. The inhibition of 2-arachidonoyl-glycerol (2-AG) biosynthesis, rather than enhancing striatal damage, protects striatal neurons from malonate-induced death: a potential role of cyclooxygenase-2-dependent metabolism of 2-AG. Cell Death Dis. 2013;4:e862.

94. Raman P, Kaplan BL, Kaminski NE. 15-Deoxy-Delta(1)(2),(1)(4)-prostaglandin J(2)-glycerol, a putative metabolite of 2-arachidonyl glycerol and a peroxisome proliferator-activated receptor gamma ligand, modulates nuclear factor of activated T cells. J Pharmacol Exp Ther. 2012;342(3):816-26.

95. Raman P, Kaplan BL, Thompson JT, Vanden Heuvel JP, Kaminski NE. 15-Deoxy-delta12,14-prostaglandin J2-glycerol ester, a putative metabolite of 2-arachidonyl glycerol, activates peroxisome proliferator activated receptor gamma. Mol Pharmacol. 2011;80(1):201-9.

96. Yang H, Zhang J, Andreasson K, Chen C. COX-2 oxidative metabolism of endocannabinoids augments hippocampal synaptic plasticity. Molecular and cellular neurosciences. 2008;37(4):682-95.

97. Vila A, Rosengarth A, Piomelli D, Cravatt B, Marnett LJ. Hydrolysis of prostaglandin glycerol esters by the endocannabinoid-hydrolyzing enzymes, monoacylglycerol lipase and fatty acid amide hydrolase. Biochemistry. 2007;46(33):9578-85.

98. Xie S, Borazjani A, Hatfield MJ, Edwards CC, Potter PM, Ross MK. Inactivation of lipid glyceryl ester metabolism in human THP1 monocytes/macrophages by activated organophosphorus insecticides: role of carboxylesterases 1 and 2. Chem Res Toxicol. 2010;23(12):1890-904.

99. Wang R, Borazjani A, Matthews AT, Mangum LC, Edelmann MJ, Ross MK. Identification of palmitoyl protein thioesterase 1 in human THP1 monocytes and macrophages and characterization of unique biochemical activities for this enzyme. Biochemistry. 2013;52(43):7559-74.

100. Long JZ, Cravatt BF. The metabolic serine hydrolases and their functions in mammalian physiology and disease. Chem Rev. 2011;111(10):6022-63.

101. Simon GM, Cravatt BF. Activity-based proteomics of enzyme superfamilies: serine hydrolases as a case study. J Biol Chem. 2010;285(15):11051-5.

102. Dodson G, Wlodawer A. Catalytic triads and their relatives. Trends Biochem Sci. 1998;23(9):347-52.

103. Patricelli MP, Lovato MA, Cravatt BF. Chemical and mutagenic investigations of fatty acid amide hydrolase: evidence for a family of serine hydrolases with distinct catalytic properties. Biochemistry. 1999;38(31):9804-12.

104. Blow DM, Birktoft JJ, Hartley BS. Role of a buried acid group in the mechanism of action of chymotrypsin. Nature. 1969;221(5178):337-40.

105. Polgar L. The catalytic triad of serine peptidases. Cell Mol Life Sci. 2005;62(19-20):2161-72.

106. Polgar L, Bender ML. The nature of general base-general acid catalysis in serine proteases. Proc Natl Acad Sci U S A. 1969;64(4):1335-42.

107. Jung G, Ueno H, Hayashi R. Proton-relay system of carboxypeptidase Y as a sole catalytic site: studies on mutagenic replacement of his 397. J Biochem. 1998;124(2):446-50.

108. Hedstrom L. Serine protease mechanism and specificity. Chem Rev. 2002;102(12):4501-24.

109. Clark JD, Schievella AR, Nalefski EA, Lin LL. Cytosolic phospholipase A2. J Lipid Mediat Cell Signal. 1995;12(2-3):83-117.

110. Mignatti P, Rifkin DB. Plasminogen activators and matrix metalloproteinases in angiogenesis. Enzyme Protein. 1996;49(1-3):117-37.

111. Seidah NG, Chretien M. Eukaryotic protein processing: endoproteolysis of precursor proteins. Curr Opin Biotechnol. 1997;8(5):602-7.

112. Kato GJ. Human genetic diseases of proteolysis. Hum Mutat. 1999;13(2):87-98.

113. Smyth MJ, O'Connor MD, Trapani JA. Granzymes: a variety of serine protease specificities encoded by genetically distinct subfamilies. J Leukoc Biol. 1996;60(5):555-62.

114. Liu Y, Patricelli MP, Cravatt BF. Activity-based protein profiling: the serine hydrolases. Proc Natl Acad Sci U S A. 1999;96(26):14694-9.

115. Cravatt BF, Wright AT, Kozarich JW. Activity-based protein profiling: from enzyme chemistry to proteomic chemistry. Annu Rev Biochem. 2008;77:383-414.

116. Balls AK, Jansen EF. Stoichiometric inhibition of chymotrypsin. Adv Enzymol Relat Subj Biochem. 1952;13:321-43.

117. Balls AK, Jansen EF. Proteolytic enzymes. Annu Rev Biochem. 1952;21:1-28.

118. Tipper DJ, Strominger JL. Mechanism of action of penicillins: a proposal based on their structural similarity to acyl-D-alanyl-D-alanine. Proc Natl Acad Sci U S A. 1965;54(4):1133-41.

119. Blumberg PM, Strominger JL. Five penicillin-binding components occur in Bacillus subtilis membranes. J Biol Chem. 1972;247(24):8107-13.

120. Suginaka H, Blumberg PM, Strominger JL. Multiple penicillin-binding components in Bacillus subtilis, Bacillus cereus, Staphylococcus aureus, and Escherichia coli. J Biol Chem. 1972;247(17):5279-88.

121. Jessani N, Liu Y, Humphrey M, Cravatt BF. Enzyme activity profiles of the secreted and membrane proteome that depict cancer cell invasiveness. Proc Natl Acad Sci U S A. 2002;99(16):10335-40.

122. Jessani N, Humphrey M, McDonald WH, Niessen S, Masuda K, Gangadharan B, et al. Carcinoma and stromal enzyme activity profiles associated with breast tumor growth in vivo. Proc Natl Acad Sci U S A. 2004;101(38):13756-61.

123. Nomura DK, Long JZ, Niessen S, Hoover HS, Ng SW, Cravatt BF. Monoacylglycerol lipase regulates a fatty acid network that promotes cancer pathogenesis. Cell. 2010;140(1):49-61.

124. Jessani N, Niessen S, Wei BQ, Nicolau M, Humphrey M, Ji Y, et al. A streamlined platform for high-content functional proteomics of primary human specimens. Nat Methods. 2005;2(9):691-7.

125. Leung D, Hardouin C, Boger DL, Cravatt BF. Discovering potent and selective reversible inhibitors of enzymes in complex proteomes. Nat Biotechnol. 2003;21(6):687-91.

126. Li W, Blankman JL, Cravatt BF. A functional proteomic strategy to discover inhibitors for uncharacterized hydrolases. J Am Chem Soc. 2007;129(31):9594-5.

127. Long JZ, Li W, Booker L, Burston JJ, Kinsey SG, Schlosburg JE, et al. Selective blockade of 2-arachidonoylglycerol hydrolysis produces cannabinoid behavioral effects. Nat Chem Biol. 2009;5(1):37-44.

128. Greenbaum D, Baruch A, Hayrapetian L, Darula Z, Burlingame A, Medzihradszky KF, et al. Chemical approaches for functionally probing the proteome. Mol Cell Proteomics. 2002;1(1):60-8.

129. Ahn K, Johnson DS, Fitzgerald LR, Liimatta M, Arendse A, Stevenson T, et al. Novel mechanistic class of fatty acid amide hydrolase inhibitors with remarkable selectivity. Biochemistry. 2007;46(45):13019-30.

130. Long JZ, Nomura DK, Vann RE, Walentiny DM, Booker L, Jin X, et al. Dual blockade of FAAH and MAGL identifies behavioral processes regulated by endocannabinoid crosstalk in vivo. Proc Natl Acad Sci U S A. 2009;106(48):20270-5.

131. Adibekian A, Martin BR, Chang JW, Hsu KL, Tsuboi K, Bachovchin DA, et al. Confirming target engagement for reversible inhibitors in vivo by kinetically tuned activity-based probes. J Am Chem Soc. 2012;134(25):10345-8.

132. Karas M, Bachmann D, Bahr U, Hillenkamp F. Matrix-assisted ultraviolet laser desorption of non-volatile compounds. International Journal of Mass Spectrometry and Ion Processes. 1987;78:53-68.

133. Miura D, Fujimura Y, Tachibana H, Wariishi H. Highly Sensitive Matrix-Assisted Laser Desorption Ionization-Mass Spectrometry for High-Throughput Metabolic Profiling. Analytical Chemistry. 2009;82(2):498-504.

134. Holle A, Haase A, Kayser M, Höhndorf J. Optimizing UV laser focus profiles for improved MALDI performance. Journal of Mass Spectrometry. 2006;41(6):705-16.

135. Rouzer CA, Marnett LJ. Non-redundant functions of cyclooxygenases: oxygenation of endocannabinoids. J Biol Chem. 2008;283(13):8065-9.

136. Nirodi CS, Crews BC, Kozak KR, Morrow JD, Marnett LJ. The glyceryl ester of prostaglandin E2 mobilizes calcium and activates signal transduction in RAW264.7 cells. Proc Natl Acad Sci U S A. 2004;101(7):1840-5.

137. Narumiya S, Toda N. Different responsiveness of prostaglandin D2-sensitive systems to prostaglandin D2 and its analogues. Br J Pharmacol. 1985;85(2):367-75.

138. Watanabe T, Narumiya S, Shimizu T, Hayaishi O. Characterization of the biosynthetic pathway of prostaglandin D2 in human platelet-rich plasma. J Biol Chem. 1982;257(24):14847-53.

139. Murphy RC, Barkley RM, Zemski Berry K, Hankin J, Harrison K, Johnson C, et al. Electrospray ionization and tandem mass spectrometry of eicosanoids. Anal Biochem. 2005;346(1):1-42.

140. Blair IA, Barrow SE, Waddell KA, Lewis PJ, Dollery CT. Specific Quantitative-Determination of 6-Oxo-Prostaglandin-F 1-Alpha in Human-Plasma. Adv Prostag Thromb L. 1983;11:197-205.

141. Barrow SE, Heavey DJ, Ennis M, Chappell CG, Blair IA, Dollery CT. Measurement of Prostaglandin-D2 and Identification of Metabolites in Human-Plasma during Intravenous-Infusion. Prostaglandins. 1984;28(6):743-54.

142. Kingsley PJ, Rouzer CA, Saleh S, Marnett LJ. Simultaneous analysis of prostaglandin glyceryl esters and prostaglandins by electrospray tandem mass spectrometry. Anal Biochem. 2005;343(2):203-11.

143. Rowlinson SW, Crews BC, Lanzo CA, Marnett LJ. The binding of arachidonic acid in the cyclooxygenase active site of mouse prostaglandin endoperoxide synthase-2 (COX-2). A putative L-shaped binding conformation utilizing the top channel region. J Biol Chem. 1999;274(33):23305-10.

144. Hong HH, Wang YS. Derivatization with girard reagent t combined with LC-MS/MS for the sensitive detection of 5-formyl-2 '-deoxyuridine in cellular DNA. Analytical Chemistry. 2007;79(1):322-6.

145. Kalgutkar AS, Kozak KR, Crews BC, Hochgesang GP, Jr., Marnett LJ. Covalent modification of cyclooxygenase-2 (COX-2) by 2-acetoxyphenyl alkyl sulfides, a new class of selective COX-2 inactivators. J Med Chem. 1998;41(24):4800-18.

146. Kulmacz RJ, Miller JF, Jr., Pendleton RB, Lands WE. Cyclooxygenase initiation assay for hydroperoxides. Methods Enzymol. 1990;186:431-8.

147. Kalgutkar AS, Crews BC, Rowlinson SW, Marnett AB, Kozak KR, Remmel RP, et al. Biochemically based design of cyclooxygenase-2 (COX-2) inhibitors: facile conversion of nonsteroidal antiinflammatory drugs to potent and highly selective COX-2 inhibitors. Proc Natl Acad Sci U S A. 2000;97(2):925-30.

148. Gierse JK, Hauser SD, Creely DP, Koboldt C, Rangwala SH, Isakson PC, et al. Expression and Selective-Inhibition of the Constitutive and Inducible Forms of Human Cyclooxygenase. Biochemical Journal. 1995;305:479-84.

149. Barnett J, Chow J, Ives D, Chiou M, Mackenzie R, Osen E, et al. Purification, characterization and selective inhibition of human prostaglandin G/H synthase 1 and 2 expressed in the baculovirus system. Biochim Biophys Acta. 1994;1209(1):130-9.

150. Yang P, Felix E, Madden T, Fischer SM, Newman RA. Quantitative high-performance liquid chromatography/electrospray ionization tandem mass spectrometric analysis of 2- and 3-series prostaglandins in cultured tumor cells. Anal Biochem. 2002;308(1):168-77.

151. Rouzer CA, Jacobs AT, Nirodi CS, Kingsley PJ, Morrow JD, Marnett LJ. RAW264.7 cells lack prostaglandin-dependent autoregulation of tumor necrosis factor-alpha secretion. J Lipid Res. 2005;46(5):1027-37.

152. Brodie AF, Lipmann F. Identification of a gluconolactonase. J Biol Chem. 1955;212(2):677-85.

153. Tjoelker LW, Wilder C, Eberhardt C, Stafforini DM, Dietsch G, Schimpf B, et al. Anti-inflammatory properties of a platelet-activating factor acetylhydrolase. Nature. 1995;374(6522):549-53.

154. Shum AK, Alimohammadi M, Tan CL, Cheng MH, Metzger TC, Law CS, et al. BPIFB1 is a lung-specific autoantigen associated with interstitial lung disease. Sci Transl Med. 2013;5(206):206ra139.

155. Pullamsetti SS, Savai R, Dumitrascu R, Dahal BK, Wilhelm J, Konigshoff M, et al. The role of dimethylarginine dimethylaminohydrolase in idiopathic pulmonary fibrosis. Sci Transl Med. 2011;3(87):87ra53.

156. Nomura DK, Lombardi DP, Chang JW, Niessen S, Ward AM, Long JZ, et al. Monoacylglycerol lipase exerts dual control over endocannabinoid and fatty acid pathways to support prostate cancer. Chem Biol. 2011;18(7):846-56.

157. Walker JM, Huang SM. Cannabinoid analgesia. Pharmacol Ther. 2002;95(2):127-35.

158. Pertwee RG. Cannabinoid receptors and pain. Prog Neurobiol. 2001;63(5):569-611.

159. Valenzano KJ, Tafesse L, Lee G, Harrison JE, Boulet JM, Gottshall SL, et al. Pharmacological and pharmacokinetic characterization of the cannabinoid receptor 2 agonist, GW405833, utilizing rodent models of acute and chronic pain, anxiety, ataxia and catalepsy. Neuropharmacology. 2005;48(5):658-72.

160. Whiteside GT, Gottshall SL, Boulet JM, Chaffer SM, Harrison JE, Pearson MS, et al. A role for cannabinoid receptors, but not endogenous opioids, in the antinociceptive activity of the CB2-selective agonist, GW405833. Eur J Pharmacol. 2005;528(1-3):65-72.

161. Di Marzo V, Bisogno T, De Petrocellis L. Endocannabinoids and related compounds: walking back and forth between plant natural products and animal physiology. Chem Biol. 2007;14(7):741-56.

162. Kogan NM, Mechoulam R. The chemistry of endocannabinoids. J Endocrinol Invest. 2006;29(3 Suppl):3-14.

163. Maccarrone M, van der Stelt M, Rossi A, Veldink GA, Vliegenthart JF, Agro AF. Anandamide hydrolysis by human cells in culture and brain. J Biol Chem. 1998;273(48):32332-9.

164. Blankman JL, Simon GM, Cravatt BF. A comprehensive profile of brain enzymes that hydrolyze the endocannabinoid 2-arachidonoylglycerol. Chem Biol. 2007;14(12):1347-56.

165. Alhouayek M, Masquelier J, Cani PD, Lambert DM, Muccioli GG. Implication of the anti-inflammatory bioactive lipid prostaglandin D2-glycerol ester in the control of macrophage activation and inflammation by ABHD6. Proc Natl Acad Sci U S A. 2013;110(43):17558-63.

166. Ross MK, Borazjani A, Wang R, Crow JA, Xie S. Examination of the carboxylesterase phenotype in human liver. Arch Biochem Biophys. 2012;522(1):44-56.

167. Quiroga AD, Lehner R. Role of endoplasmic reticulum neutral lipid hydrolases. Trends Endocrinol Metab. 2011;22(6):218-25.

168. Ghosh S. Cholesteryl ester hydrolase in human monocyte/macrophage: cloning, sequencing, and expression of full-length cDNA. Physiol Genomics. 2000;2(1):1-8.

169. Lu JY, Hofmann SL. Thematic review series: lipid posttranslational modifications. Lysosomal metabolism of lipid-modified proteins. J Lipid Res. 2006;47(7):1352-7.

170. Lu JY, Hofmann SL. Inefficient cleavage of palmitoyl-protein thioesterase (PPT) substrates by aminothiols: implications for treatment of infantile neuronal ceroid lipofuscinosis. J Inherit Metab Dis. 2006;29(1):119-26.

171. Crow JA, Bittles V, Herring KL, Borazjani A, Potter PM, Ross MK. Inhibition of recombinant human carboxylesterase 1 and 2 and monoacylglycerol lipase by chlorpyrifos oxon, paraoxon and methyl paraoxon. Toxicol Appl Pharmacol. 2012;258(1):145-50.

172. Wang A, Dennis EA. Mammalian lysophospholipases. Biochim Biophys Acta. 1999;1439(1):1-16.

173. Weltzien HU. Cytolytic and membrane-perturbing properties of lysophosphatidylcholine. Biochim Biophys Acta. 1979;559(2-3):259-87.

174. Silverman BA, Weller PF, Shin ML. Effect of erythrocyte membrane modulation by lysolecithin on complement-mediated lysis. J Immunol. 1984;132(1):386-91.

175. Kelly RA, O'Hara DS, Mitch WE, Smith TW. Identification of NaK-ATPase inhibitors in human plasma as nonesterified fatty acids and lysophospholipids. J Biol Chem. 1986;261(25):11704-11.

176. Martonosi A, Donley J, Halpin RA. Sarcoplasmic reticulum. 3. The role of phospholipids in the adenosine triphosphatase activity and Ca++ transport. J Biol Chem. 1968;243(1):61-70.

177. Shier WT, Baldwin JH, Nilsen-Hamilton M, Hamilton RT, Thanassi NM. Regulation of guanylate and adenylate cyclase activities by lysolecithin. Proc Natl Acad Sci U S A. 1976;73(5):1586-90.

178. Lands WE. Metabolism of glycerolipides; a comparison of lecithin and triglyceride synthesis. J Biol Chem. 1958;231(2):883-8.

179. Lands WE. Stories about acyl chains. Biochim Biophys Acta. 2000;1483(1):1-14.

180. Waku K, Nakazawa Y. Acyltransferae activity to 1-acyl-, 1-O-alkenyl-, and 1-O-alkyl-glycero-3-phosphorylcholine in Ehrlich ascites tumor cells. J Biochem. 1972;72(2):495-7.

181. Quinn MT, Kondratenko N, Parthasarathy S. Analysis of the monocyte chemotactic response to lysophosphatidylcholine: role of lysophospholipase C. Biochim Biophys Acta. 1991;1082(3):293-302.

182. Ross BM, Kish SJ. Characterization of lysophospholipid metabolizing enzymes in human brain. J Neurochem. 1994;63(5):1839-48.

183. Zhang YY, Deems RA, Dennis EA. Lysophospholipases I and II from P388D1 macrophage-like cell line. Methods in enzymology. 1991;197:456-68.

184. Lepage N, Roberts KD. Purification of lysophospholipase of human spermatozoa and its implication in the acrosome reaction. Biology of reproduction. 1995;52(3):616-24.

185. Gross RW, Sobel BE. Rabbit myocardial cytosolic lysophospholipase. Purification, characterization, and competitive inhibition by L-palmitoyl carnitine. J Biol Chem. 1983;258(8):5221-6.

186. Sunaga H, Sugimoto H, Nagamachi Y, Yamashita S. Purification and properties of lysophospholipase isoenzymes from pig gastric mucosa. Biochem J. 1995;308 (Pt 2):551-7.

187. Sugimoto H, Hayashi H, Yamashita S. Purification, cDNA cloning, and regulation of lysophospholipase from rat liver. J Biol Chem. 1996;271(13):7705-11.

188. Zhang YY, Dennis EA. Purification and characterization of a lysophospholipase from a macrophage-like cell line P388D1. J Biol Chem. 1988;263(20):9965-72.

189. Garsetti DE, Ozgur LE, Steiner MR, Egan RW, Clark MA. Isolation and characterization of three lysophospholipases from the murine macrophage cell line WEHI 265.1. Biochim Biophys Acta. 1992;1165(2):229-38.

190. Wang A, Deems RA, Dennis EA. Cloning, expression, and catalytic mechanism of murine lysophospholipase I. J Biol Chem. 1997;272(19):12723-9.

191. Wang A, Loo R, Chen Z, Dennis EA. Regiospecificity and catalytic triad of lysophospholipase I. J Biol Chem. 1997;272(35):22030-6.

192. Devedjiev Y, Dauter Z, Kuznetsov SR, Jones TL, Derewenda ZS. Crystal structure of the human acyl protein thioesterase I from a single X-ray data set to 1.5 A. Structure. 2000;8(11):1137-46.

193. Wang A, Yang HC, Friedman P, Johnson CA, Dennis EA. A specific human lysophospholipase: cDNA cloning, tissue distribution and kinetic characterization. Biochim Biophys Acta. 1999;1437(2):157-69.

194. Gibson DG, Young L, Chuang RY, Venter JC, Hutchison CA, 3rd, Smith HO. Enzymatic assembly of DNA molecules up to several hundred kilobases. Nat Methods. 2009;6(5):343-5.

195. Studier FW. Protein production by auto-induction in high density shaking cultures. Protein Expr Purif. 2005;41(1):207-34.

196. Di Marzo V, Bisogno T, De Petrocellis L, Melck D, Orlando P, Wagner JA, et al. Biosynthesis and inactivation of the endocannabinoid 2-arachidonoylglycerol in circulating and tumoral macrophages. Eur J Biochem. 1999;264(1):258-67.

197. Di Marzo V, De Petrocellis L, Bisogno T. The biosynthesis, fate and pharmacological properties of endocannabinoids. Handb Exp Pharmacol. 2005(168):147-85.

198. Duncan JA, Gilman AG. A cytoplasmic acyl-protein thioesterase that removes palmitate from G protein alpha subunits and p21(RAS). J Biol Chem. 1998;273(25):15830-7.

199. Sugiura T, Kishimoto S, Oka S, Gokoh M. Biochemistry, pharmacology and physiology of 2-arachidonoylglycerol, an endogenous cannabinoid receptor ligand. Prog Lipid Res. 2006;45(5):405-46.

200. Basavarajappa BS. Critical enzymes involved in endocannabinoid metabolism. Protein Pept Lett. 2007;14(3):237-46.

201. Ahn K, McKinney MK, Cravatt BF. Enzymatic pathways that regulate endocannabinoid signaling in the nervous system. Chem Rev. 2008;108(5):1687-707.